# COMBINATION DRUG DISCOVERY IN THE TREATMENT OF MULTIDRUG-RESISTANT PRECLINICAL MODELS OF BREAST CANCER

by

Xingjian Zhai

Submitted in partial fulfillment of the requirements
for the degree of Master of Science

at
Dalhousie University
Halifax, Nova Scotia
September 2021

**Table of Contents**

## List of Tables

## List of Figures

**Abstract**

Therapeutic resistance is the culprit behind most cancer-related relapse and death, accounting for over 90% chemotherapeutic intervention failures. To combat the genetic and phenotypical abnormalities associated with resistant cancer cells, combination therapy takes the centre stage. Here, we identified a commercially available molecule, which we renamed as “BC-2021,” and its ability to sensitize multidrug-resistant triple-negative and hormone receptor-positive breast cancer cells to the challenge of Taxol in short-term and longer-term *in vitro* studies. 1µM of BC-2021 alone did not pose acute cytotoxicity towards non-cancerous cells, whereas 1µM of BC-2021 in combination with 585nM of PLX induced apoptosis among resistant breast cancer cells. It is noteworthy that the observed cell death was not accompanied by elevated total or mitochondrial reactive oxygen species, nitric oxide levels, and microtubule stabilization. Instead, the combination regimen predominantly induced extensive G2/M phase cell cycle arrest, resulting in BC-2021 dose-dependent nuclear fragmentation.

**Acknowledgements （感谢）**

首先，我要感谢我的妈妈 (dúndún)。在过去的二十二年里，我们共同看世界，一起成长。在此同时，我们也经历了生活中的喜怒哀乐和一日三餐。你以身作则，教会了我许多东西：快乐，善良，选择，独立和真我。因为有你无条件的支持和理解，我才会有这么好的平台。在求学的道路上有你的陪伴很给力！有时想起咱俩过吃炒面的日子 -- 我们拥有的并不多，但依旧像现在这样无比的开心。美好的生活来之不易，我们要感激生活，健康，平安，让彼此放心，别的都是浮云。在这儿，我们共同期待未来的征程!

I also appreciate my master's supervisor, Dr. Yassine El Hiani for his enthusiasm, approachability, and dedication to my professional developments at Dalhousie. What's unique about our close-knit lab is that every lab day is a happy day.

No one makes it through graduate school alone. I want to thank Dr. Alex Quinn, Dr. Ketul Chaudhary, Dr. Thomas Pulinilkunnil, and Dr. Xianping Dong for making such a supportive Supervisory Committee and offering many insightful chats after work.

One thing that I unexpectedly discovered during my graduate studies is a passion for teaching. Dr. Marie-Soleil Beaudoin and Dr. Elizabeth Cowley helped me realize my potential in this profession, and I hope to excel in it just as you both have.

Last but not least, I thank the Dalplex and staff members in the Sherriff Hall Dining Hall. The dining hall has great food and allows me to eat unlimited amounts, fuelling me to break my own powerlifting records again and again. You both have become inseparable parts of my graduate career!

# CHAPTER 1 INTRODUCTION

## Chapter 1.1 Comprehensive Overview of Breast Cancer

### 1.1.1 Physiology and development of the breast

The human breast consists of parenchymal and stromal elements. The parenchyma gives rise to “tree-like” ducts that lead to secretory acini, while the stroma, mainly composed of adipose tissues, supports the development of the parenchyma (1). Fetal breast development begins in the first trimester with the thickening of the mammary ridges, also known as the milk lines, producing primary mammary buds (2). Guided by inductive factors of the mesenchyme, primary mammary buds depress into the mesenchyme, canalize, and form secondary buds that subsequently give rise to lactiferous ducts by the end of the second trimester. At the time of birth, fetal breast presents complex branching and remodeling with vascular infiltration, albeit with very limited secretory capacity. Postnatal morphological and functional developments of the breast stroma and parenchyma often follow distinct growth kinetics up until puberty, where sexually dimorphic development of the breast takes place under hormonal regulation (3). Under the regulation of estrogen and human epidermal growth factor (ErbB2), the post-natal female breast epithelium forms a bi-layered ductal structure, consisting of an outer myoepithelial basal layer and an inner luminal layer and begins ductal outgrowth (4, 5). The primary ducts that lead to the nipple branch into a series of segmented and sub-segmented ducts. Importantly, sub-segmented ducts culminate with the alveolar terminal duct lobular units (TDLUs), the basic functional units of the breast and the epithelial structures that produce milk during lactation (6). Exterior to the ductal

branches are a constellation of stromal components, including fibroblasts, smooth muscles, blood vessels, immune cells, and adipose tissue, which continues to develop until progesterone induces functional remodification of the breast again during pregnancy (7-12).

The functions of the female breasts are to produce milk for breastfeeding and transmit sexual pleasure. From a glandular perspective, female breast produces milk that contains all essential nutrients and bioactive factors that enable infants to survive and build up immunity during the first 6 months of life (13, 14). Mechanistically, when a baby suckles, the level of prolactin in the blood increases, stimulating the production of breast milk by cells lining the alveoli. Simultaneously, suckling-induced release of oxytocin facilitates the contraction of myoepithelial cells surrounding the milk-collecting alveolar ducts to squeeze the milk out (15). As an auxiliary function, human breast subjected to tactile stimulation transmits sexual pleasure through activation of the cerebellum and paracentral lobule, the genital region of the primary sensory cortex (16). Overall, the female breast functions to provide vital nutrients for the newborn while mediating complex endocrine signaling. The complete structural development of the human breast spans through decades and is subjected to constant remodeling by hormones, making human breast prone to undergoing pathophysiological changes, the most common of which includes the initiation and progression of breast malignancies (17).

### 1.1.2 Breast cancer epidemiology

Breast cancer (BC) is the second leading cause of death among women in Canada, affecting approximately 27,000 women with 5,400 dying each year (18). Statistically, one in eight women will be diagnosed with BC during their lifetime and one in 33 women will die from it, making it the most common cancer among Canadian women. Age is a major risk factor as 83% of BC incidences are detected in women over the age of 50 (19). Globally, BC is a serious health concern affecting predominantly women with approximately 2.3 million confirmed diagnoses and 685,000 deaths reported in 2020 alone (20). Interestingly, women in developed countries, such as France, Australian, and the US, for instance, are at higher risk of developing BC compared to women in other developing countries (21, 22). Indeed, in a developed country like Canada, BC incidence rates have risen steadily since the 1990s, yet mortality has thankfully been declining, thanks to improved access to healthcare resources, such as early detection as well as advanced diagnostic tools, and wider scope of research (19). Despite its high prevalence, BC has a rather high 5-year relative survival rate (87.2%) compared to that of all cancers combined (63%) (23). This high relative survival rate is further reflected in localized breast cancer cases, the 5-year relative survival rate of which is as high as 99%, highlighting the critical need for early diagnosis and intervention in the management of BC (24).

### 1.1.3 Clinical diagnosis and subtyping of breast cancer

Despite common clinical applications of preliminary check-up technologies, such as mammography and breast ultrasound imaging, the only definitive way to diagnose BC is through tissue biopsy, whereby a sample of breast tissue is removed from the patient using either a needle or via surgical means and sent for laboratory testing (25).

A tissue biopsy assesses tumor stage, grade, and receptor status to characterize the spread, aggressiveness, and clinical subtype of BC, respectively. The tumor stage is determined according to the guidelines in the American Joint Committee on Cancer (AJCC) TNM system, reporting on tumor (T) size, status of regional lymph nodes (N) containing cancer, and extent of distant metastases (M), all accompanied by a numerical number following each lettered parameter to indicate the severity of tumor development and extent of spread (26-28). Tumor grade, as an indicator for tumor aggressiveness, establishes the extent of morphological abnormality between cancer cells and their healthy counterparts. To standardize tumor grading, the Scarff-Bloom-Richardson (SBR) grading scheme is applied in BC, systematically characterizing the differentiation status of cancer cells centred on three parameters, namely tubule formation, nuclear size, and mitotic count, a high score for each of which is associated with aggressive phenotype (29). For instance, well-differentiated cancer cells, also known as low-grade cancer cells, resemble their healthy counterparts and typically have lower growth rates and better prognosis compared to poorly differentiated, high-grade cancer cells. Furthermore, immunohistochemistry (IHC) offers a rapid, affordable, and cost-effective way to categorize BC based on the presence of specific cellular markers.

The three widely used markers for receptor status of BC include estrogen receptor (ER), progesterone receptor (PR), and human epidermal growth factor receptor 2 (HER2) (30). Coupled with phenotypical measurements of tumor size, nodal involvement, and degree of metastasis, receptor status revealed by IHC can provide clinical insights for BC management and treatment.

### 1.1.4 Intrinsic subtyping of breast cancer

While IHC offers a glimpse into the clinical subtypes of BC cells, it does not encapsulate the intrinsic molecular abnormality associated with these cells. Therefore, genomic profiling is implemented to complement the results obtained from clinical IHC to guide therapeutic interventions.

The PAM (Prediction Analysis of Microarray) 50 classifier, designed by Parker and colleagues, is a widely used microarray analysis of 50 oncogenes that categorizes BC into 4 distinct intrinsic subtypes based on gene expression profiles: luminal A, luminal B, HER2-enriched, basal-like breast cancer (31, 32). Each intrinsic subtype was then mapped to an IHC-based clinical BC subtype with unique characteristics as outlined in Figure 1.1 (33). Among these intrinsic subtypes, the luminal A subtype encompasses low-grade, estrogen and progesterone receptor-positive BC with limited metastatic potential holding the best prognosis. The luminal B subtype, on the other hand, differs from luminal A by having lower progesterone receptor expression and the occasional presence of HER2. Most notably, luminal B breast cancer expresses higher proliferation marker Ki-67, conferring shorter disease-free survival and worse outcome (34, 35).

HER2-enriched and basal-like breast cancer subtypes, which is primarily made up of triple-negative breast cancer, hold the poorest prognosis and are often accompanied by deficient or absent expression of hormone receptors. These tumors are usually high-grade, presenting a multitude of molecular abnormalities in cell proliferation, metabolism, DNA damage response, and growth factor signaling while carrying a high risk of recurrence (36, 37). Thanks to the advent of anti-HER2 monoclonal antibodies, HER-2 breast cancer has been relatively manageable (38). But, on the other hand, the lack of expression of hormone receptors and HER2-overexpression makes triple-negative breast cancer a grim medical dilemma, rendering targeted therapy ineffective and restricting therapeutic options to specific chemotherapeutic agents, which present toxicities to both cancerous and non-cancerous cells (39, 40).

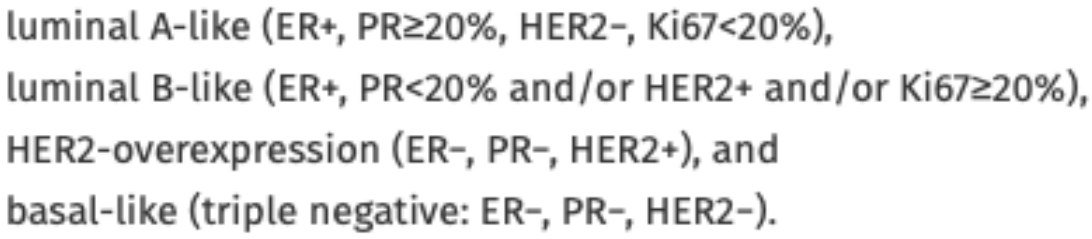


**Figure 1.1. Tabulated summary of immunohistochemical markers and their biopsy quantification in the four major intrinsic subtypes of breast cancer.** This figure is extracted from Tsang, J. Y. S. and Tse, G. M. (2020). Molecular Classification of Breast Cancer. *Advances in Anatomic Pathology.*

## Chapter 1.2 Chemotherapy for Breast Cancer

### 1.2.1 Hormone receptor-positive breast cancer

The mainstay therapeutic option for hormone receptor-positive breast cancers is endocrine therapy, using selective estrogen receptor modulators (SERMs), for instance. However, endocrine therapy is only effective against early-stage, low-grade hormone receptor-positive breast tumors and that the menopausal status of the patient may influence the efficacy of endocrine therapy (41, 42). As a result, adjuvant chemotherapy becomes an ideal candidate to decrease recurrence and improve overall disease-free survival, especially for advanced, high-grade hormone receptor-positive breast cancer. Particularly, meta-analyses and randomized trials revealed that taxane and anthracycline-based regimens are most efficacious against receptor-positive, HER2-negative breast cancer and that patients' overall survival is improved upon receiving concurrent treatment of taxanes and anthracyclines (43, 44).

Mechanistically, anthracyclines and taxanes work cohesively. Anthracyclines (doxorubicin, daunorubicin, epirubicin) intercalate into DNA bases and inhibit topoisomerase II, an enzyme essential for relieving the flexural and torsional strain of supercoiled DNA during DNA replication, causing extensive nucleic acid damages (45, 46). Taxanes (paclitaxel, docetaxel), on the other hand, predominantly exert their cytotoxicity downstream of anthracyclines by stabilizing microtubule disassembly through intercalating at the β-tubulin subunit (47, 48). As microtubules must tether and allocate genomic DNA to daughter cells with high fidelity during mitosis to maintain cell survival, taxane-mediated disruption of microtubule structure and function results in

cell cycle arrest at the G2 (Growth)/ M (Mitosis) phase, leading to apoptosis (49). As a result, anthracyclines compromises genomic integrity of target cells, and taxanes induce further cellular damages by inhibiting microtubule dynamicity and stopping the allocation of genomic materials into daughter cells during cell division.

While the most superior adjuvant chemotherapy for hormone-receptor positive, HER2-negative breast cancer remains anthracycline and taxane-based regimen, patients with history of cardiac disease are at risk for anthracycline-induced cardiotoxicity (50). To mediate this dilemma, alternative regimens, such as docetaxel and cyclophosphamide-based regimen, can be prescribed, albeit recommended only for patients with early-stage and lower-risk breast cancer (51).

### 1.2.2 HER2$^{+}$-positive breast cancer

Encoded by *erbB2* located in chromosome region 17q12, HER2 is a membrane-bound glycoprotein that forms heterodimers with other epidermal growth factor receptor members (EGFR, HER3, HER4) to mediate tyrosine kinase signaling (52). Many of these signaling pathways, such as mitogen-activated protein kinase (MAPK) and phosphatidylinositol 3-kinase / protein kinase B (PI3K/AKT), are oncogenic, fuelling cell survival and proliferation (53). Indeed, IHC staining reveals that 20-30% of human breast cancer cases are characterized by HER2 overexpression (54). Patients with HER2-enriched breast cancers generally have poor prognosis and relatively high metastatic potential. Nonetheless, the progression of these cancers can be managed using tyrosine kinase inhibitors (lapatinib) and humanized anti-HER2 monoclonal antibodies, such as

trastuzumab (Herceptin) and pertuzumab (Perjeta). However, tyrosine kinase inhibitors and anti-HER2 monoclonal antibodies are most effective against cancer cells drastically enriched with HER2. Cancer cells with moderate HER2 overexpression may not receive optimal therapeutic benefits solely from targeted HER2-based interventions (55, 56). Indeed, network meta-analysis of more than a dozen clinical trials with over 37,000 patients concluded that, to achieve superior overall and disease-free survival, chemotherapy is often required along with trastuzumab and lapatinib in early and locally advanced HER2-positive breast cancer patients (57).

The optimal chemotherapeutic agent to be used in partnership with anti-HER2 therapies remains to be highly individualized. This individualized therapeutic design is due to varying extent of drug efficacy and toxicity profiles among patients. For instance, anthracycline and trastuzumab-based regimen leads to cardiotoxicity, causing therapy withdrawal (58). To lessen cardiotoxicity, patients can be prescribed with a regimen consisting of either docetaxel, carboplatin and trastuzumab (TCH) or paclitaxel and trastuzumab concurrently (59, 60). However, taxane and trastuzumab-based intervention may lead to peripheral neuropathy. Fortunately, genomic profiling of single-nucleotide polymorphisms (SNPs) could identify patients who are genetically predisposed to adverse drug effects associated with such regimen, enhancing adherence and clinical output (61, 62). Similarly, incorporation of weekly paclitaxel and carboplatin, an alkylating agent that induces DNA crosslinks, into tri-weekly trastuzumab and pertuzumab regimen is associated with high pathological complete response rates, namely the lack of all signs of cancer in tissue samples after chemotherapeutic

treatment, and manageable toxicities (63). As a result, the effective management of $HER2^{+}$-positive breast cancer requires a combination of chemotherapy and monoclonal antibodies, the administration cycle and dosing schedule of which may vary individually to strike a balance between efficacy and toxicity.

### 1.2.3 Triple-negative breast cancer

As triple-negative breast cancer (TNBC) lacks expression of hormone receptors and HER2 overexpression, hormonal and targeted HER2-based therapies do not demonstrate clinical utility. This leaves chemotherapy as the principal systemic mode of intervention for TNBC patients.

To date, a broad spectrum of chemotherapeutic agents have been indicated for TNBC patients. Overall, chemotherapeutic agents targeting TNBC can be classified as alkylating agents (64), taxanes (65-67), antimetabolites (68), and topoisomerase inhibitors (69, 70) based on their mechanism of action (Figure 1.2-1.5). Although anthracycline and paclitaxel-based regimens remain the gold standard chemotherapy for TNBC patients, the clinical prescription of these chemotherapeutic depends on the intrinsic molecular characteristics of TNBC and that the molecular heterogeneity of TNBC confers variable sensitivity and response to these chemotherapeutic agents. For instance, despite of the differences across ethnic populations, 10-20% of TNBC patients harbor mutations in the *breast cancer gene 1/2* (*BRCA1/2*) (71). BRCA1 and 2 are tumor suppressor proteins that mediate DNA damage repair, cell cycle arrest, and elicit apoptosis (72, 73). Although pervasive DNA damages and mutations due to deficient

BRCA1/2-mediated DNA repair may enhance the pathophysiology and oncogenesis of TNBC, this deficient DNA repair serves as a molecular Achilles' heel associated with TNBC and can, therefore, be exploited for therapeutic design (74). Indeed, BRCA1/2-deficient TNBC cells are particularly sensitive to the genotoxic alkylating agents as these agents exacerbate DNA damage of BRCA1/2-mutant TNBC cells to the point where cell viability is no longer possible. For instance, clinical studies show that platinum-based alkylating agents (cisplatin, carboplatin) outperform platinum-free, taxane-based regimen in terms of drug efficacy and progression-free survival for TNBC patients harboring *BRCA1/2* mutations (75-79). In addition to alkylating agents, other genotoxic chemotherapeutics, such as DNA damage response inhibitors (poly adenosine diphosphate-ribose polymerase inhibitors) and topoisomerase inhibitors (anthracyclines, irinotecan), which induce DNA double-strand breaks during replication, may serve as excellent alternatives for *BRCA*-mutated TNBC patients (80-82). Therefore, even though paclitaxel is regarded as a potent, highly versatile agent that can be used in just about every clinical subtype of breast cancer, the *BRCA1/2* mutation status associated with TNBC sets a precedent whereby the therapeutic benefits of using DNA-damaging chemotherapeutic agents outweigh those derived from classical paclitaxel (83, 84). Due to the aggressive and metastatic nature of TNBC, TNBC patients bear the brunt of undergoing excruciating drug therapies while facing the grim reality of shortened disease-free interval.

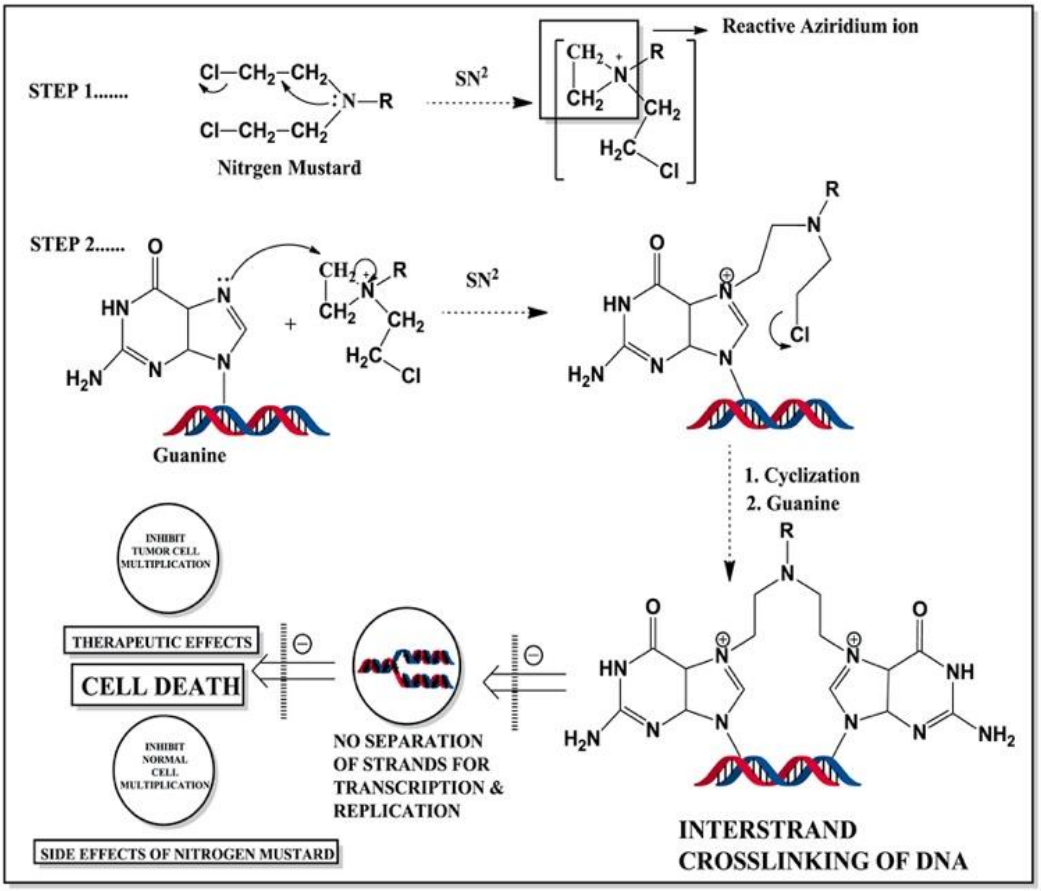


**Figure 1.2. Mechanism of action of the bi-functional alkylating agent nitrogen mustard reacting with a guanine base and causing inter-strand DNA crosslinks through two sequential nucleophilic substitution reactions.** This figure is extracted from Singh, R. K., Kumar, S., Prasad, D. N., & Bhardwaj, T. R. (2018). Therapeutic journey of nitrogen mustard as alkylating anticancer agents: Historic to future perspectives. *European Journal of Medicinal Chemistry*.

**A.**

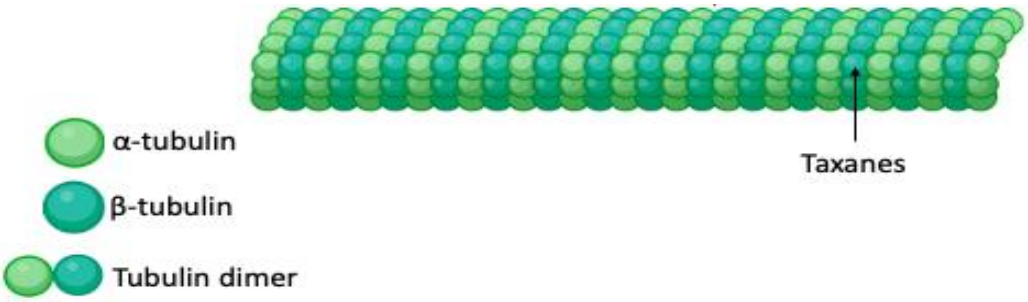


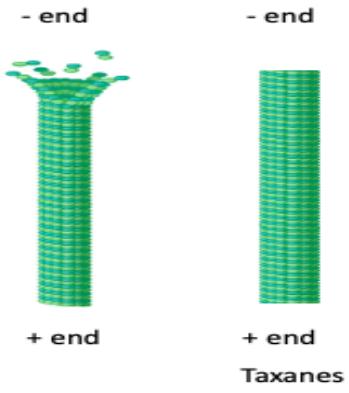


Created with BioRender

**B.**

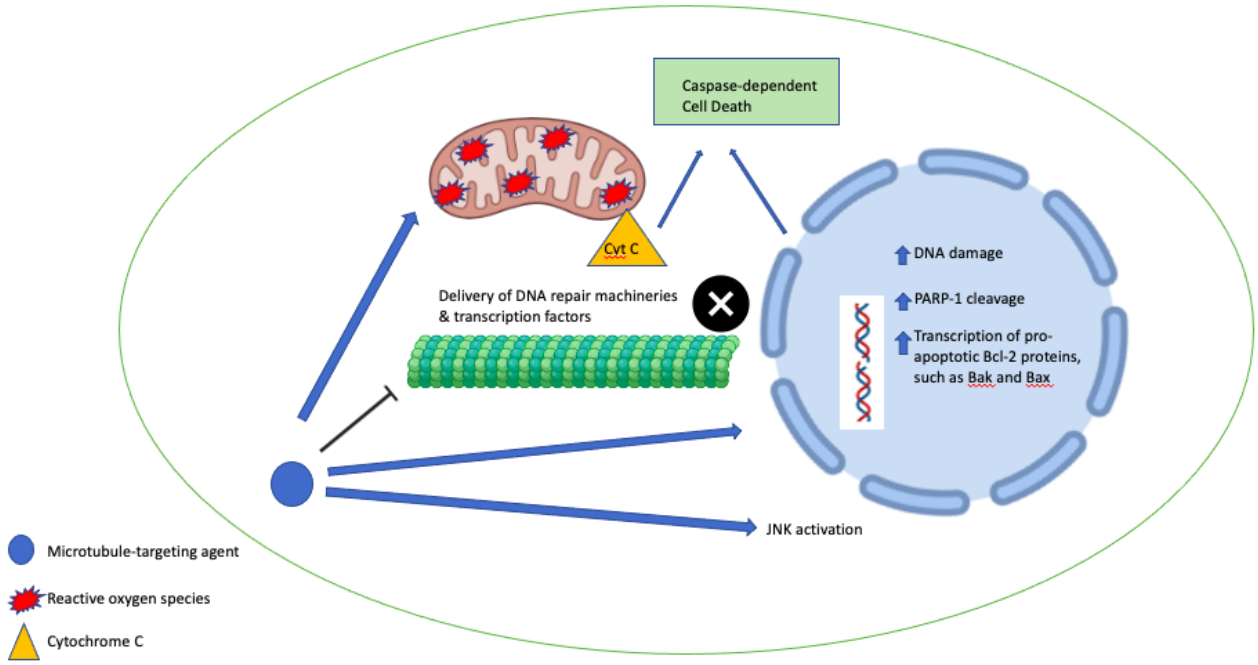


Created with BioRender

**Figure 1.3. Mechanism of action of taxanes.** A) Taxanes, as microtubule-targeting agents, intercalate at ß-tubulin of microtubules to prevent microtubule depolymerization. B) Taxanes exert cytotoxicity through multiple aspects. Taxanes primarily act by stabilizing microtubules and blocking their cellular transport, including transcription factors and proteins essential for DNA repair. Besides, taxanes induce intrinsic, mitochondria and caspase-dependent cellular apoptosis through promoting reactive oxygen species production, mitochondrial permeability, and leakage of cytochrome C. These series of actions lead to poly ADP-ribose polymerase 1 (PARP-1) cleavage and result in DNA fragmentation, a phenotypical hallmark of apoptosis.

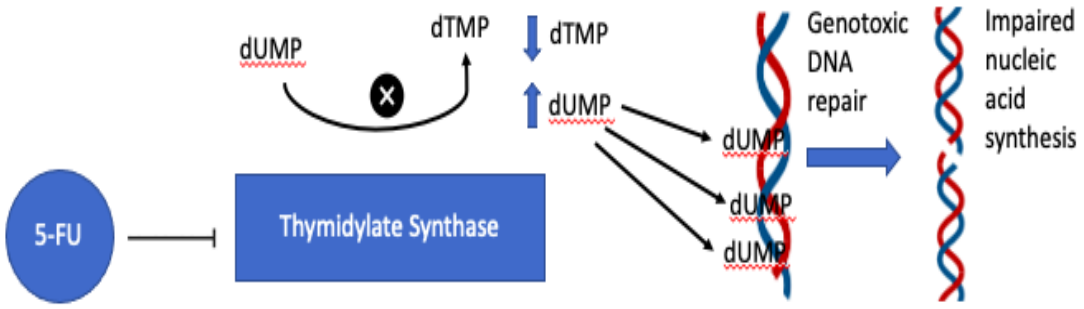


**Figure 1.4. Mechanism of action of the antimetabolite 5-fluorauracil (5-FU).** Used widely in breast cancer, 5-FU inhibits the conversion of deoxyuridine monophosphate (dUMP) to deoxythymidine monophosphate (dTMP) by thymidylate synthase. This leads to cellular depletion of dTMP and increased concentration of dUMP, resulting in decreased pyrimidine synthesis and global DNA damage, respectively.

**A.**

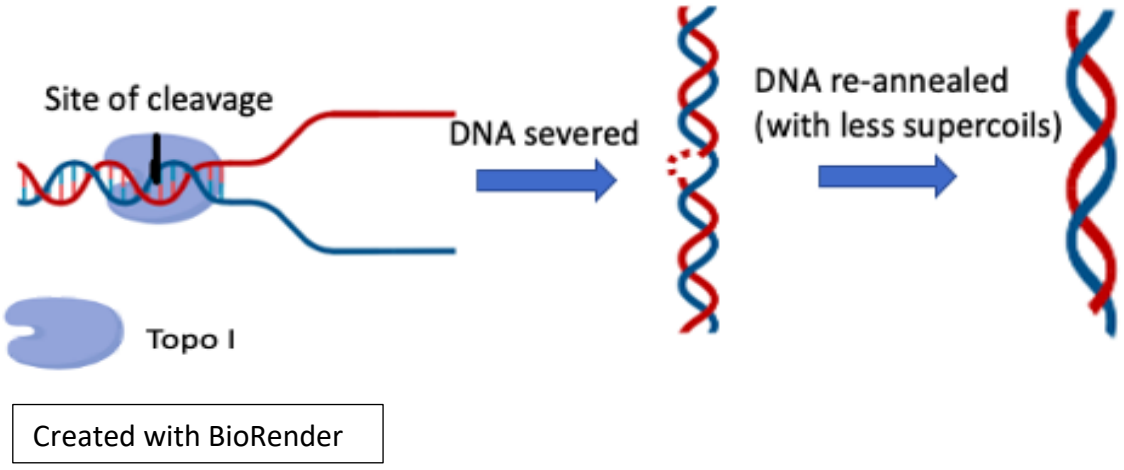


**B.**

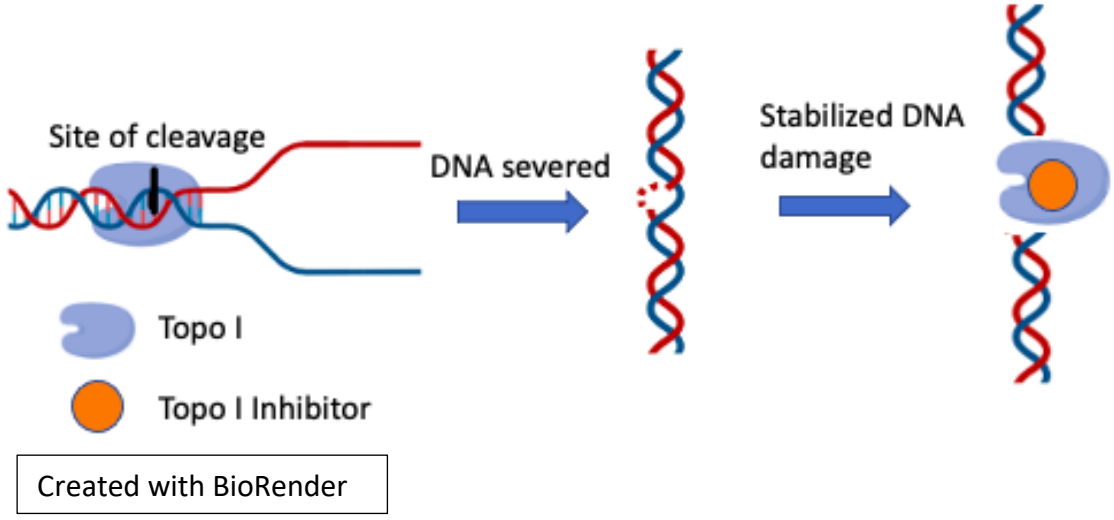


**Figure 1.5. Mechanism of action of mammalian topoisomerase I (Topo I) and topo I inhibitors.** A) Topo I relieves torsion strain arisen from DNA unwinding by creating a single-strand nick and allowing a single strand to pass through the nick before resealing the DNA. B) Topo I inhibitor stabilizes topo I-DNA complex, preventing DNA re-annealing and prolonging the exposure of the genotoxic DNA breakage, leading to cell death.

## Chapter 1.3 Molecular Mechanisms of Breast Cancer Chemotherapeutic Resistance

Cancer cells can become insensitive to therapeutic interventions via either intrinsic resistance, also known as primary resistance, or acquired resistance. Intrinsic resistance arises largely because of the heterogeneous and/or pre-existing genetic composition of cancer cells that confer them varying levels of predisposition to therapeutic treatment. Acquired chemoresistance, on the other hand, often occurs due to adaptative evolutions at the molecular level that allow cancer cells to become insensitive to repeated exposure to antineoplastics. Once resistant, cancer cells may metastasize and invade secondary organs, accounting for over 90% of all failed attempts of chemotherapeutic treatment (85). This renders cancer therapeutic resistance a burning global health concern. This present section will summarize mechanistic perspectives regarding the acquisition of cancer therapeutic resistance with a primary focus on breast cancer and preface novel strategies to combat this issue.

### 1.3.1 Intrinsic resistance

Intrinsic resistance is defined by the initial lack of response of cancers to treatment, upon first exposure. This is predominantly attributed to the population-wide genomic heterogeneity and genetic instability among cancer cells. In immunotherapy, the lack of tumor antigens or the failure to present tumor antigens at the cell surface can result in intrinsic resistance (86, 87). This concept is also appropriate for the case of triple-negative breast cancer (TNBC), where hormonal deprivation or targeted HER-2-based therapy used to treat conventional hormone receptor or HER2-positive breast

cancers fail due to the absence of druggable receptors on the cell surface. Other major contributors to recurring relapses include cancer-initiating stem cells (CSCs) (88). Depending on the cancer type, these CSCs may lack specific mediators of apoptosis-inducing DNA repair machineries, become resistant to apoptosis (89). Using the Cluster of Differentiation system, studies have identified molecular markers for these CSCs, making it feasible to sort and isolate those stem cells from the rest of the population (90). In breast cancer, for instance, these CSCs are characterized by $CD44^{+}/CD24^{-/low}$ and demonstrate the ability to reconstitute parental tumors in xenografts (91, 92). Contrary evidence also exists to indicate that the so-called CSCs, instead of being a distinct type of tumor cells, just represent an alternate functional state of cancer. However, evidence does tilt towards the notion that CSCs exist in many cases of hematological malignancies but not so much so for solid tumors (93-95). Thus, the ability to precisely ascertain the presence of CSCs remains a controversy in oncology research and is one that needs further dialogue having considered the context-dependent nature of cancer as well as the diverse forms of manifestation and phenotypic plasticity of CSCs. Nevertheless, in a tumor cell population, a small number of residual drug-resistant cancer cells, if left un-eradicated, may proliferate and clonally expand into more genetically diverse offspring population over time, making therapeutic efficacy and response onset critical factors when it comes to cancer treatment.

### 1.3.2 Acquired resistance

Acquired resistance can be viewed as an outcome of natural selection at the molecular level. Drugs can induce a variety of responses among cancer cells. Some drug responses are lethal, while others trigger adaptive strategies. During the acquisition of chemoresistance, cancer cells undergo changes at the genomic and proteomic levels (96, 97). Common mediators of acquired chemoresistance in breast cancer include aberrant membrane transporters (impaired drug entry and enhanced drug efflux), metabolic inactivation as well as lysosomal compartmentalization of chemotherapeutics, and genomic instability (dysregulated expression of oncogenes and tumor suppressors). The intricacy and coordination of these responses offers clinical insights into the underlying molecular vulnerability of resistant cancer cells.

#### 1.3.2.1 Aberrant membrane transporters

Among the most primitive defense mechanisms against chemotherapeutic intrusion are drug entry and efflux systems. Resistant cancer cells have managed to minimize drug access and maximize drug extrusion by manipulating the expression, localization, and function of membrane transporters. For instance, methotrexate, an antimetabolite, enters cells through reduced folate carriers (RFC). CpG island methylation of the RFC promoter silences the expression of such promoter, conferring methotrexate resistance in triple-negative MDA-MB-231 breast cancer cells (98). Indeed, the intracellular uptake of many weak-base chemotherapeutics are predominantly mediated by either passive diffusion or facilitated transport. The

extracellular microenvironment of tumors is notoriously acidic, which is largely due to the Warburg Effect, where cancer cells preferentially use glycolysis as the main pathway to acquire energy due to its astounding speed and efficiency in energy production and generate lactate as a result. The extracellular enrichment of lactate results in an acidic extracellular microenvironment. Such acidic extracellular microenvironment acts as a natural barrier by neutralizing and preventing weak-base chemotherapeutic compounds from reaching the cytosol, decreasing cytosolic drug bioavailability, and leading to therapeutic resistance (99, 100). For chemotherapeutics that gain cytosolic access through specialized membrane transporters, especially bulky drugs, many of them are substrates of organic anion transporting peptides (OATPs), a member of the solute carrier (SLC) superfamily (101). With decreased expression of OATPs, cancer cells can develop therapeutic resistance. For instance, paclitaxel-resistant breast cancer cells showed reduced OATP1B3 expression compared to that of their sensitive counterparts (102). In line with this evidence, loss of OATP1B3 leads to taxane resistance in prostate and liver cancer (103, 104). Since OATP1B3 is downregulated in many types of resistant cancer cells, it is often used as a marker to predict drug sensitivity and patient outcome (105, 106). Besides limiting drug influx, cancer cells, on many occasions, simultaneously upregulate drug efflux machineries. Among the most prominent drug efflux transporters are the ATP-binding cassette (ABC) transporters. Some of the most well-studied members that confer multidrug resistance within the ABC transporter superfamily include P-glycoprotein (P-gp), multi-drug resistance protein 1 (MRP1), and breast cancer resistant protein (BCRP/ABCG2/MXR/ABCP) (107). In breast cancer, P-gp and BCRP

overexpression is notoriously prevalent regardless of immunophenotype (108). Structurally, these enzymes have transmembrane domains that dictate the conformation of their substrates and nucleotide-binding regions that catalyze ATP hydrolysis to power active transport of xenobiotics and drug molecules with various properties (109). For ABC transporters to work efficiently in chemo-resistant cells, in addition to the intrinsic ATPase activity originated from the nucleotide-binding domains of the enzymes themselves, a robust supply of ATP from the mitochondria also seems necessary (110). Transfection or overexpression of these transporters shows decreased cytoplasmic drug concentration and confers cancer therapeutic resistance (111). Moreover, these transporters can also be modified epigenetically. For instance, hypomethylation of the *ABCB1* downstream promoter results in increased expression of P-glycoprotein and subsequently confers paclitaxel resistance in MCF7 breast cancer cells (112, 113). This showcases the multifaceted regulation of ABC transporters in cancer and the diverse ways in which cellular machineries can be "hijacked" to acquire therapeutic resistance.

#### 1.3.2.2 Metabolic inactivation of chemotherapeutic agents

Once situated in the cytosol, chemotherapeutic agents may undergo extensive metabolic inactivation and lysosomal sequestration in resistant cancer cells. Cellular biotransformation of drugs requires Phase I and Phase II drug-metabolizing enzymes, whereby Phase I enzymes activate prodrugs through redox reactions and Phase II enzymes, which are made of predominantly of transferases, add hydrophilic and soluble

moieties onto drugs to facilitate their excretion (114, 115). Upregulation of these drug-metabolizing enzymes confers accelerated drug detoxification kinetics, setting the stage for therapeutic resistance. This phenomenon is observed in breast cancer cells after prolonged exposure to chemotherapeutic agents. For instance, extensive exposure to methotrexate in breast cancer cell models results in the induction of UGT1A6, a Phase II UDP-glucuronosyltransferase, leading to enhanced glucuronidation activity and decreased drug sensitivity (116, 117). Moreover, GSTP1 overexpression is associated with resistance to docetaxel, paclitaxel, and doxorubicin (118, 119). Interestingly, GSTP1 also triggers breast cancer drug resistance through activating autophagy, another cellular clearance mechanism, in response to doxorubicin challenge, further highlighting the collaborative nature of drug metabolism in drug-resistant breast cancer (120).

#### 1.3.2.3 Lysosomal compartmentalization of chemotherapeutics

In the event that drug-metabolizing enzymes reach saturation, chemo-resistant cells bear the brunt of the cytotoxic effects associated with chemotherapeutic agents through either enhanced antioxidant capacity, to buffer chemotherapeutic-induced oxidative stress, or lysosomes, which intracellular sequester chemotherapeutic compounds (121-123). Considering that many chemotherapeutic compounds are weak bases, the acidic and degradative environment of the lysosomes can target chemotherapeutics for sequestration and elimination (124). This process can occur passively, whereby small-molecular-weight, lipophilic, and weak base agents become trapped inside lysosomes after traversing both the plasma and lysosomal membrane

(125). Alternatively, lysosomal sequestration of chemotherapeutic compounds can occur actively, whereby P-glycoproteins localized to lysosomal membrane actively suction drug substrates from the cytosol into the lysosomes (126). These instances have been reported in triple-negative breast cancers, where P-gps localized to the plasma and lysosomal membrane can mediate drug efflux out to the extracellular space and into the lysosomal lumen for degradation, respectively, diminishing the therapeutic efficacy of P-gp substrates, such as paclitaxel (127). Conversely, the inhibition of lysosomal function, such as autophagy, using hydroxychloroquine potentiates anti-estrogen responsiveness in $ER^+$ breast cancer, further elucidating the importance of higher kinetics of lysosomal activity and autophagy in chemoresistance (128). Indeed, increased autophagic response has been confirmed in paclitaxel-resistant hormone receptor-positive MCF7 breast cancer cells (129).

Remarkably, not only can entrapped chemotherapeutic agents become degraded in lysosomes, but they can also stimulate further lysosomal biogenesis through transcriptional coupling. Mechanistically, as weak-base chemotherapeutics enter lysosomes, they become rapidly protonated. Some of these protonated agents initiate physical contact with the hydrophilic phospholipid portion of the lysosomal membrane, interfering with their packing and spatial arrangement. This fluidization of the lysosomal membrane lipid composition causes proteins bound to it, such as the mammalian target of rapamycin complex 1 (mTORC1), to dissociate. The dissociation of mTORC1 from the lysosomal membrane attenuates its phosphorylation and subsequent cytoplasmic retention of transcription factor EB (TFEB), triggering the nuclear translocation of TFEB

and activation of its downstream transcriptional machineries for coordinated lysosomal expression and regulation (CLEAR) network of genes (130). The transcription of the CLEAR gene network then results in upregulated autophagy through increased lysosomal biogenesis, further potentiating lysosomal entrapment of weak-base chemotherapeutics and fueling chemoresistance in a positive feedback loop (131, 132). To summarize, even if chemotherapeutics break through the barriers imposed by the acidic tumoral extracellular environment and diminished expression of drug transporters and reach the cytosol, drug inactivation and degradation can occur through various drug-metabolizing enzymes and organellar sequestration.

#### 1.3.2.4 Genomic instability

When chemotherapeutic agents cannot be eliminated through the means mentioned above, the genome-wide amplification of oncogenes and downregulation of tumor suppressors collectively shield resistant cancer cells from activating chemotherapeutic-mediated apoptotic responses. For instance, when *MYCN* is overexpressed, it drives cell growth, proliferation, and metabolism (133). In the context of triple-negative breast cancer, *MYCN* overexpression is associated with resistance to bromodomain and extra-terminal motific (BET) inhibitors (134). Besides, *MYCC* overexpression is linked to doxorubicin and paclitaxel resistant in breast cancer potentially due to its anti-apoptotic and cycle-cycle promoting properties (135, 136). Moreover, as another oncogene, the human epidermal growth factor receptor 2 (*ErbB2*) is amplified in 15-30% breast cancers (137). Not only does *ErbB2* activate proliferative

signaling pathways, but it can also rewire cellular migration, which is associated with the loss of cell polarity, and subsequent resistance to apoptosis (138). On the other end of the spectrum, downregulation of tumor suppressors mediates drug resistance by enabling cells to circumvent apoptosis following chemotherapeutic challenge. The most prevalent example is the downregulation of tumor-suppressor p53, also known as the guardian of the genome. P53 interacts with a variety of transcription factors to modulate gene expression in response to stress and DNA damage (139). In breast cancer, mutant p53 increases nuclear translocation of nuclear factor erythroid 2-related factor 2 (Nrf2) and activates specific the transcription of NRF2 target genes to enhance proteasome function, conferring resistance to proteasomal inhibitors (140). Furthermore, mutant p53 in mammary adenocarcinoma may also upregulate pro-survival signaling molecules, such as Bcl-xL, in acquiring gemcitabine resistance (141). Collectively, genomic instability manifested in the dysregulated oncogenic and tumor-suppressive signaling landscape contributes to the development therapeutic resistance by inhibiting chemotherapeutic-induced apoptotic responses.

### 1.3.3 Need for novel therapeutic strategies

To acquire chemoresistance, cancer cells reprogram their epigenome, genome, proteome, and metabolome to evade drug target response and decrease intracellular bioavailability of therapeutic agents. Some mutation-driven drug resistance can be overcome by simply administering higher drug dosages. However, due to non-specific cytotoxicity, high-dose chemotherapy is unfavorable and only used as a last resort (142).

This then prompts the exploration of other therapeutic strategies to tackle chemoresistance.

Given the advancement of the “omics” era, many genes and signaling pathways are starting to be uncovered. These cellular signatures serve as promising disease biomarkers and patient outcome predictors, providing invaluable clinical guidance for drug development. In light of the multifarious pathways resistant cancer cells can sabotage, common strategies to disarm chemoresistance involve the use of combinatorial drug regimen. Some chemotherapeutics, when combined, generate synergistic therapeutic outcome by either targeting a wider spectrum of oncogenic processes or enhancing the bioavailability or potency of other agents in the combination. As a result, combination therapy can make use of multiple cytotoxic agents in the same combination, such as gemcitabine and paclitaxel in the treatment of metastatic breast cancer, or combine known cytotoxic agents with a molecule that is not cytotoxic by itself but can facilitate the disposition of other chemicals, i.e., ABC transporter inhibitors, also known as chemo-sensitizers (143-145). Regardless of how the combinatorial paradigm is constructed, identifying appropriate and actionable drug targets as molecular vulnerabilities associated with the development and presentation of chemoresistance is of paramount importance.

## Chapter 1.4 Combination Therapy to Overcome Breast Cancer Therapeutic Resistance

### 1.4.1 Polychemotherapy

Polychemotherapy refers to the combination of two or more chemotherapeutic agents with the goal of obtaining a better clinical response with an acceptable toxicity profile. Polychemotherapy achieves greater clinical efficacy by mostly diversifying subcellular targets or facilitating additive or synergistic drug-drug interactions (146).

#### 1.4.1.1 Taxane-based regimens

Taxanes are the most common chemotherapeutics indicated for breast cancer patients. The chief purposes of combining taxanes with other therapeutic agents are to overcome taxane drug resistance and reduce taxane adverse effects (147). Historically, paclitaxel had been administered alongside cyclophosphamide, 5-fluorauracil, and mitoxantrone in metastatic breast cancers (148). To overcome drug resistance and relapse, the consensus nowadays is to administer taxane (paclitaxel or docetaxel, e.g.) and anthracycline (doxorubicin, e.g.) either in sequence or concurrently (149). However, for patients developing resistance to both taxanes and anthracyclines, alternative combinations of conjugated taxanes and platinum-based alkylating agents can be considered. For instance, as of July 2021, albumin-bound paclitaxel (nab-paclitaxel) in combination with carboplatin entered Phase IV clinical trial for the treatment of triple-negative breast cancer (150-152). To counteract drug resistance, albumin-bound paclitaxel, compared to the traditional, solvent-based paclitaxel, has faster and deeper tumor penetration capacity and is associated with milder toxicities, leading to generally

higher overall survival and pathological complete response rates (153, 154). While functionally similar, the use of carboplatin in replacement of cisplatin as part of the combination regimen is expected to considerably alleviate toxicity and drug-induced mutagenicity associated with cisplatin, thereby promoting regimen adherence (155-157).

#### 1.4.1.2 Platinum-based regimens

Regarding the 20% TNBC patients harboring BRCA1/2 mutations and their inherent sensitivity to DNA-damaging compounds, combinatorial regimen consisting of cisplatin and paclitaxel is reported to achieve high pathological complete response rates (158). For metastatic TNBC patients who have acquired resistance to either taxane or anthracycline-based treatment, cisplatin in combination with either vinorelbine or gemcitabine can act as an alternative salvage regimen with acceptable tolerability and clinical outcomes (159). Besides TNBC, cisplatin in combination with Anvirzel, a plant extract with anti-cancer property, exhibits synergistic cytotoxicity in hormone receptor-positive MCF7 cells compared to monotherapy of either alone (160).

#### 1.4.1.3 Antimetabolite-based regimens

Although antimetabolites are not classified as first-line therapy in breast cancer, they can be applied to mitigate instances of drug resistance against other agents. For instance, combination chemotherapy consisting of mitomycin C and methotrexate was effective for 10-20% HER2-negative metastatic breast cancer patients resistant to

aggressive therapeutic interventions involving eribulin, vinorelbine, and bevacizumab (161). Furthermore, capecitabine, an antimetabolite disrupting nucleotide synthesis, may be used in combination with docetaxel among metastatic breast cancer patients previously exposed to anthracycline-based regimen (162). For non-metastatic but advanced breast cancer patients, 5-fluorauacil in combination with sodium-folinate is preferred over capecitabine (163). Although not directly prolonging overall survival of taxane and anthracycline-refractory metastatic breast cancer patients, the incorporation of the antimetabolite gemcitabine into vinorelbine increased progression-free survival compared to vinorelbine alone (164).

**Table 1. Use of polychemotherapy to tackle breast cancer drug resistance**

| Combinatorial Drug Class | Components | Description | References |
|---|---|---|---|
| Taxane and anthracycline-based regimens | Albumin-bound paclitaxel (nab-paclitaxel) + carboplatin | Current in phase IV clinical trial applied to triple-negative breast cancer patients resistant to conventional anthracycline and taxane-based regimens | 150 |
| | Liposomal doxorubicin + trastuzumab | Indicated for anthracycline-refractory HER2-overexpressing breast cancer | 165 |
| Platinum-based regimens | Cisplatin + paclitaxel | Indicated for TNBC patients harboring BRCA1/2 mutations | 158 |
| | Cisplatin + vinorelbine /gemcitabine | Indicated for metastatic TNBC patients resistant to conventional anthracycline and taxane-based regimens | 159 |
| | Cisplatin + Anvirzel | Produces synergistic efficacy in hormone receptor-positive breast cancer. | 160 |
| Antimetabolite-based regimens | Mitomycin C + methotrexate | Indicated for 10-20% HER2-negative metastatic breast cancer patients resistant to eribulin, vinorelbine, and bevacizumab. | 161 |
| | Capecitabine + docetaxel | Metastatic breast cancer patients resistant to anthracycline-based regimens | 162 |
| | 5-fluorauracil + sodium folinate | Indicated for advanced, non-metastatic breast cancer patients | 163 |
| | Gemcitabine+ vinorelbine | Prolongs progression-free survival compared to vinorelbine alone in metastatic breast cancer previously resistant to | 164 |

| | | | |
|---|---|---|---|
| | | taxane and anthracycline-based regimens | |

### 1.4.2 Chemosensitizers

#### 1.4.2.1 ABC transporter inhibitors

As discussed in 1.3.2.1, drug-resistant breast cancer cells tend to overexpress P-gp, MRP, and BCRP. Since these transporters mediate the clearance and extrusion of a plethora of chemotherapeutic agents, inhibiting ABC transporters enhances intracellular drug retention. Clinically, many ABC transporter inhibitors are used in conjunction with chemotherapeutic agents to overcome therapeutic resistance. For instance, bergapten and xanthotoxin decrease mitoxantrone efflux in the hormone receptor-positive MCF7 cells overexpressing BCRP (166). Verapamil (p-gp inhibitor), probenecid (MRP inhibitor), and genistein (BCRP inhibitor) each sensitizes SN38-resistant the hormone receptor-positive T47D ductal carcinoma cells to SN38 challenge (167, 168). In addition, P-gp blockade with verapamil synergizes with paclitaxel in killing doxorubicin-resistant MCF7 cells and induce cell cycle arrest and upregulate apoptosis (169). On the same note, functional inhibition of P-gp using diltiazem potentiates doxorubicin cytotoxicity in MCF7 cells (170). Remarkably, some p-gp inhibitors, on their own, pose manageable cytotoxicity, making them promising leads for future drug development especially following the development of second and third-generation P-gp inhibitors (171, 172). Considering the broad spectrum of substrates P-gp, MRP, and BCPR can accommodate, one therapeutic challenge underlying ABC transporter inhibitor design is substrate / inhibitor specificity overlap and the consequential drug-drug interactions (173-178).

#### 1.4.2.2 Antioxidant inhibitors

Reactive oxygen species (ROS) plays a pivotal role in breast cancer oncogenesis by enhancing cell proliferation, facilitating angiogenesis, and initiating epithelial-mesenchymal transition (179-182). To circumvent cell deaths from elevated ROS, cancer cells, especially drug-resistant ones, often upregulate antioxidant defense and drug metabolizing mechanisms, such as glutathione (GSH) and glutathione-S-transferases (GSTs) involved in drug conjugation and subsequent elimination (183). This is evident in multidrug-resistant MCF7 breast cancer cell where genetic knockdown of *GST1* restores chemosensitivity of resistant cells to the cytotoxicity of 5-fluorauracil, doxorubicin, and cisplatin, all of which are known to increase ROS levels (184). Pharmacologically, GSH-inhibiting compound buthionine sulfoximine sensitizes antihormone-resistant breast cancer MCF7 cells to estrogen-induced apoptosis (185). Furthermore, ethacrynic acid (EA), a GSH inhibitor, in combination with DACHPt, a precursor of oxaliplatin, increases cellular platinum accumulation and enhances platinum-based therapeutic efficacy by 4.6 fold in MCF7 cells (186). Yet, auranofin, a GSTP1-1 inhibitor, is found to significantly enhance ROS level and leads to synergistic apoptosis in combination with nutlin-3a and trametinib in MCF7 cells, respectively (187, 188). Similarly, in triple-negative breast cancer, inhibiting gamma-glutamylcysteine ligase, the enzyme responsible for *de novo* synthesis of GSH, sensitizes TNBC to ROS-mediated killing (189, 190). It is evident that combining antineoplastics aimed at promoting ROS with antioxidant defense inhibitors induces redox imbalance, leading to death of drug-resistant breast cancer cells.

#### 1.4.2.3 MicroRNA-based therapeutics

Owing to its ease of administration through local and parenteral injection routes as well as high tissue uptake, microRNA (miRNA)-based therapeutics have become a research hotspot with many undergoing preclinical and clinical trials in recent years (191, 192). As a versatile mode of therapy, miRNA-based therapeutics' advantage goes hand in hand with its major downfall – "too many (unknown) targets with one (miRNA) effect (TMTME)" (193). Nevertheless, transcriptomic profiling has elucidated miRNAs that may act as the molecular Achilles' heel in modulating breast cancer chemosensitivity, identifying targetable disease biomarkers for combination drug discovery.

Multiple miRNAs regulate chemosensitivity and could be potentially incorporated into combination regimen. For instance, miR-424-5p enhanced TNBC sensitivity to Taxol cytotoxicity by potentially targeting the PTEN/PI3K/AKT/mTOR axis while upregulating apoptotic response elements, such as p53, BAX, and cleavage of pro-caspase 3 (194). Differential RNA-seq analysis also revealed that inhibiting miR-355-5p and Let-7c-5p-mediated suppression of CXCL9, CCR7, and SOCS1 reverses MCF7 resistance to taxanes (195). Furthermore, co-loading of doxorubicin and miR-34 in hyaluronic acid-chitosan nanoparticles into the triple-negative MDA-MB-231 cells enhances antitumor effects of doxorubicin through suppressing the expression of anti-apoptotic proto-oncogene *Bcl-2* (196). Of note, miRNAs also regulate the expression of ABC transporters, the principal culprit of breast cancer drug resistance (197). For instance, downregulation of miR-326 is associated with elevated MRP1 as well as

etoposide and doxorubicin resistance in MCF7 cells (198). Conversely, upregulation of miR-132 and miR-212 drives BCRP-mediated doxorubicin efflux, promoting doxorubicin resistance in MCF7 cells (199). This differential expression of miRNAs contextualizes the complex regulatory landscape and clinical utility of incorporating miRNAs in combination regimen to combat breast cancer drug resistance.

**Table 2. Utility of chemosensitizers to tackle breast cancer drug resistance**

| Chemosensitizer Classes | Drug Name | Role in Chemo-sensitization | References |
|---|---|---|---|
| ABC transporter inhibitors | Verapamil | Inhibits p-glycoprotein, sensitizing MDA-MB-231 cells to proteasome inhibitors | 200 |
| | Tariquidar | Inhibits p-glycoprotein, potentiating paclitaxel concentration in hormone receptor-positive MCF7 BC cells | 201 |
| | Sulbactam, Quercetin | Reduces expression of ABC transporters to potentiate doxorubicin toxicity in multiple TNBC cell lines | 202, 203 |
| | Tanshinone IIA (Tan IIA) | Inhibits PTEN/AKT and ABC transporters to enhance doxorubicin efficacy in MCF7 cells | 204 |
| GSH inhibitors | Buthionine sulfoximine | Reduces glutathione, *Bcl-2*, *phospho-Bcl-2*, and *Bcl-xL* expression and upregulates *BAX* expression in estrogen-deprived MCF7:2A cells | 185 |
| | Ethacrynic acid | Inhibits GST-mediated conjugation of GSH to oxaliplatin, enhancing cytosolic oxaliplatin in MCF7 cells | 186 |
| | Auranofin | Causes cell cycle arrest at the sub-G1 phase, induces mitochondrial stress, and activates caspase-3/7 and PARP cleavage in MCF7 cells | 187 |
| | Buthionine sulfoximine | Inhibits gamma-glutamylcysteine ligase, sensitizing multiple TNBC cell lines to ROS | 189 |
| miRNA-based therapeutics | miR-298 | Represses expression of P-gp, conferring doxorubicin resistance in MDA-MB-231 cells. | 205 |

| | | | |
|---|---|---|---|
| | miR-424-5p | Sensitizes MDA-MB-231 cells to Taxol by downregulating cdk2 to induce G2 cell cycle arrest and modulating apoptosis-related factors, including p53, c-Myc, and Bcl-2. | 194 |
| | miR-326 | Represses *MRP1* expression to confer etoposide and doxorubicin resistance in MCF7 cells | 198 |
| | miR-132-212 | Represses PTEN-AKT/NF-κB signaling and modulates BCRP-mediated doxorubicin efflux in drug-resistant MCF7 cells | 199 |

## Chapter 1.5 Research Direction and Objectives

We have identified a new molecule, which, when being administered alongside the chemotherapeutic agent paclitaxel (PLX), shows sustained cytotoxicity against multidrug-resistant triple-negative (MDA-MB-231) and hormone receptor-positive MCF7 breast cancer cell lines. For confidentiality and proprietary considerations, the molecule is named “BC-2021,” the identity of which will not be revealed until further systematic drug characterization is conducted. We hypothesize that BC-2021 restores chemosensitivity of multidrug-resistant breast cancer cells to the challenge of PLX and can result in sustained cell death when being co-administered along with PLX. This research aims to describe the combinatorial regimen consisted of BC-2021 and PLX in killing drug-resistant breast cancer cells through assessing:

1) The extent of cell death post-combinatorial drug treatment
2) The level of global and mitochondrial reactive oxygen species and nitric oxide
3) The distribution of cell cycle progression
4) The transcription of apoptosis and cell cycle checkpoint regulators
5) The overall cellular autophagy
6) The morphological manifestation of organelles (nucleus and microtubules)

# CHAPTER 2 MATERIALS AND METHODS

## 2.1 Cell Lines

Cells lines used in this thesis can be broadly categorized as chemo-sensitive and paclitaxel-resistant cells. The following chemo-sensitive cell lines are acquired from the American Type Culture Collection (ATCC), with the exception of the BHK (Baby Hamster Kidney) fibroblast cell line being a gift from Ms. Christina Irving (Dalhousie University, Department of Physiology and Biophysics):

| | |
|---|---|
| MDA-MB-231: Human Triple-negative Breast Cancer Cells | ATCC-HTB-26 |
| MCF-10A: Human Breast Epithelial cells | ATCC-CRL-10317 |
| MCF-7: Human Receptor-positive Breast Cancer Cells | ATCC-HTB-22 |
| BHK: Baby Hamster Kidney fibroblasts | Gift from Ms. Christina Irving |

The following paclitaxel-resistant cell lines were originally generated by Dr. Kerry Goralski (Dalhousie University, College of Pharmacy) and are obtained as gifts from Dr. Denis Dupré (Dalhousie University, Department of Pharmacology):

| |
|---|
| MDA-MB-231 PLX (R): Paclitaxel-resistant Triple-negative Breast Cancer Cells |
| MCF-7 PLX (R): Paclitaxel-resistant Receptor-positive Breast Cancer Cells |

Paclitaxel (PLX) resistance is achieved through continuously culturing the aforementioned cell lines with increasing dosage of PLX (Sigma), beginning with 0.1 nM

PLX until a final concentration of 585 nM (5mg/mL) PLX is reached. To maintain drug resistance, PLX-resistant cells are maintained in 10% Fetal Bovine Serum (Thermo Fisher Scientific), 1% Penicillin-Streptomycin-supplemented (Thermo Fisher Scientific) Dulbecco's Modified Eagle Medium (Thermo Fisher Scientific) containing 585 nM of PLX inside a humidified, 95% air/ 5% $CO_2$ atmosphere at 37˚C, which are the default culturing conditions in this thesis unless stated otherwise.

**2.2 Drug Treatment**

Many experiments illustrated in this thesis are based on cells treated with a strategic combination of PLX and BC-2021. BC-2021 is a commercially available compound that, through this thesis work, demonstrates potent anti-cancerous effects against multidrug-resistant triple-negative (MDA-MB-231) and receptor-positive (MCF7) breast cancer cells when being administered alongside PLX. In essence, this thesis work repurposes a commercially available compound and extends its therapeutic potential to the treatment of resistant breast cancer cells.

Drugs of interest, including PLX and BC-2021, were previously diluted in Dimethyl Sulfoxide (DMSO) to constitute their respective lab stock concentration: PLX (585nM) and BC-2021 (25mM). Prior to treatment with lab stock drugs, cells are seeded and allowed to settle to the bottom of cell culture plates for 24 hours under culturing conditions. Lab stock drugs are added to fresh pre-warmed cell culture media at their desired working concentration before appropriate volume of drug-containing media is dispensed to cell culture plates. For experimental conditions that require low

concentration of drug, DMSO-diluted stock drugs are further diluted in sterile dd$H_2O$ before being added to cell culture media. Media is not changed until the desired drug incubation period has been reached. For all drug treatment experiments presented in this thesis, the vehicle control condition receives equimolar concentration of DMSO as that used in the highest drug dosage condition.

**2.3 MTT Assay**

MTT assay is a colorimetric assay that allows for interpretation of cell proliferation based on overall cellular metabolic activity. Based on the growth rate of cell lines, 3,000 cells are seeded in each well of a 96-well plate (Thermo Scientific Biolite) and allowed to settle to the bottom of the well over a period of 24 hours under culturing conditions before being subjected to drug treatment for 24, 48, and 72 hours. Once the desired drug treatment period has been reached, MTT formazan powder (1-(4,5-Dimethylthiazol-2-yl)-3,5-diphenylformazan, Sigma) is then diluted in phosphate-buffered saline (Gibco) at 5mg MTT formazan powder/1 mL of PBS before being combined with serum-free cell culture media at a 1:1 ratio. Subsequent to removal of cell culture media, 100 µL of MTT-media mixture is then dispensed to each well followed by 3-hour incubation in dark under culturing conditions. After incubation, MTT-media solution is gently removed. 150 µL of DMSO solvent is then added to each well and the plate is placed on a room-temperature shaker in dark and subject to 15 minutes of shaking to allow sufficient solvation of formazan crystals. The plate is then read by a spectrophotometer at Optical Density (OD) of 570 nm wavelength using the ADLD

software. The OD readouts for each time point and condition are then collected and plotted using GraphPad Prism 8 as both raw OD readouts and normalized OD readouts.

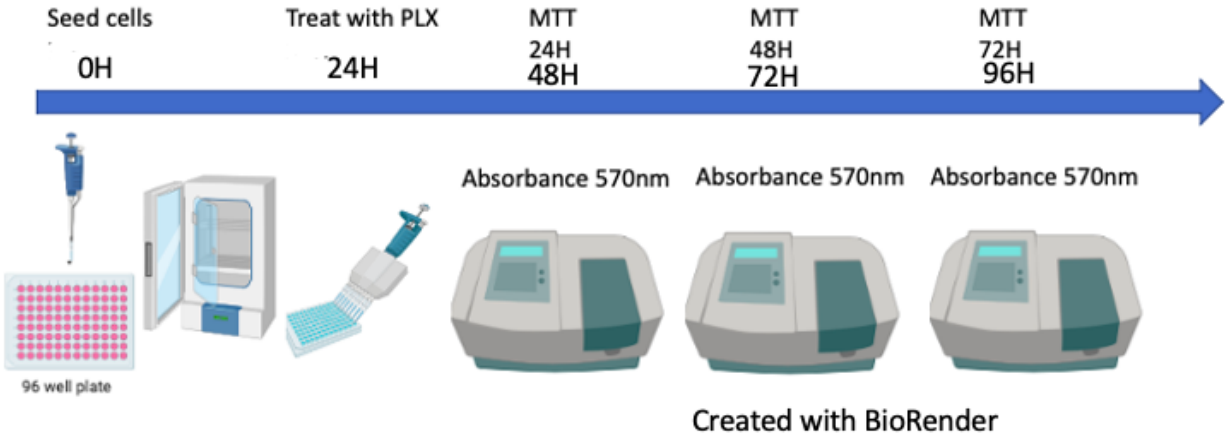


**2.4 Colony Formation Assay**

Colony Formation Assay is a visualizable quantitative assay to measure cell survival after drug incubation over a 14-day period. 500 cells are seeded into each well of a 6-well plate (Thermo Fisher Scientific) and allowed 24 hours to settle to the bottom of the well. Fresh culture media containing desired drug concentrations is applied to each well for 7 days at a time before removal of the media and addition of fresh drug-containing media for another 7-day incubation period. At the end of the 14-day drug incubation, culture media is removed, and cells are washed twice with PBS. 2 mLs of 1% methylene blue (3, 7-bis(Dimethylamino)phenazathionium chloride) (Sigma) diluted in methanol (Thermo Fisher Scientific) are applied to each well for 30 minutes before being decanted and washed with sink water. Blue cellular colonies are quantified through

direct visualization. Total colony numbers for cells exposed to combinatorial regimen are tallied and normalized to the DMSO+585nM PLX vehicle-control group.

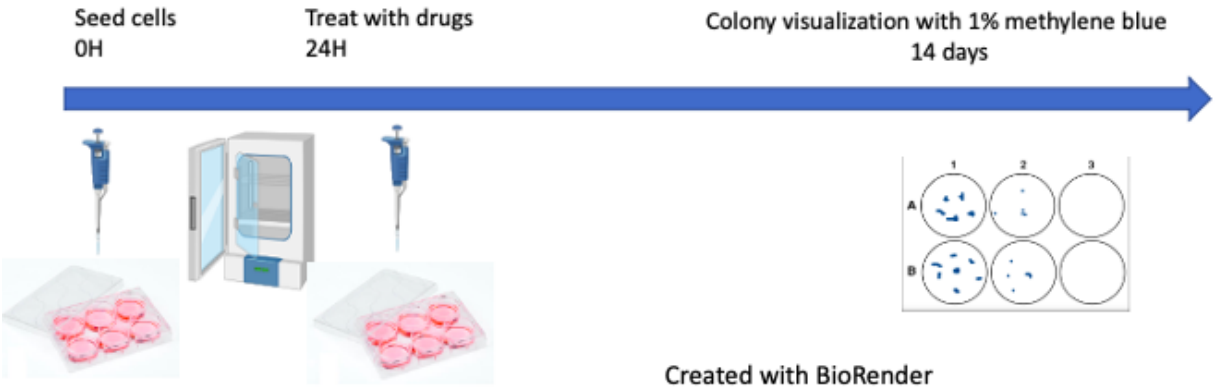


## 2.5 Flow Cytometry

The following sections detail the cellular staining procedure for flow cytometry experiments. These flow cytometry experiments pertain to the study of cell cycle, the assessment of cellular as well as mitochondrial reactive oxygen species, nitric oxide, overall autophagic flux and modality of cell death. All flow cytometry readouts come in the form of mean fluorescence intensity (MFI), which are analyzed by FCS Express 7 (De Novo Software).

### 2.5.1 eFluor™ 780 Fixable Viability Dye Staining

150,000 cells are seeded and allowed to settle for 24 hours under culturing conditions into a 35-mm cell culture dish (Thermo Fisher Scientific) before being treated with drugs of desired concentration for 72 hours. After drug treatment, cells are trypsinized, centrifuged at 1000 RPM for 5 minutes, and washed twice with PBS before

being stained with 75 µL of staining mixture containing 1µL of eFluor™ 780 Fixable Viability Dye (Thermo Fisher Scientific) diluted in 1000µL of PBS in dark at room temperature for 20 minutes. Following staining, cells are washed twice with PBS and are either run immediately on the BD LSR Fortessa SORP on low speed using the 780/60 band pass filter or fixed with 4% paraformaldehyde for 10 minutes in dark at room temperature. Upon completion of fixation, cells are washed twice with 1-mL fluorescent-activated cell sorting (FACS) wash buffer (PBS+1% Bovine Serum Albumin+0.2% Sodium Azide) and subsequently resuspended in 500µL of FACS wash buffer before being stored in 4˚C fridge in dark to be processed further on the BD LSR Fortessa SORP instrument. Positive control involves placing cells on 65˚C heat block for 10 minutes and mixing 1:1 ratio of stained live and dead cell population to obtain differential fluorescence intensity based on cell viability. Negative control is unstained cell population.

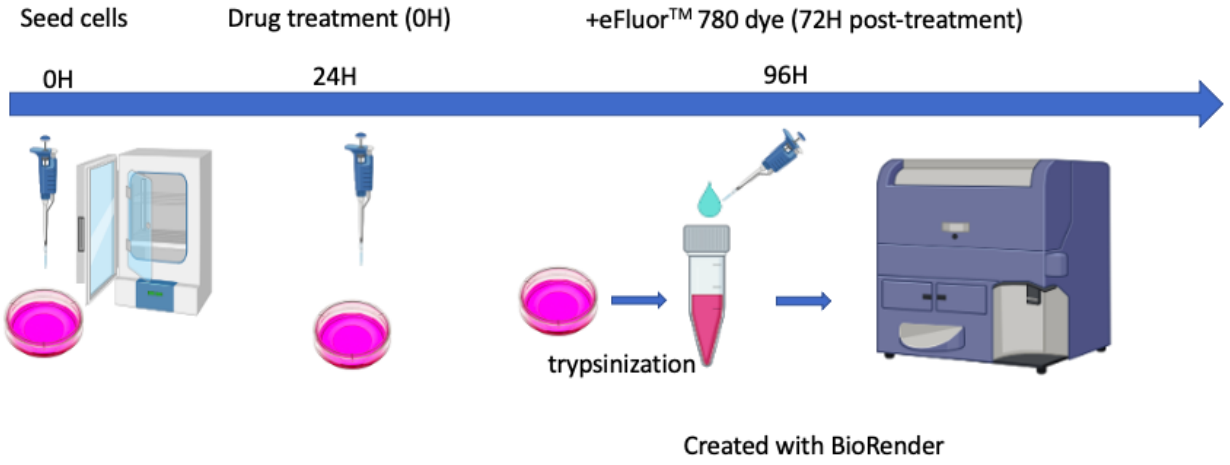

### 2.5.2 Propidium Iodide Staining for Cell Cycle Analysis

300,000 cells are seeded into a 6-cm cell culture dish (Thermo Fisher Scientific) and allowed to settle for 24 hours under culturing conditions before receiving 16-hour treatment of serum-free growth media for cell cycle synchronization. Once cell cycle synchronization is complete, 10% FBS-supplemented growth media containing desired concentration of drugs is applied to cells for 24 hours under culturing conditions. Cells are trypsinized and then washed twice with PBS prior to staining with eFluor™ 780 Fixable Viability Dye as mentioned above to distinguish dead cells from the entire cell population. Following staining with eFluor™ 780, strong fluorescence signals of which label dead cells, cells undergo fixation. During fixation, cells are exposed to gradual, drop-wise addition of ice-cold 70% ethanol while being simultaneously vortexed. Cells suspended in ice-cold 70% ethanol are then placed in 4˚C fridge for another 24 hours to allow for thorough fixation. Once fixation is complete, ethanol is removed by pelleting cells down through 10-minute centrifugation at 3000 RPM at 4˚C. Cell pellets are then washed twice with 3 mLs of PBS following the aforementioned centrifugation conditions before being re-suspended in 500 µL of PI solution ([PI (Thermo Fisher Scientific)] =10 mg/mL, [RNase A (Thermo Fisher Scientific)] = 20 mg/mL diluted in PBS). Resuspended cells are placed in dark at room temperature for 1 hour. To avoid collecting cell clumps, cell clumps are filtered out using round-bottom polystyrene test tubes with cell strainer snap cap (Falcon) before being run on low speed using the 780/60 band pass filter to detect fluorescence signals of eFluor™ 780 Fixable Viability Dye and the 585/42 band pass filter on CytoFlex (Beckman Coulter) for those of propidium iodide. To analyze cell

cycle distribution within the live cell population, only the e780-negative population is used as a basis to measure distribution of PI fluorescence intensity. Histograms depicting distribution of PI fluorescence intensity and its corresponding event number are gathered and the mean fluorescence intensity value, for each sample, is analyzed using FCS Express 7.

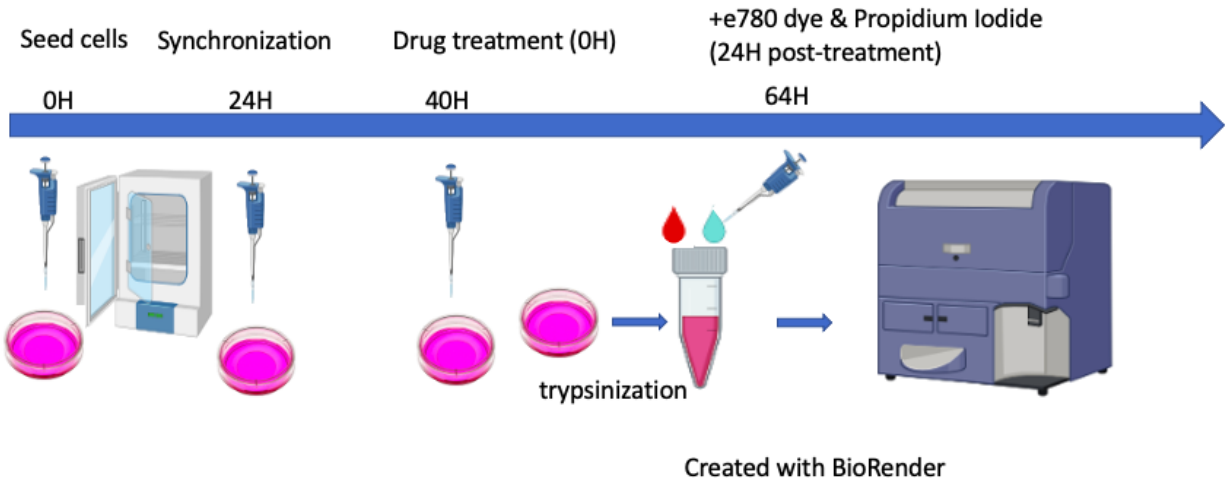


### 2.5.3 FITC-Annexin V / 7-AAD (7-Aminoactinomycin D) Staining for Assessment of Apoptosis

Early-stage apoptosis is characterized by a series of structural changes of the plasma membrane, such as flipping of the cell membrane and the exposure of cytoplasmic-facing phospholipid phosphatidylserine to the extracellular milieu. Annexin V, as a phospholipid-binding protein, has high binding affinity to phosphatidylserine after its exposure to the extracellular side during early-stage apoptosis. Late-stage apoptosis and necrosis, on the other hand, involve the direct exposure of intracellular

genomic content, and, therefore can be detected by binding to common intercalating agents, such as 7-AAD (7-Aminoactinomycin D) and propidium iodide. To determine the precise modality of cell deaths, cells are stained with FITC-conjugated Annexin V and 7-AAD according to manufacturer's instruction of FITC Annexin V Apoptosis Detection Kit with 7-AAD (BioLegend). 150,000 cells are seeded and allowed to settle for 24 hours under culturing conditions in a 35-mm cell culture dish before being treated with drugs of desired concentration for 24 and 48 hours for R231 cells and 72 hours for MCF7R cells. Once drug treatment is complete, cells are washed twice with PBS and resuspended in 100-µL Annexin V Binding Buffer. Subsequently, 5 µLs of FITC Annexin V and 5 µLs 7-AAD Viability Staining Solution are added to the 100-µL cell suspension. Each sample is briefly vortexed and incubated in the dark at room temperature for 15 minutes before being dispensed to a FACS tube containing 400 µLs of Annexin V Binding Buffer placed in an icebox. Samples are then read on the BD Celesta cytometer (BD Biosciences) on low speed using FITC and 7-AAD-specific detectors. Cells treated with 9.8 mM of $H_2O_2$ for 2 hours and stained with Annexin V only are used as the single-channel Annexin V positive control, whereas cells subjected to higher incubation period with same dosage of $H_2O_2$ and stained with 7-AAD only are used as the single-channel 7-AAD positive control. Compensation is adjusted manually on FCS Express 7 to minimize fluorescence signal spillover. Quadrant gating positionality is determined by fluorescence signals of single-channel FITC-Annexin V and 7-AAD from cell population with a 1:1 mixture of live, untreated cells and $H_2O_2$-treated cells.

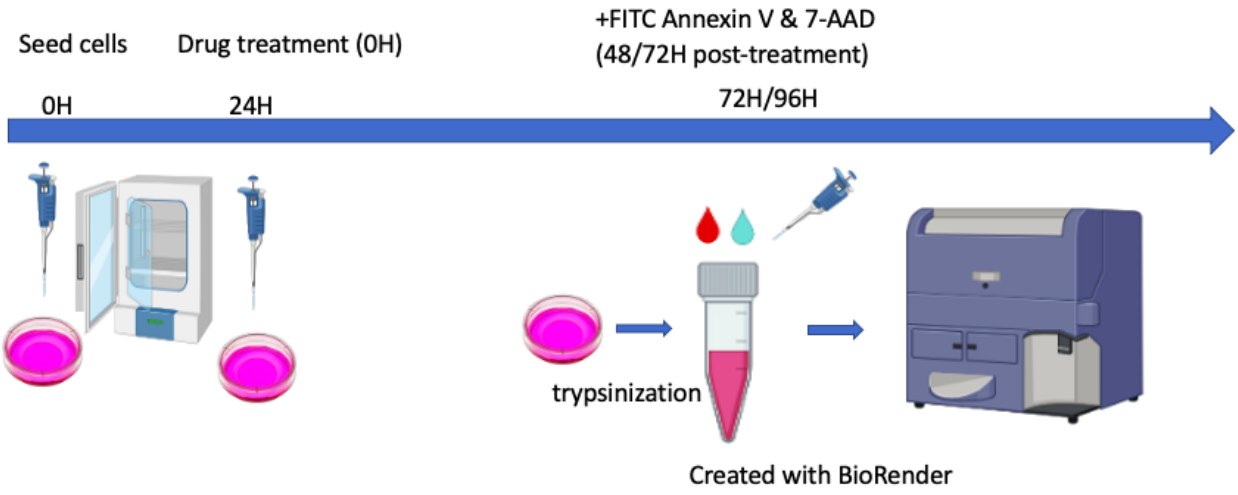


### 2.5.4 Autophagy Assay

Autophagy is measured in accordance to the Autophagy Assay Kit's manufacturer's protocol (Abcam; ab139484). 150,000 cells are seeded and allowed to settle for 24 hours in a 35-mm cell culture dish under culturing conditions before being treated with drugs of desired concentration for 8, 16, and 24 hours. As a positive control, autophagy is induced by overnight treatment with 500-nM DMSO-reconstituted lyophilized autophagy inducer, rapamycin. On the day of the experiment, cells are collected via centrifugation at 1000 RPM for 5 minutes and subsequently washed twice and resuspended in 250 µLs of 1X Autophagy Assay Buffer provided in the Autophagy Assay Kit supplemented with 5% FBS. 250 µLs of Autophagy Green dye staining solution is applied to the cell suspension for 30 minutes at room temperature in the dark. Afterwards, cells are collected via centrifugation at 1000 RPM for 5 minutes and washed with 1X Autophagy Assay Buffer prior to being resuspended in 500 uL of fresh 1X Assay

Buffer and read on low speed using the FITC-specific detector of the BD Celesta cytometer.

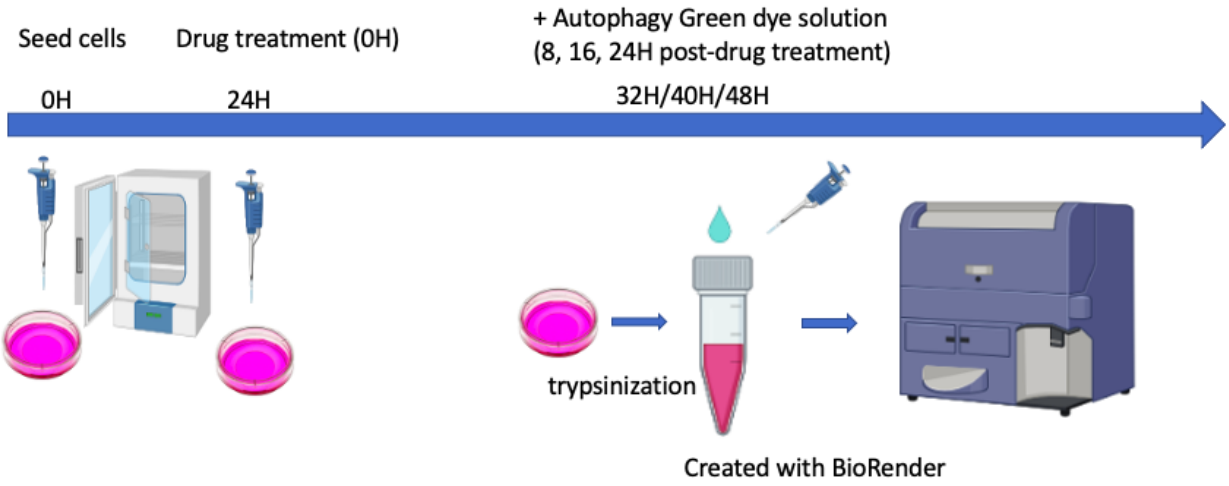


**2.5.5 CM-$H_2$DCFDA Staining for Quantification of Total Reactive Oxygen Species (tROS)**

70,000 cells are seeded in 12-well plates and allowed to settle for 24 hours under culturing conditions before being treated with drugs of desired concentration for 8, 16, and 24 hours. 30 minutes prior to staining, cells are treated with 9.8 mM of $H_2O_2$ as a positive control. Cells are centrifuged at 1,000 RPM for 5 minutes and washed with PBS twice before staining with viability dye and CM-$H_2$DCFDA (Thermo Fisher Scientific) staining mixture (1µL of eFluor™ 780 Fixable Viability Dye and 1 µL of DMSO-constituted 5 mM CM-$H_2$DCFDA diluted in 1000 µLs of PBS per sample) in dark at room temperature for 30 minutes. Cells are washed once with PBS and then read on the band pass filter set 525/40 for CM-$H_2$DCFDA and filter set 780/60 for eFluor™ 780 Fixable Viability Dye. The distribution of fluorescence intensity of CM-$H_2$DCFDA and its corresponding event

number is plotted out of live, or e780-negative, cell population. Mean fluorescence intensity of CM-$H_2$DCFDA is reported by FCS Express 7.

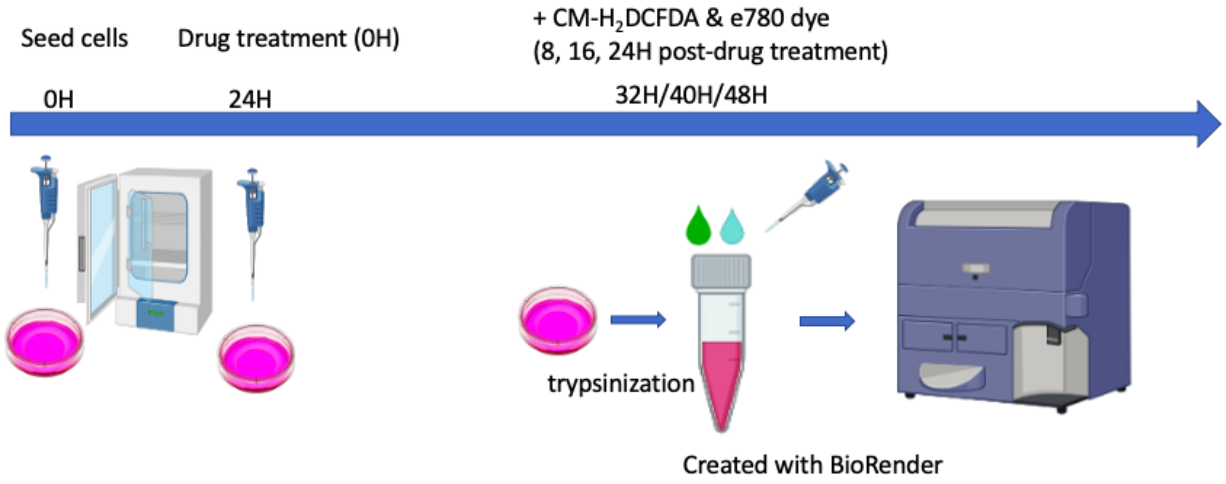


**2.5.6 MitoSOX Red Staining to Quantify Mitochondrial Reactive Oxygen Species (mitoROS)**

70,000 cells are seeded in 12-well plates and allowed to settle for 24 hours under culturing conditions before being treated with drugs of desired concentration over 8, 16, and 24 hours. 8 hours prior to staining, cells were treated with 50uM of FCCP (carbonyl cyanide-p-trifluoromethoxyphenylhydrazone) as a positive control. Cells are centrifuged at 1,000 RPM for 5 minutes and washed twice with PBS before staining with viability dye and MitoSOX Red reagent (Thermo Fisher Scientific) staining mixture (1µL of eFluor™ 780 Fixable Viability Dye and 1 µL of DMSO-constituted 5 mM MitoSOX Red reagent diluted in 1000 µLs of PBS per sample) in dark at room temperature for 30 minutes. Cells

are washed once with PBS and then read on the band pass filter set 585/42 for MitoSOX Red and filter set 780/60 for eFluor™ 780 Fixable Viability Dye. The distribution of fluorescence intensity of MitoSOX Red and its corresponding event number is plotted out of live, or e780-negative, cell population. Mean fluorescence intensity of MitoSOX Red, which is reflective of the level of mitochondrial ROS, is reported by FCS Express 7.

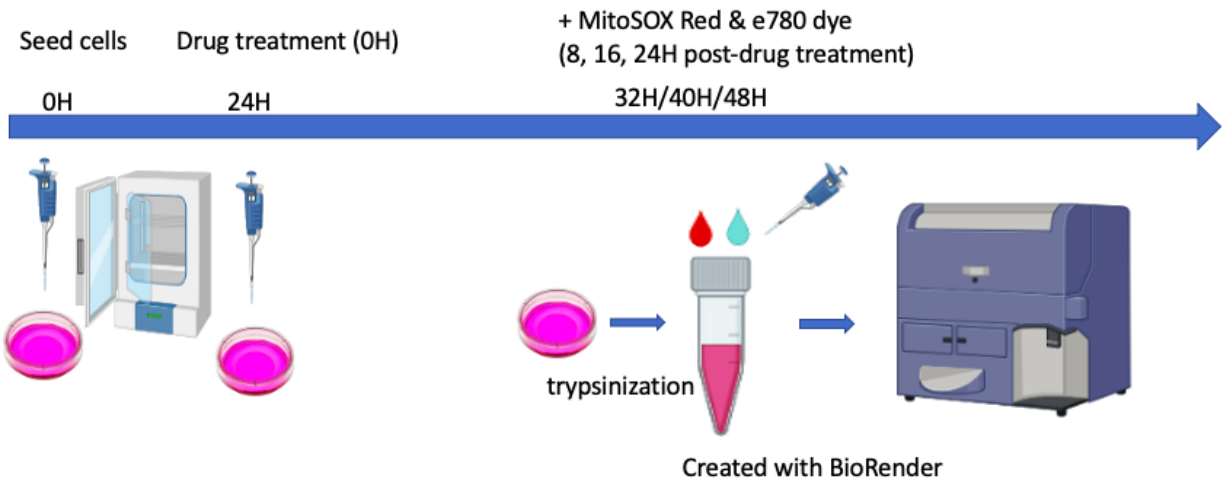


**2.5.7 DAF-FM Diacetate Staining for Quantification of Nitric Oxide (NO)**

70,000 cells are seeded in 12-well plates and allowed to settle for 24 hours under culturing conditions before being treated with drugs of desired concentration over 8, 16, and 24 hours. 8 hours prior to staining, cells were treated with 2000-nM PLX as a positive control. Cells are centrifuged at 1,000 RPM for 5 minutes and washed with PBS twice before staining with viability dye and DAF-FM diacetate (4-Amino-5-Methylamino-2', 7'-Difluorofluorescein Diacetate, Thermo Fisher Scientific) staining mixture (1µL of eFluor™ 780 Fixable Viability Dye and 1 µL of DMSO-constituted 5 mM DAF-FM diacetate diluted in 1000 µLs of PBS per sample) in dark at room temperature for 30

minutes. Cells are washed once with PBS and then read on the band pass filter set 525/40 for DAF-FM diacetate and 780/60 for eFluor™ 780 Fixable Viability Dye. The distribution of fluorescence intensity of DAF-FM diacetate and its corresponding event number is plotted out of live, or e780-negative, cell population. Mean fluorescence intensity of DAF-FM diacetate is reported by FCS Express 7.

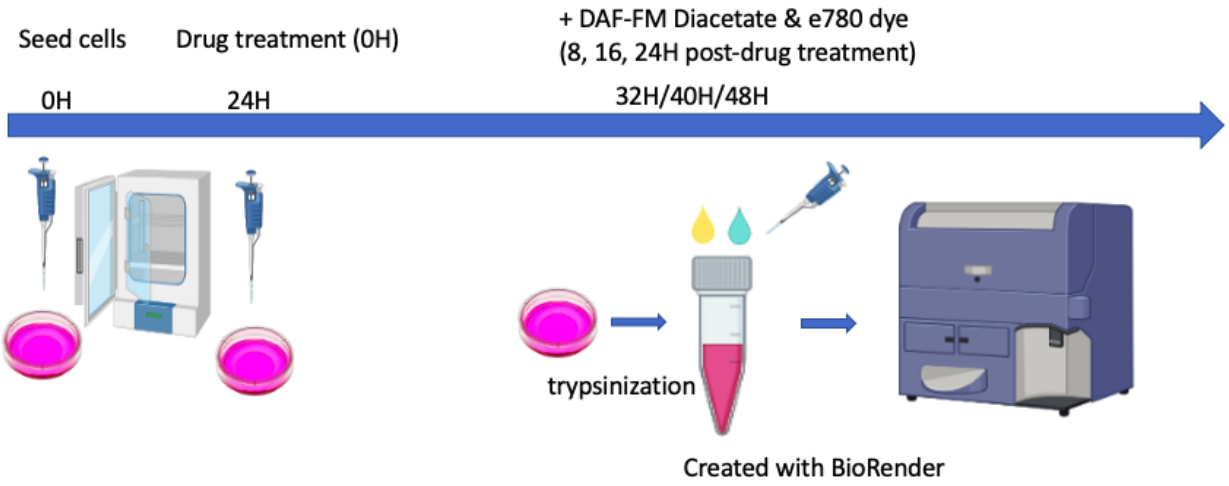


**2.6 Gap Closure Assay**

30,000 cells were seeded into each well of the 2-well culture insert (Ibidi) on a 35-mm culture plate (Thermo Fisher Scientific) and allowed to adhere to the bottom of the plate overnight under culturing conditions. A pair of forceps is used to remove the insert the next day. Cells are washed twice with 0.5% FBS-supplemented growth media. Cells are then exposed to 0.5% FBS-supplemented growth media containing drugs of desired concentration, after which a picture of the gap is captured immediately at the 0-hour time point using an inverted light microscope at 10X magnification. Cells are then

placed back to their culturing conditions for 16 hours before another image at the same spot is taken using the aforementioned parameters.

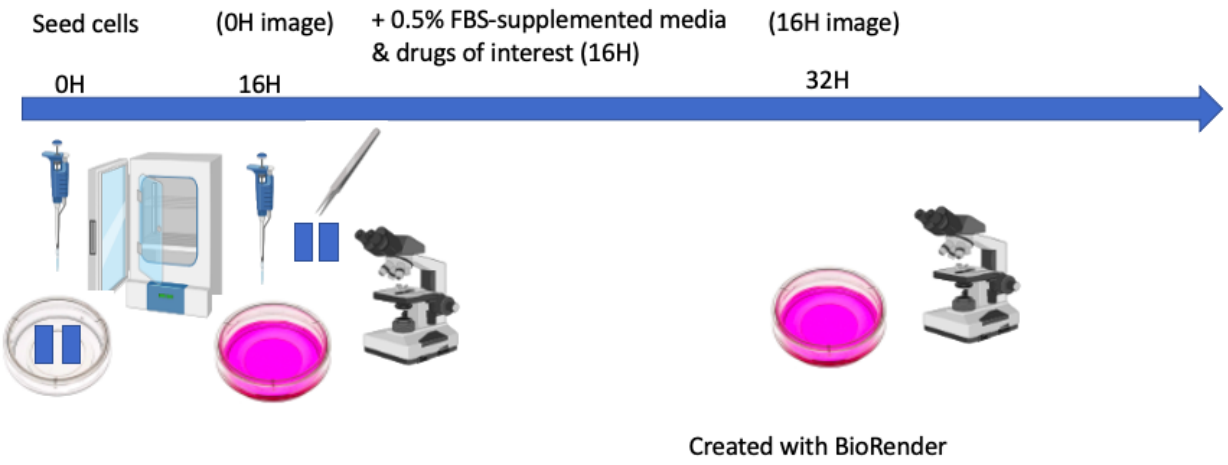


**2.7 Quantitative Reverse Transcription Polymerase Chain Reaction (RT-qPCR)**

800,000 cells are seeded and allowed to settle on a 10-cm culture dish (Thermo Fisher Scientific) under culturing conditions for 24 hours before drug treatment. Following 16-hour drug treatment, 1mL of Trizol reagent (Thermo Fisher Scientific) is used isolate total RNA. 2 µgs of total RNA are used to perform cDNA conversion following manufacturer's protocol associated with SuperScript First-Strand Synthesis System for RT-PCR (Thermo Fisher Scientific). Regions of interest within cDNA are amplified using specific primers (Table 3) and quantified using the SsoAdvanced Universal SYBR Green Supermix (BioRad) and the BioRad CFX96 Real-time PCR Detection System. mRNA expression cycle threshold (Ct) values are calculated after normalization to the expression level of the housekeeping 3-phosphate dehydrogenase (GAPDH)

reference gene using the Livak and Schmittgen's $2^{-\triangle\triangle CT}$ method. The endpoint of these results translate into fold changes in the expression level of genes of interest, reported relative to those in the vehicle control (DMSO-treated) sample.

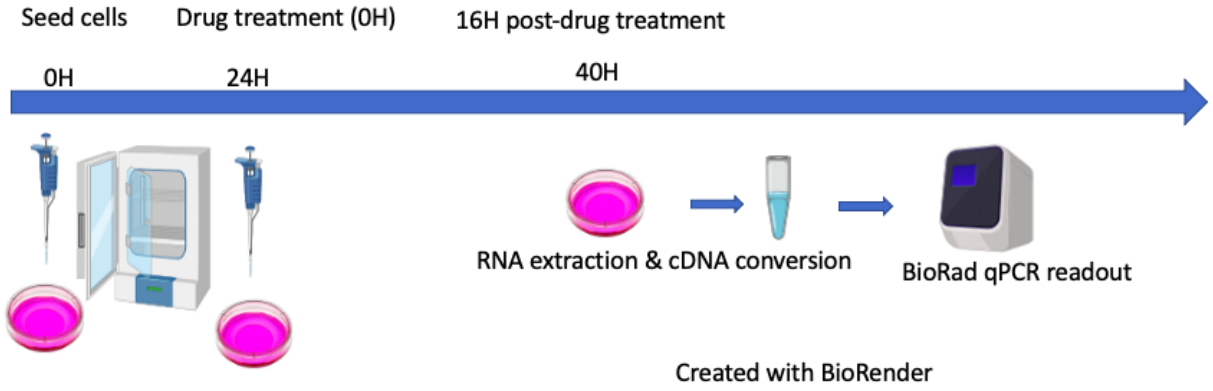


**Table 3. Primer Sequence Table**

| **Gene Name** | Forward Primer Sequence (5' – 3') | Reverse Primer Sequence (5' – 3') |
|---|---|---|
| *GAPDH* | GACAGTCAGCCGCATCTTCT | GCGCCCAATACGACCAAATC |
| *ATF2* | TGTGAATTCTGCCAGGCAAT | CTCGTTGGTAAAACGCTGGC |
| *BAD* | CTCCGGAGGATGAGTGACGA | CACCAGGACTGGAAGACTCG |
| *BAX* | GCAGATCATGAAGACAGGGGC | TGCCACTCGGAAAAAGACCT |
| *Bcl-2* | GGATCCAGGATAACGGAGGC | GGGCCAAACTGAGCAGAGTC |
| *Bcl-xL* | ACTGGTTGAGCCCATCCCTA | GGGCATCCAAACTGCTGCTG |
| *Bim* | ACAGAGCCACAAGACAGGAG | ACCATTGCACTGAGATAGTGGT |

| | | |
|---|---|---|
| *p53* | ATTGGCCAGACTGCCTTCCG | TCCCAGAATGCAAGAAGCCGC |
| *RB1* | ACACAACCCAGCAGTTCGAT | GGGTGTTCGAGGTGAACCAT |
| *TNF-α* | CCCAGGGACCTCTCTCTAACA | GCTTGAGGGTTTGCTACATCATG |
| *TGF-β* | AGGGCTACCATGCCAACTTC | CCCGGGTTATGCTGGTTGTA |

**2.8 Confocal Microscopy**

Confocal microscopy is used to quantify nuclear fragmentation incidence rate and elucidate the fluorescence intensity of microtubules as targets of paclitaxel after a time-course drug treatment.

**2.8.1 Imaging and Quantification of Nuclear Fragmentation**

Autoclaved coverslips are allowed 24 hours to settle to the bottom of a media-filled 35-mm culture plate under culturing conditions prior to removal of media. Following media removal, 150,000 cells are seeded and allowed 24 hours to adhere to the bottom of the coverslip. Drugs of desired concentration are then applied to cells over 0 and 24 hours. Following drug incubation, cells grown on coverslips are washed twice with 1X PBS and fixed with 4% paraformaldehyde (Sigma) for 15 minutes under

room temperature. Cells are washed twice with PBS before being permeabilized with 0.1% Triton X-100 (100 µL of 10% Triton X-100 (Sigma) in 9.9 mL of $ddH_2O$) followed by two washes with 1X PBS. Cells are then incubated with Alexa Fluor 555 Phalloidin (Thermo Fisher Scientific), an F-actin binding dye that defines cell membrane, and Hoechst 33342 (Thermo Fisher Scientific), a fluorescent DNA-intercalating agent, for 45 minutes in the dark at room temperature. Stained coverslips are washed three times with 1X PBS before being transferred onto microscopy glass slides (Thermo Fisher Scientific) and immersed in a droplet of 10 µLs of fluorescence mounting media (Agilent) for each coverslip. Samples are imaged immediately with 405-nm (for nuclei) and 555-nm lasers (for F-actin) under the 63X magnification of a LSM710 confocal microscope. Confocal microscopy image results are reported as nuclear fragmentation incidence rates, or the ratio of the number of fragmented nuclei over total number of cells imaged. These results are presented as bar graphs over a range of drug treatment doses.

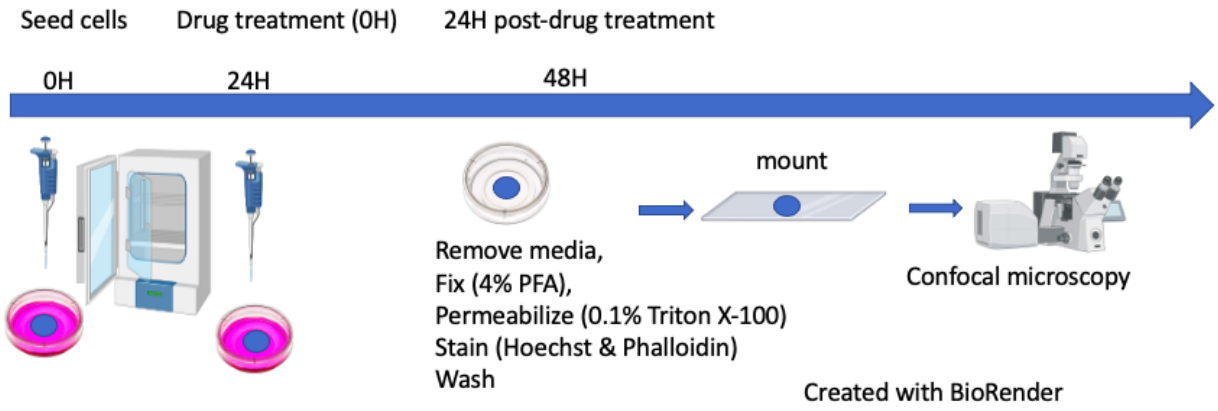

### 2.8.2 Quantification of Fluorescence Intensity of Microtubules

Autoclaved coverslips are allowed 24 hours to settle to the bottom of a media-filled 35-mm culture plate under culturing conditions prior to removal of media. Following media removal, 150,000 cells are seeded and allowed 24 hours to adhere to the bottom of the coverslip. Drugs of desired concentration are then applied to cells over 0, 1, 3, and 6 hours. Following drug incubation, cells grown on coverslips are washed twice with 1X PBS and fixed with 4% paraformaldehyde for 15 minutes under room temperature. Cells are washed twice with PBS before being permeabilized by 0.1% Triton X-100 (100 µL of 10% Triton X-100 (Sigma) in 9.9 mL of $ddH_2O$) followed by two washes with 1X PBS. Cells are then incubated with Oregon Green™ 488 Conjugate paclitaxel derivative (Thermo Fisher Scientific), a tubulin-binding agent, Alexa Fluor 555 Phalloidin, Hoechst 33342, as previously described for 45 minutes in the dark at room temperature. Stained coverslips are washed three times with 1X PBS before being transferred onto microscopy glass slides and immersed in a droplet of 10µLs of fluorescence mounting media for each coverslip. Samples are imaged immediately with 405-nm (for nuclei), 488-nm (for microtubules), and 555-nm (for F-actin) lasers under the 63X magnification of a LSM710 confocal microscope. Sample preparation and image acquisition across all biological repeats involve using the same dye concentration and identical gain and laser power. The fluorescence intensity of microtubules in any given cell is reported by ImageJ after outlining cell membrane following phalloidin staining signals and superimposing the same area onto the 488-nm laser, Oregon Green 488 paclitaxel derivative channel.

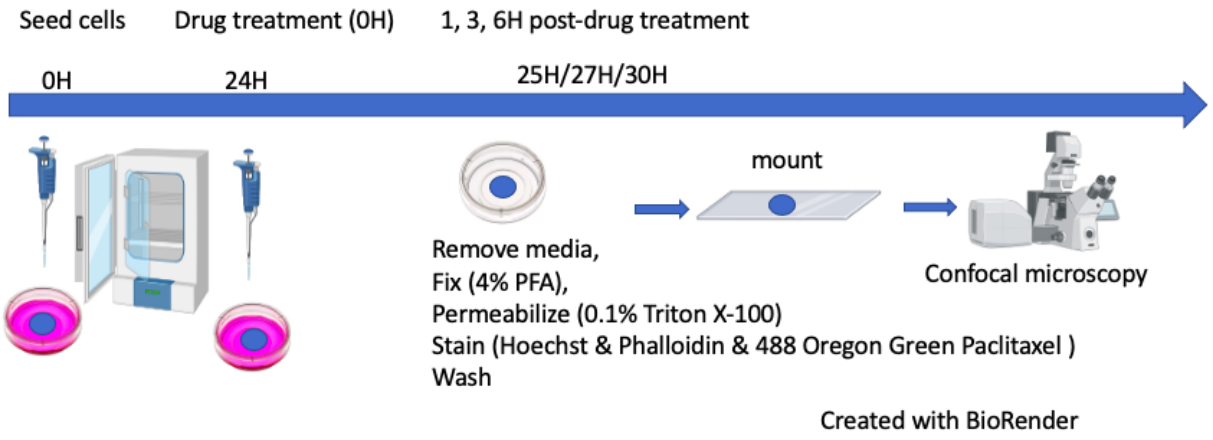


**2.9 Statistics**

Statistical significance for multiple comparisons (three or more experimental conditions) is analyzed using the Tukey post-hoc test in conjunction with one-way ANOVA, whereas Student's *t* tests are performed to analyze statistical significance between two experimental conditions. The error bars represent mean ± S.D. of the experiments. The level of statistical significance is indicated by the presence and number of asterisks used in bar graphs throughout this thesis with n.s = not significant ($p>0.05$), * = $p \leq 0.05$, ** = $p \leq 0.01$, *** = $p \leq 0.001$, and **** = $p \leq 0.0001$.

# CHAPTER 3 RESULTS

## 3.1 Validation of Paclitaxel-resistant breast cancer cell lines and sensitive counterparts

Paclitaxel-resistant triple-negative (MDA-MB-231) and receptor-positive (MCF7) cells were established through continuous culturing of the paclitaxel-sensitive, wild-type MDA-MB-231 and MCF7 cells in increasing dosage of paclitaxel (PLX) until 5mg/mL or 585nM of PLX was reached. To verify the establishment of drug resistance in our model breast cancer cell lines, 3-(4, 5-dimethylthiazol-2-yl)-2, 5-diphenyltetrazolium bromide (MTT) viability assays were conducted on PLX-resistant triple-negative breast cancer (231R) and receptor-positive breast cancer (MCF7R) cells, along with their sensitive counterparts following incubation with various doses of PLX over the span of 24, 48, and 72 hours (Figure 3.1 A-B). At 72 hours, the $IC_{50}$ values of chemo-sensitive triple-negative breast cancer (231S) and receptor-positive MCF7 (MCF7S) cells were 2.459 nM and 10.59 nM, respectively. On the contrary, 231R and MCF7R cells exhibited $IC_{50}$ values of 1.036 μM and 1.76 μM, respectively, suggesting the establishment of chemoresistance in 231R and MCF7R cells.

**A**

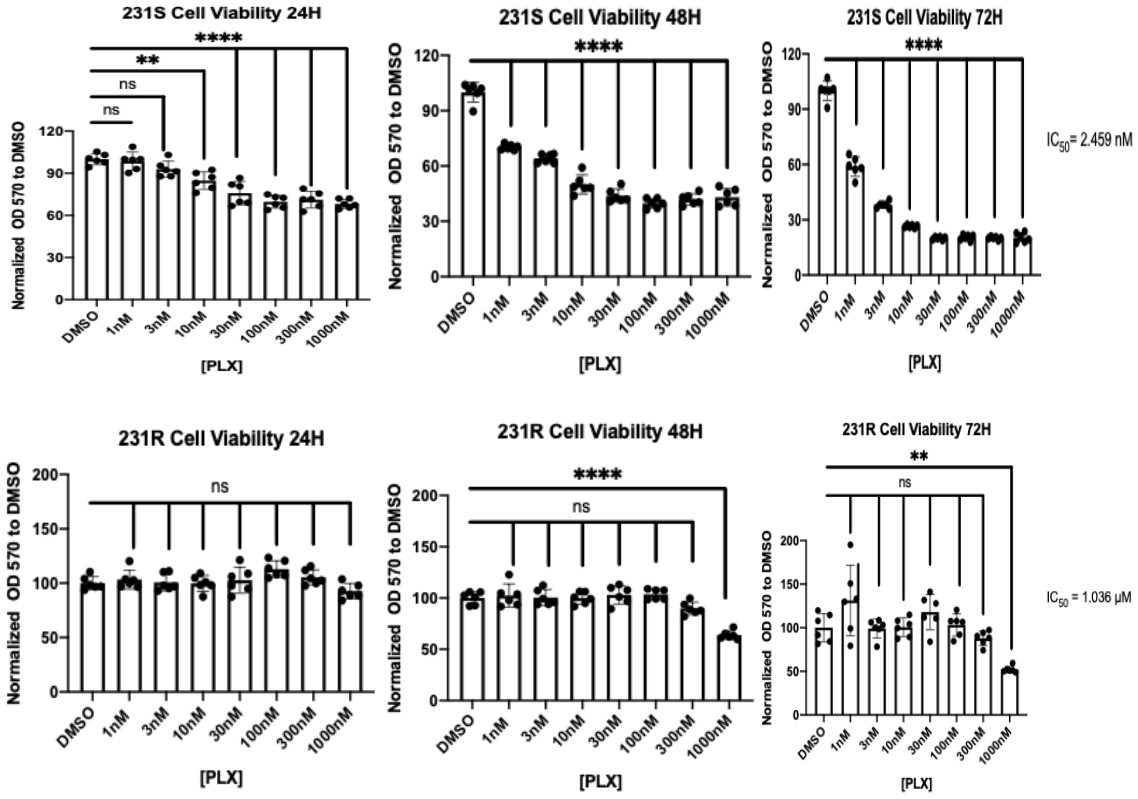
231S Cell Viability 24H
231S Cell Viability 48H
231S Cell Viability 72H
231R Cell Viability 24H
231R Cell Viability 48H
231R Cell Viability 72H
Normalized OD 570 to DMSO
[PLX]
DMSO
1nM
3nM
10nM
30nM
100nM
300nM
1000nM
ns
**
****
IC50= 2.459 nM
IC50 = 1.036 µM

**B**

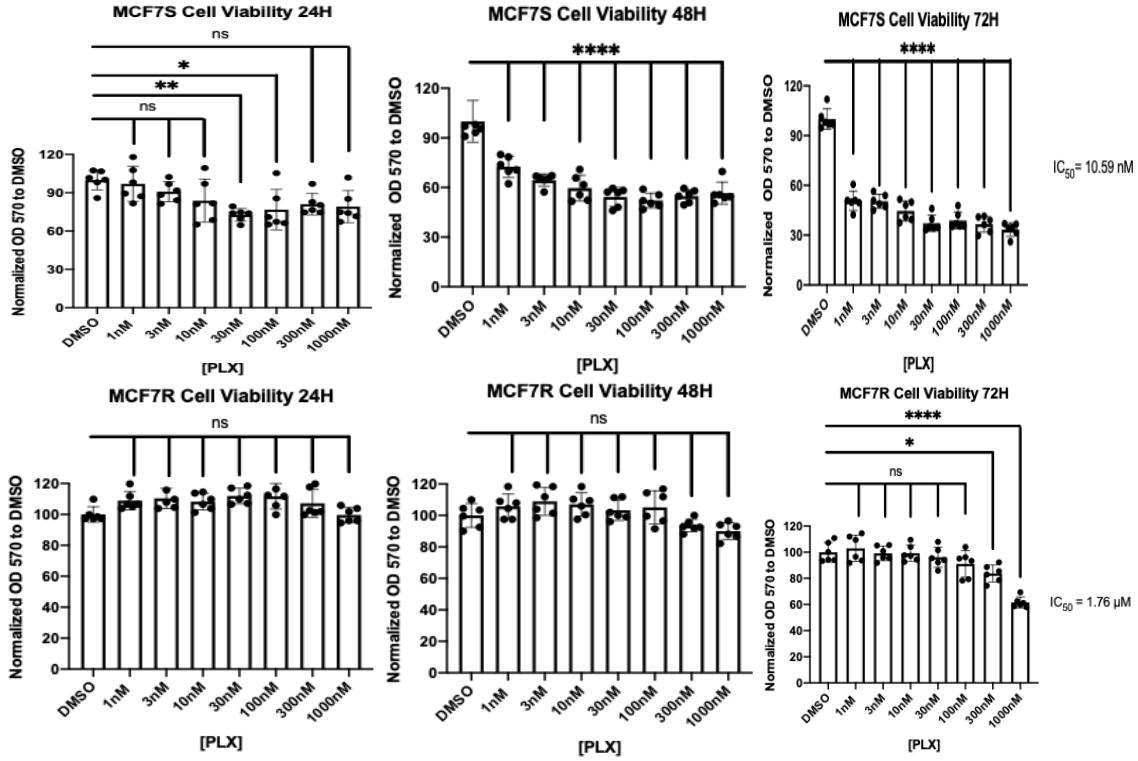
MCF7S Cell Viability 24H
MCF7S Cell Viability 48H
MCF7S Cell Viability 72H
MCF7R Cell Viability 24H
MCF7R Cell Viability 48H
MCF7R Cell Viability 72H
Normalized OD 570 to DMSO
[PLX]
DMSO
1nM
3nM
10nM
30nM
100nM
300nM
1000nM
ns
*
**
****
IC50= 10.59 nM
IC50 = 1.76 µM

**Figure 3.1. MTT cell viability assay of 231R, MCF7R, 231S, and MCF7S cells.** A) Normalized cell viability of sensitive and resistant triple-negative breast cancer MDA-MB-231 cells in response to varying concentration of PLX at 24, 48, and 72-hour treatment time points. B) Normalized cell viability of sensitive and resistant receptor-positive breast cancer MCF7 cells in response to varying concentration of PLX at 24, 48, and 72-hour treatment time points. Data are expressed as the mean ± s.d. of triplicates (n=3). All experiments were performed three times to confirm reproducibility. NS indicates $P > 0.05$, * indicates $P \leq 0.05$, ** indicates $P \leq 0.01$, and **** indicates $P \leq 0.0001$.

### 3.2 BC-2021, albeit downregulating resistant breast cancer cell viability, exerts significantly higher cytotoxicity in combination with PLX on 231R and MCF7R cells

Cell counting experiments showed that 1μM of BC-2021 alone did not reduce the viability of 231R and MCF7R cells over 24, 48, and 72-hour incubation periods (Figure 3.2 A), whereas the combination of 585nM PLX and 1μM of BC-2021 induced significant cytotoxicity on 231R and MC7R cells over these time frames (Figure 3.2 B). This effect was more pronounced over the longer-term study as evidenced by the complete eradication of clonogenicity of 231R and MCF7R cells exposed to 1μM of BC-2021 and 585nM of PLX at the 14-day interval (Figure 3.2 C). Since the concentration of PLX remained constant in the combinatorial regimen, 231R and MCF7R cells exhibited dose-dependent reduction in viability in response to the increasing concentration of BC-2021 within the combinatorial regimen, as illustrated by flow cytometric assessment of cell viability using the Fixable Viability Dye eFluor™ 780 (Figure 3.2 D). A BC-2021 dosage-dependent shift of cell population to the non-viable region was observed for 231R and MCF7R cells upon combinatorial drug treatment, further demonstrating the potent cytotoxicity of the combination of BC-2021 and PLX on resistant breast cancer cells.

**A**

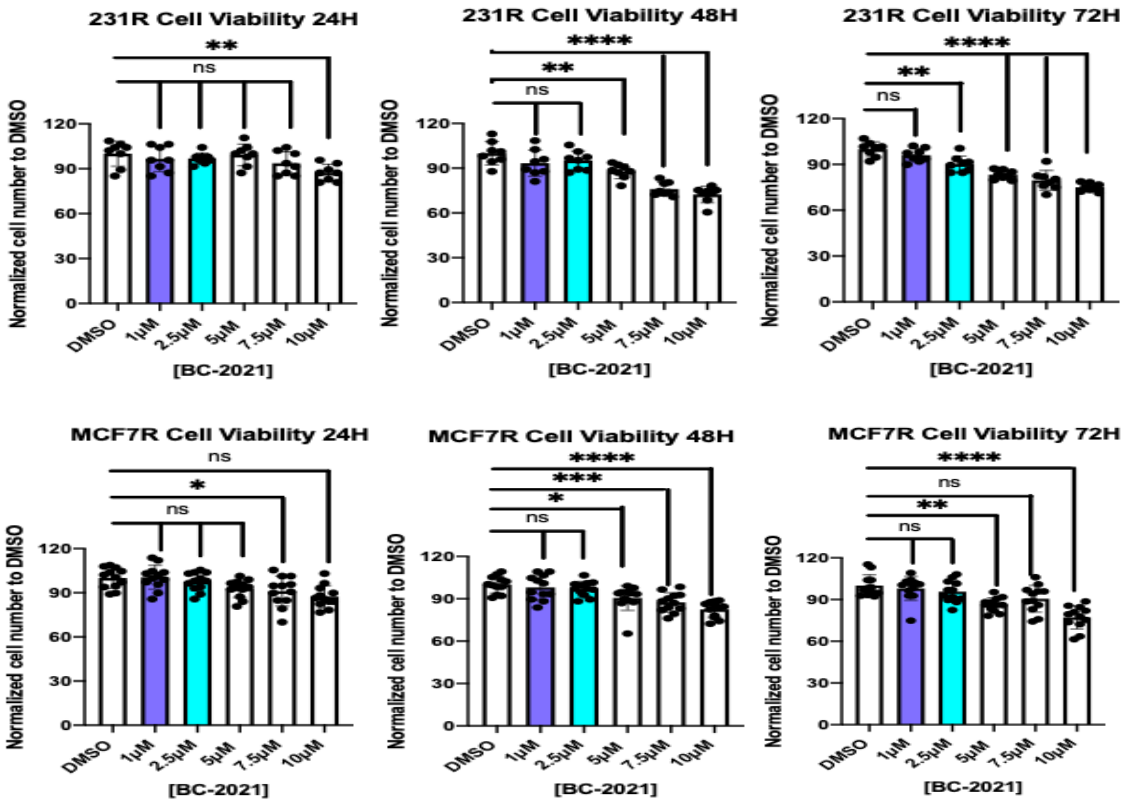
231R Cell Viability 24H
231R Cell Viability 48H
231R Cell Viability 72H
MCF7R Cell Viability 24H
MCF7R Cell Viability 48H
MCF7R Cell Viability 72H
Normalized cell number to DMSO
DMSO
1μM
2.5μM
5μM
7.5μM
10μM
[BC-2021]
ns
*
**
***
****

**B**

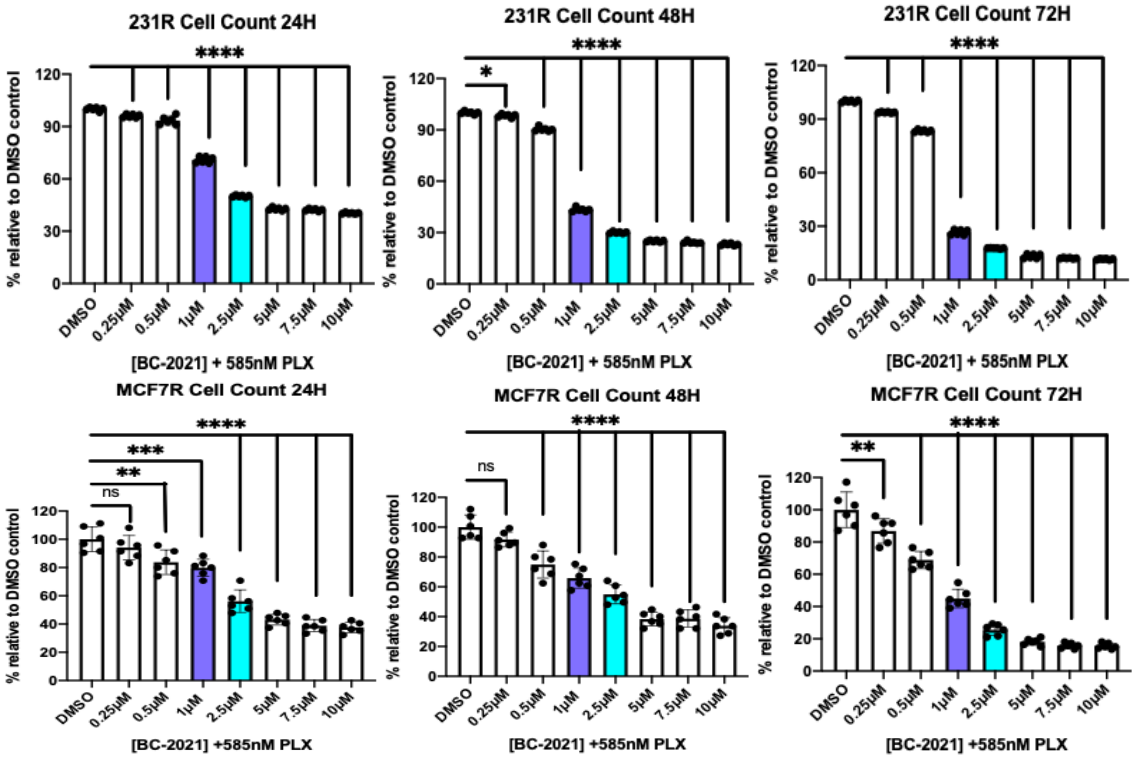
231R Cell Count 24H
231R Cell Count 48H
231R Cell Count 72H
MCF7R Cell Count 24H
MCF7R Cell Count 48H
MCF7R Cell Count 72H
% relative to DMSO control
DMSO
0.25μM
0.5μM
1μM
2.5μM
5μM
7.5μM
10μM
[BC-2021] + 585nM PLX
[BC-2021] +585nM PLX
ns

**C.**

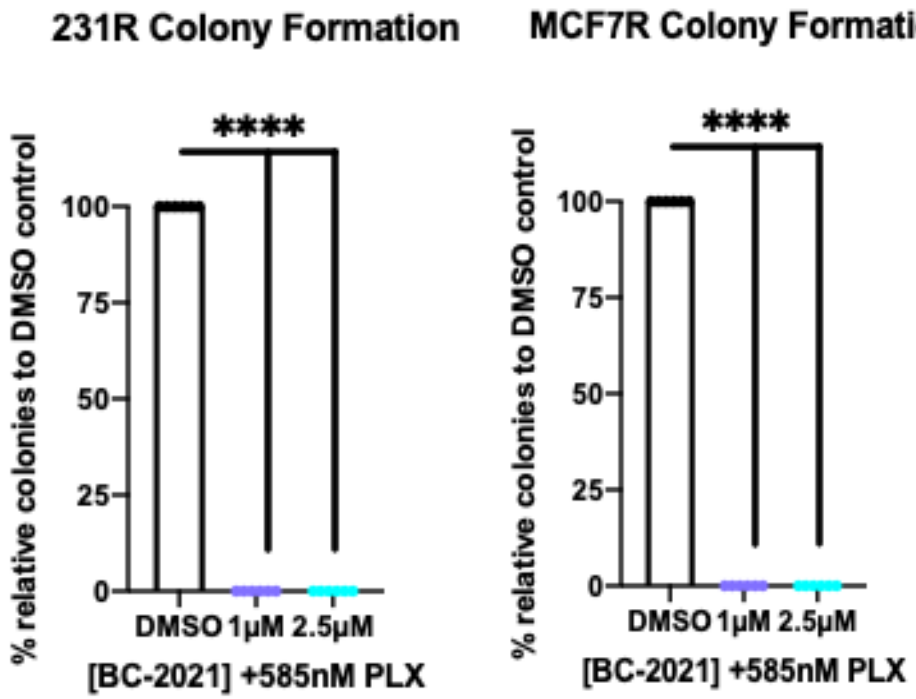
231R Colony Formation
MCF7R Colony Formation
% relative colonies to DMSO control
DMSO 1μM 2.5μM
[BC-2021] +585nM PLX

**D.**

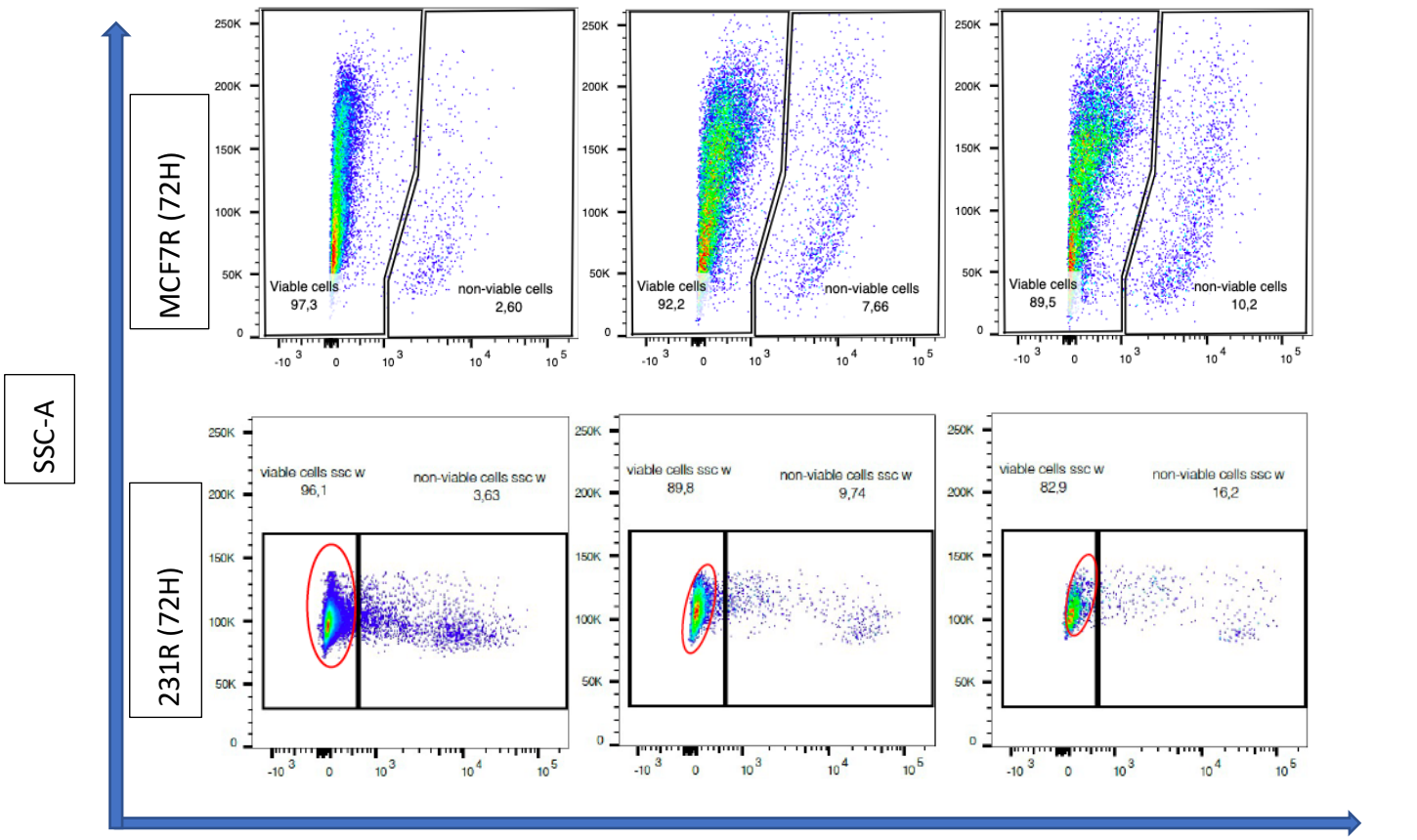


Contributed by Lauren Westhaver, *PhD Candidate*, Department of Pathology, Dalhousie University, Halifax, NS

**Figure 3.2. BC-2021 in combination with PLX induces sustained cytotoxicity on 231R and MCF7R cells.** A) Normalized cell counting of 231R and MCF7R 24, 48, and 72 hours post-BC-2021 treatment alone relative to the DMSO-treated control B) Normalized cell counting of 231R and MCF7R 24, 48, and 72 hours following combinatorial treatment with BC-2021 and 585nM PLX to relative to the DMSO and 585nM PLX-treated control. C) Normalized colony counts of 231R and MCF7R cells following combinatorial treatment with BC-2021 and 585nM PLX for 14 days relative to the colony counts of the DMSO and 585nM PLX-treated control. D) e-Fluor$^{TM}$ 780-based flow cytometric assessment of 231R and MCF7R cell viability following 72-hour combinatorial treatment with BC-2021 and 585nM PLX. e-Fluor 780$^{TM}$ viability dye, a cell membrane-impermeable dye, emits fluorescence upon binding to amine residues of proteins. Viable cells exhibit minimal e-Fluor$^{TM}$ 780 fluorescence signal, while non-viable cells exhibit significantly higher fluorescence signals as a result of the dye binding to intracellular proteins after crossing the compromised cell membrane. Flow cytometry data was acquired by Lauren Westhaver, PhD Candidate, in the Department of Pathology at Dalhousie University at the time of this writing. Data are expressed as the mean ± s.d. of triplicates (n=3). NS indicates $P > 0.05$, * indicates $P \leq 0.05$, ** indicates $P \leq 0.01$, *** indicates $P \leq 0.001$, and **** indicates $P \leq 0.0001$.

### 3.3 Combination drug-treated 231R and MCF7R cells undergo primarily apoptosis

To characterize the modality of drug-induced cell death, 231R and MCF7R cells were treated with BC-2021 alone or BC-2021 and PLX before being co-stained with FITC-conjugated Annexin V and 7-AAD. FITC-conjugated Annexin V emits fluorescence upon binding to phosphatidylserine, the externalization of which hallmarks apoptotic cell death, whereas the exclusive exhibition of 7-AAD, a DNA-intercalating agent, signifies necrotic cell death. Based on the distribution of fluorescence signals (Figure 3.3 A-B), the percentages of apoptotic ($FITC^+$ or FITC-and-7-$AAD^+$) and necrotic (7-$AAD^+$) cells for each given drug dosage or combination were quantified. BC-2021 incubation alone did not enhance overall cell death, comprising of both apoptotic and necrotic cell populations, on 231R cells (Figure 3.3 C) and MCF7R cells (Figure 3.3 D), however, BC-2021 and PLX treatment together resulted in predominantly apoptotic cell death of 231R at the 24 and 48-hour treatment intervals (Figure 3.3 E) and of MCF7R cells at the 72-hour treatment period (Figure 3.3 F), both in a BC-2021 dose-dependent manner (Figure 3.3 G). To further validate apoptotic cell death, we evaluated the extent of nuclear fragmentation, a phenotypical hallmark of apoptosis, using the fluorescent DNA-intercalating dye Hoechst 33342. Indeed, following 24-hr incubation with BC-2021 alone or BC-2021 in combination with 585nM of PLX, 231R cells exhibited a BC-2021 dose-dependent increase in nuclear fragmentation incidences (Figure 3.3 H-I), pinpointing apoptosis as the major modality of cell death following combinatorial treatment.

## A. $H_2O_2$-induced 7-AAD Staining (Positive Control)

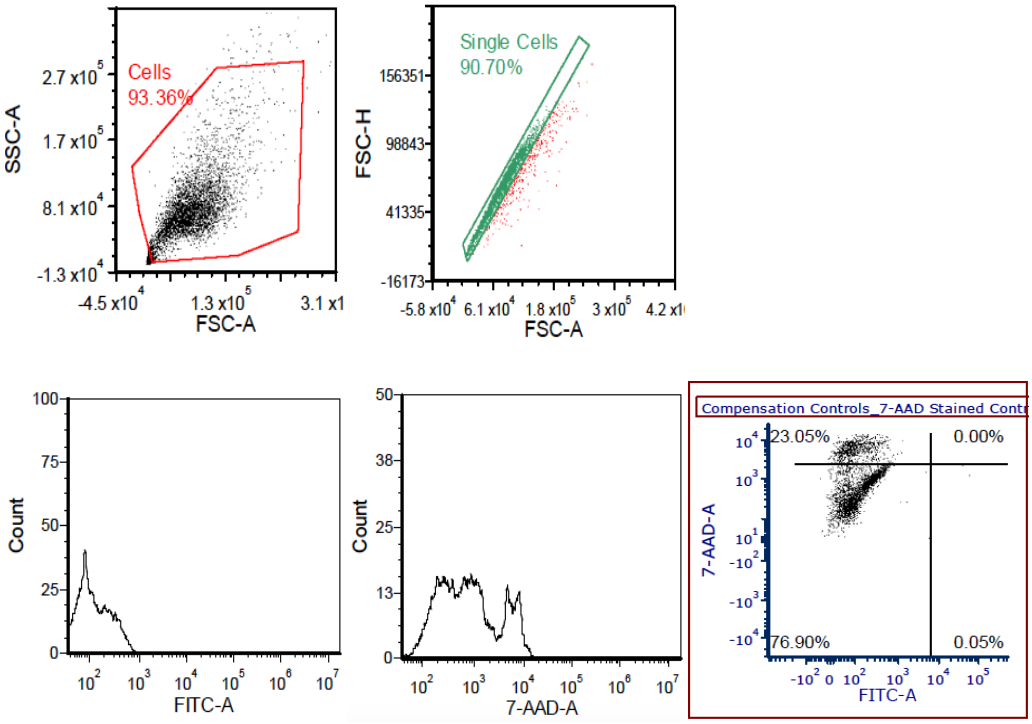


## B. $H_2O_2$-induced FITC-Annexin V Staining (Positive Control)

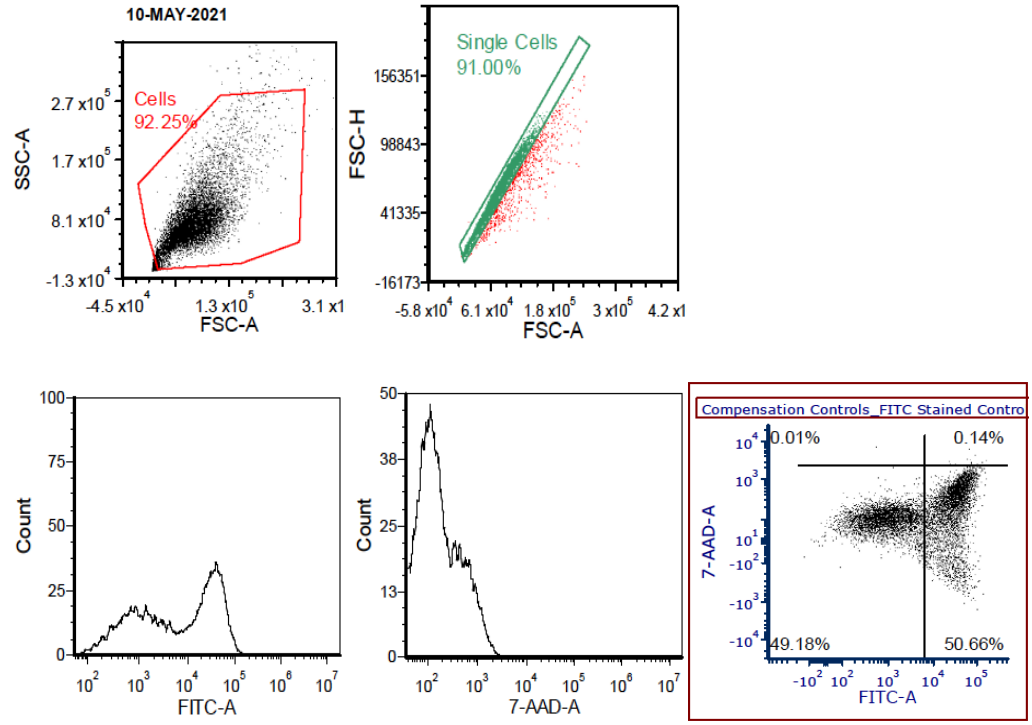

**C**

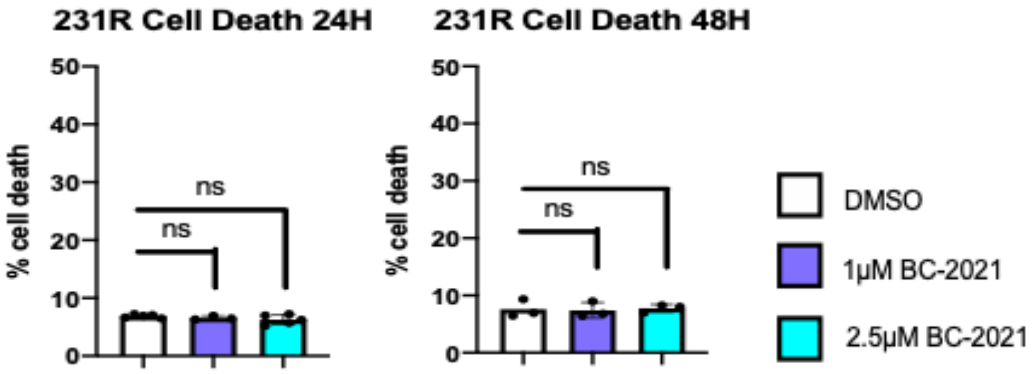
231R Cell Death 24H
231R Cell Death 48H
% cell death
50
40
30
20
10
0
ns
ns
ns
ns
DMSO
1μM BC-2021
2.5μM BC-2021

**D**

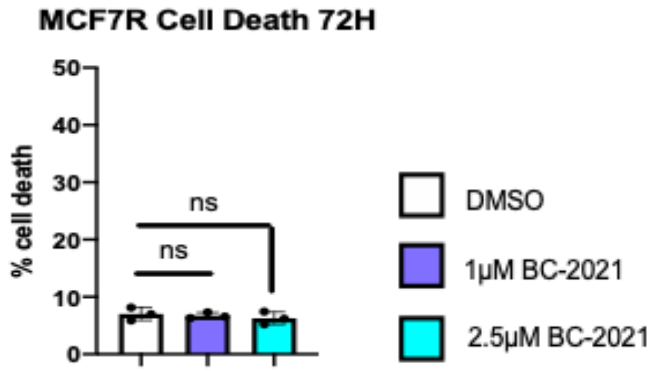
MCF7R Cell Death 72H
% cell death
50
40
30
20
10
0
ns
ns
DMSO
1μM BC-2021
2.5μM BC-2021

**E**

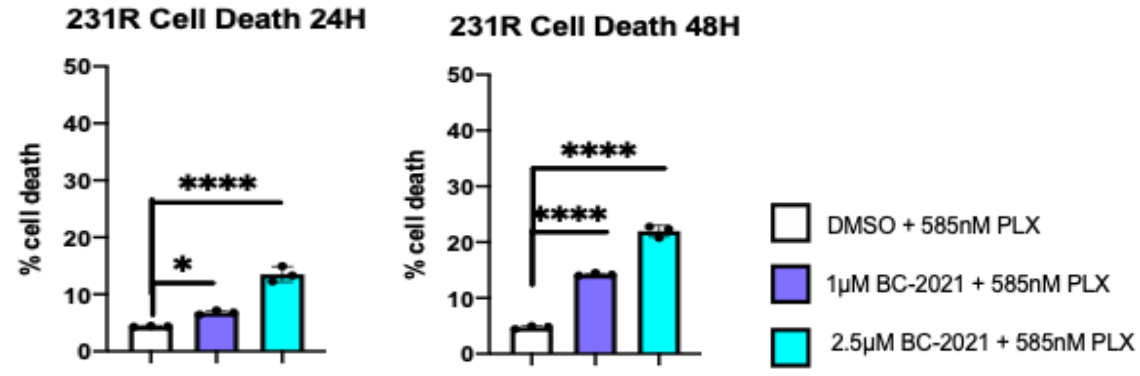
231R Cell Death 24H
231R Cell Death 48H
% cell death
50
40
30
20
10
0
****
*
****
****
DMSO + 585nM PLX
1μM BC-2021 + 585nM PLX
2.5μM BC-2021 + 585nM PLX

**F**

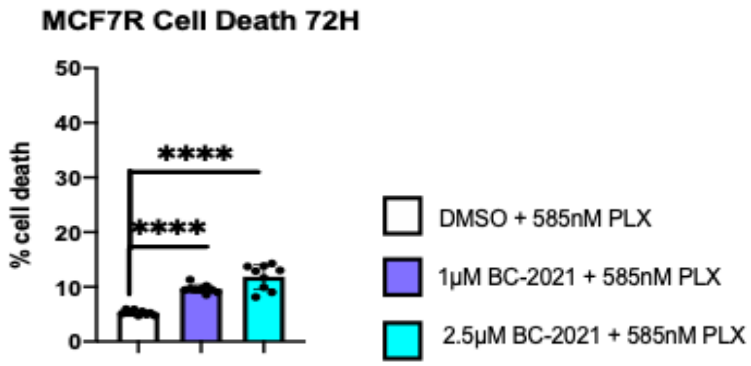
MCF7R Cell Death 72H
% cell death
50
40
30
20
10
0
****
****
DMSO + 585nM PLX
1μM BC-2021 + 585nM PLX
2.5μM BC-2021 + 585nM PLX

**G**

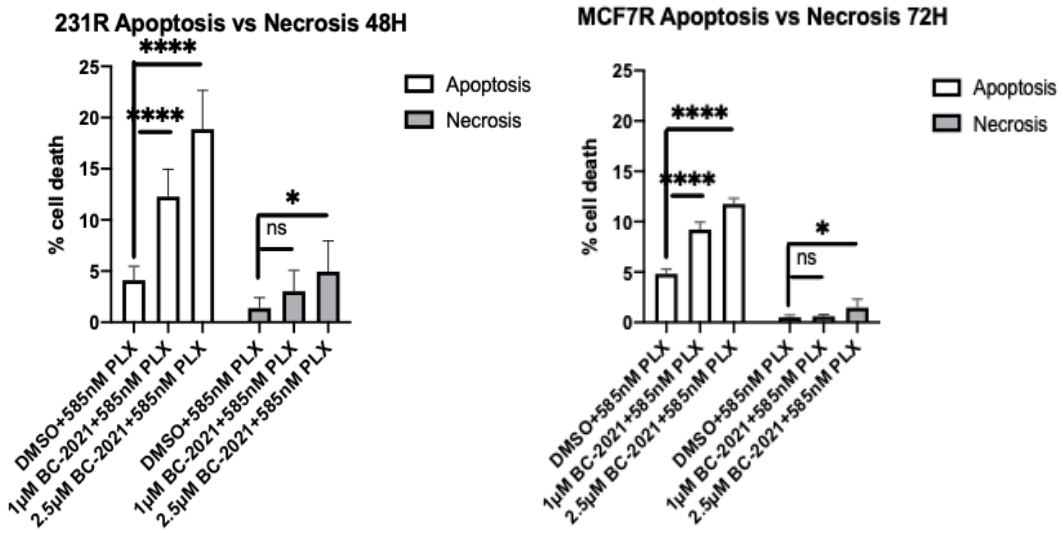
231R Apoptosis vs Necrosis 48H
% cell death
25
20
15
10
5
0
****
****
*
ns
Apoptosis
Necrosis
DMSO+585nM PLX
1μM BC-2021+585nM PLX
2.5μM BC-2021+585nM PLX
DMSO+585nM PLX
1μM BC-2021+585nM PLX
2.5μM BC-2021+585nM PLX
MCF7R Apoptosis vs Necrosis 72H
% cell death
25
20
15
10
5
0
****
****
*
ns
Apoptosis
Necrosis
DMSO+585nM PLX
1μM BC-2021+585nM PLX
2.5μM BC-2021+585nM PLX
DMSO+585nM PLX
1μM BC-2021+585nM PLX
2.5μM BC-2021+585nM PLX

**H**

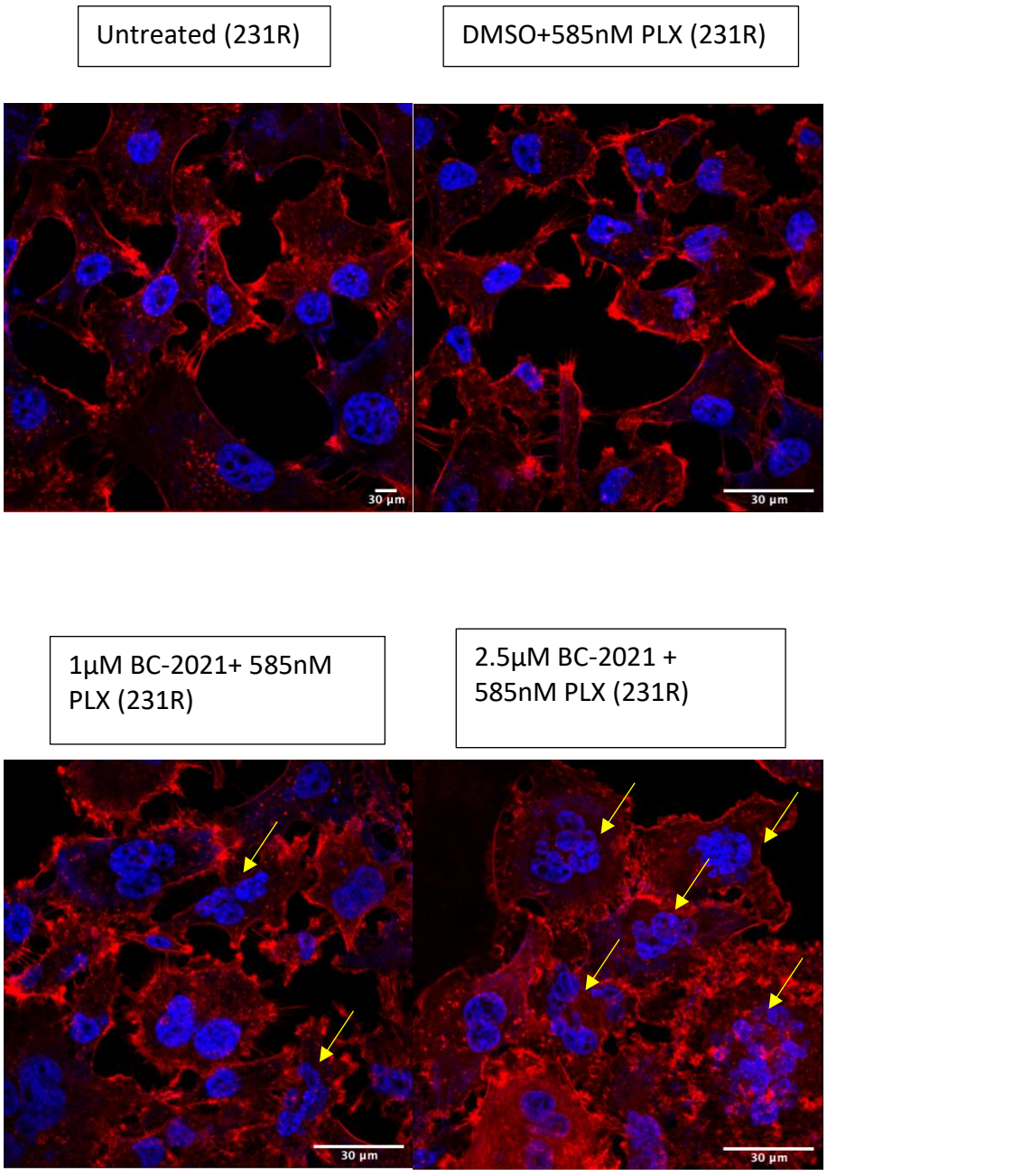
Untreated (231R)
DMSO+585nM PLX (231R)
30 µm
30 µm
1µM BC-2021+ 585nM PLX (231R)
2.5µM BC-2021 + 585nM PLX (231R)
30 µm
30 µm
Nucleus
F-actin
Nuclear fragmentation incident

I

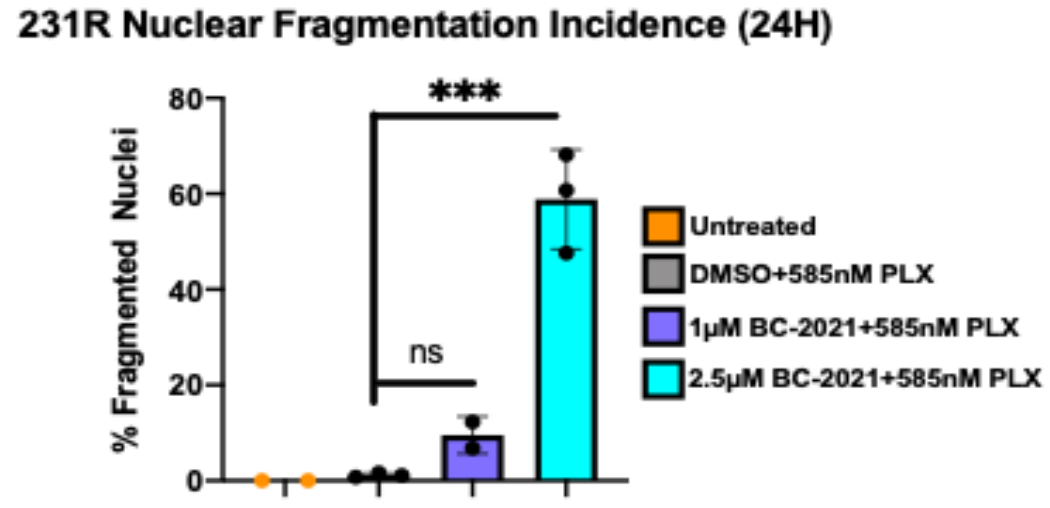
231R Nuclear Fragmentation Incidence (24H)
% Fragmented Nuclei
80
60
40
20
0
***
ns
Untreated
DMSO+585nM PLX
1μM BC-2021+585nM PLX
2.5μM BC-2021+585nM PLX

**Figure 3.3. Combination drug-treated 231R and MCF7R cells undergo primarily apoptosis.** To facilitate flow cytometry gating, 231R cells were subjected to $H_2O_2$ incubation as outlined in 2.5.3 of Materials and Methods and were subsequently stained with either 7-AAD or FITC-conjugated Annexin V to serve as single channel-stain control. Based on fluorescence signatures, A) necrotic (7-ADD$^+$) and B) apoptotic (FITC$^+$ or FITC-and-7-AAD$^+$) 231R cells were identified. Total percentage of cell death, encompassing both apoptotic and necrotic population, was tallied and reported for C) 231R cells and D) MCF7R cells cells treated with BC-2021 alone or E) with BC-2021 and 585nM of PLX at 24 and 48 hours for 231R cells as well as F) for MCF7R cells at the 72-hour interval. G) 231R and MCF7R cells both exhibit predominantly apoptotic cell death following combinatorial drug treatment. H) Validatory fluorescent confocal microscopy images displaying dose-dependent nuclear fragmentation of 231R cells following 24-hr combinatorial drug treatment with 0, 1, and 2.5µM of BC-2021 and 585nM of PLX. Nuclei, in blue, were stained by Hoechst 33342 (blue), a cell membrane-permeable DNA minor groove-binding agent. Cell boundary, in red, was outlined by the F-actin-binding chemical phalloidin. All images were acquired using the Zeiss LSM 710 Confocal Microscope at 63X magnification. I) Quantification of percent fragmented nuclei, or the total number of 231R cells exhibiting fragmented nuclei out of the entire cell population, post-drug treatment revealed a dose-dependent increase in nuclear fragmentation, the phenotypical hallmark of apoptosis. Data are expressed as the mean ± s.d. of triplicates (n=3). NS indicates $P>0.05$, * indicates $P \leq 0.05$, *** indicates $P \leq 0.001$, and **** indicates $P \leq 0.0001$.

### 3.4 The combination of BC-2021 and PLX downregulates 231R and MCF7R cell viability by disposing 231R and MCF7R cells, but not sensitive counterparts, to PLX cytotoxicity

Given that the combinatorial administration of BC-2021 and PLX leads to drastic and sustained killing of 231R and MCF7R cells, it was of interest to study whether BC-2021 acts by potentiating the therapeutic efficacy of PLX. To test this hypothesis, 231S and MCF7S cells were treated with DMSO, 2.5μM of BC-2021, 5nM of PLX, and 2.5μM of BC-2021 along with 5 nM of PLX for 24, 48, and 72 hours. 2.5μM of BC-2021 in combination with 5nM of PLX did not result in greater 231S or MCF7S cell death compared to 5-nM PLX challenge alone, suggesting that BC-2021 does not act solely by potentiating the therapeutic efficacy of PLX (Figure 3.4 A). Instead, cell counting following the sequential single and double-agent incubation of BC-2021 and PLX paradigm (Figure 3.4 B) revealed that the combination of BC-2021 and PLX downregulated 231R and MCF7R cell viability specifically by predisposing resistant cells to PLX-mediated cytotoxicity, as evidenced in the 30-40% reduction of viability among 231R and MCF7R cells relative to the DMSO-treated control group following 24-hour pre-treatment with BC-2021 and 72 hours of PLX incubation immediately afterwards (Figure 3.4 C).

**A.**

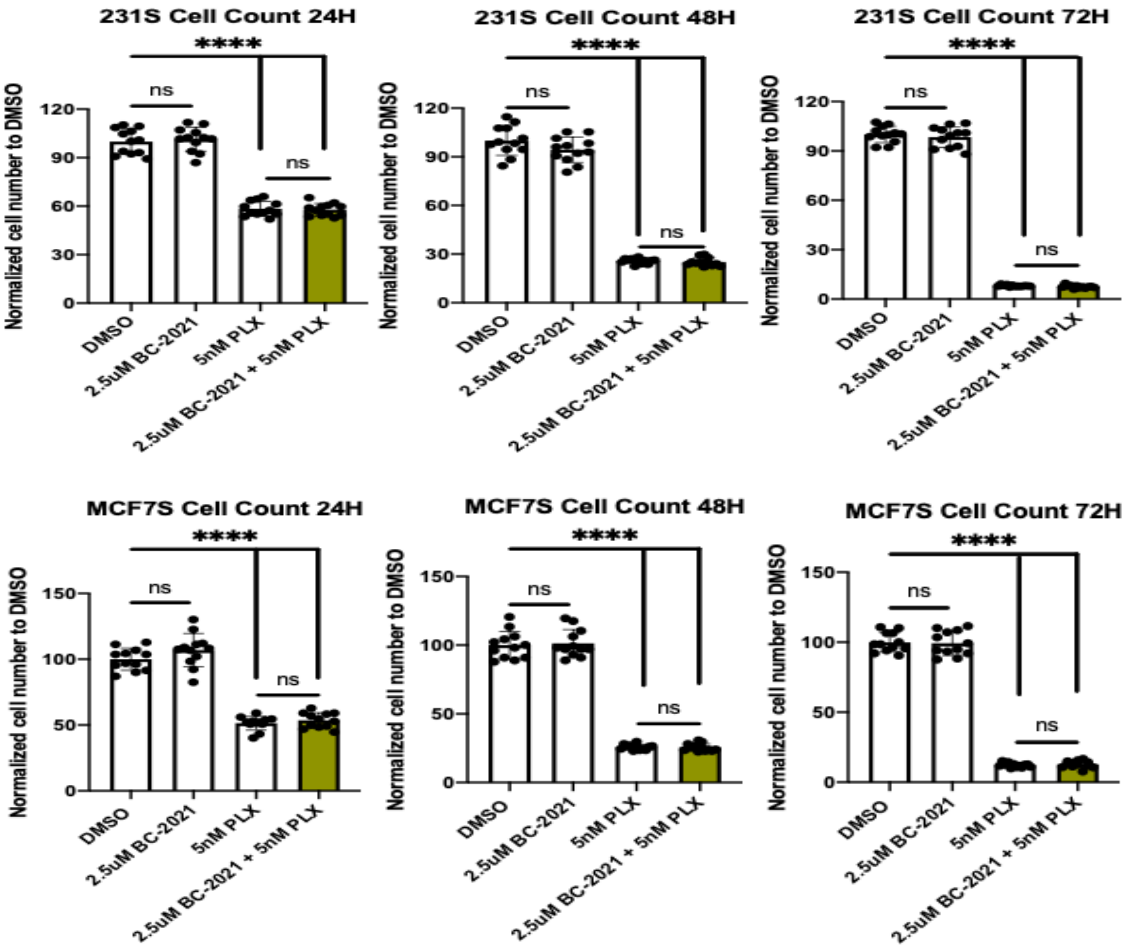
231S Cell Count 24H
231S Cell Count 48H
231S Cell Count 72H
MCF7S Cell Count 24H
MCF7S Cell Count 48H
MCF7S Cell Count 72H
Normalized cell number to DMSO
****
ns
DMSO
2.5uM BC-2021
5nM PLX
2.5uM BC-2021 + 5nM PLX

**B.**

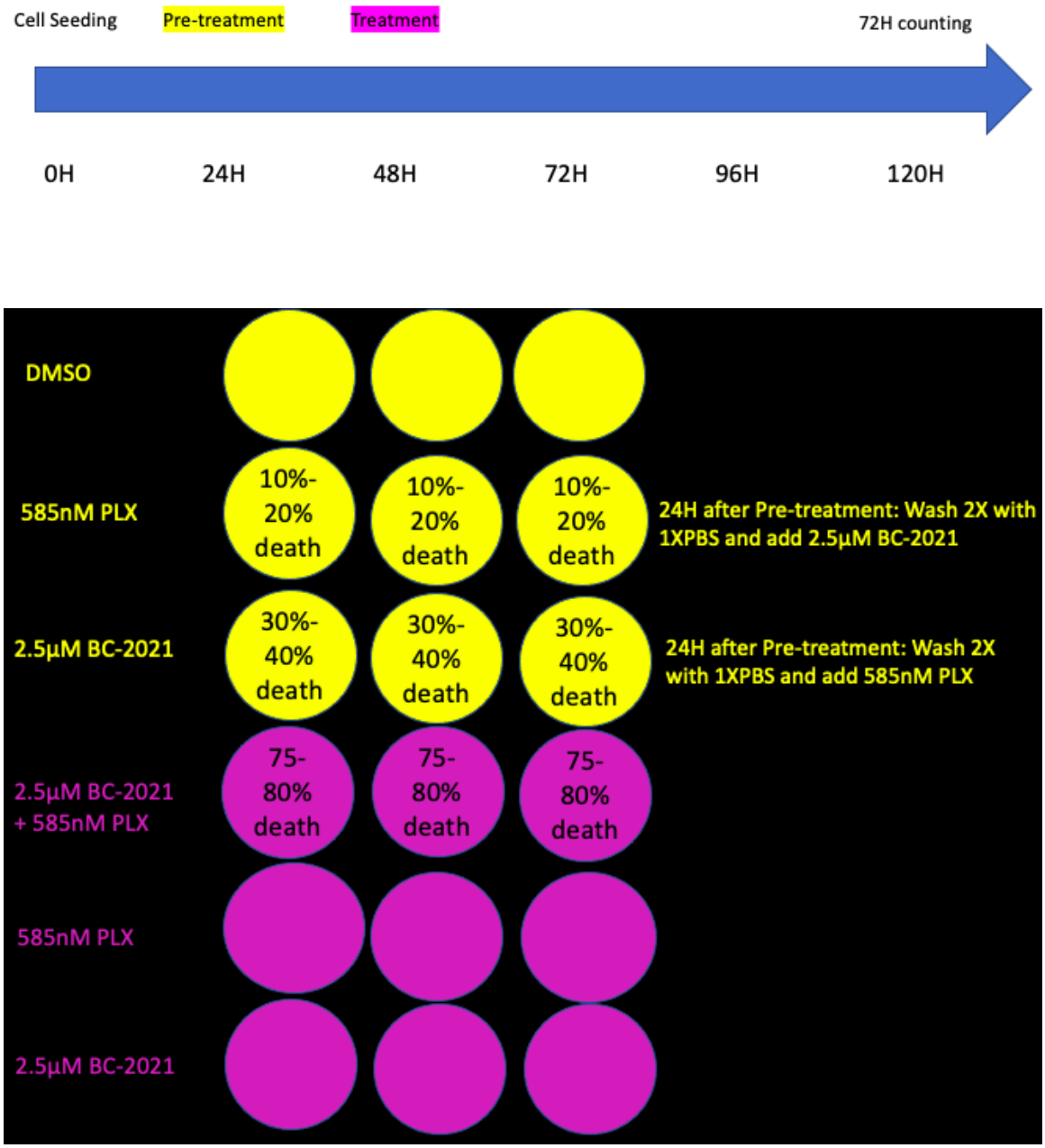
Cell Seeding
Pre-treatment
Treatment
72H counting
0H
24H
48H
72H
96H
120H
DMSO
585nM PLX
10%-20% death
10%-20% death
10%-20% death
24H after Pre-treatment: Wash 2X with 1XPBS and add 2.5µM BC-2021
2.5µM BC-2021
30%-40% death
30%-40% death
30%-40% death
24H after Pre-treatment: Wash 2X with 1XPBS and add 585nM PLX
2.5µM BC-2021 + 585nM PLX
75-80% death
75-80% death
75-80% death
585nM PLX
2.5µM BC-2021

**C.**

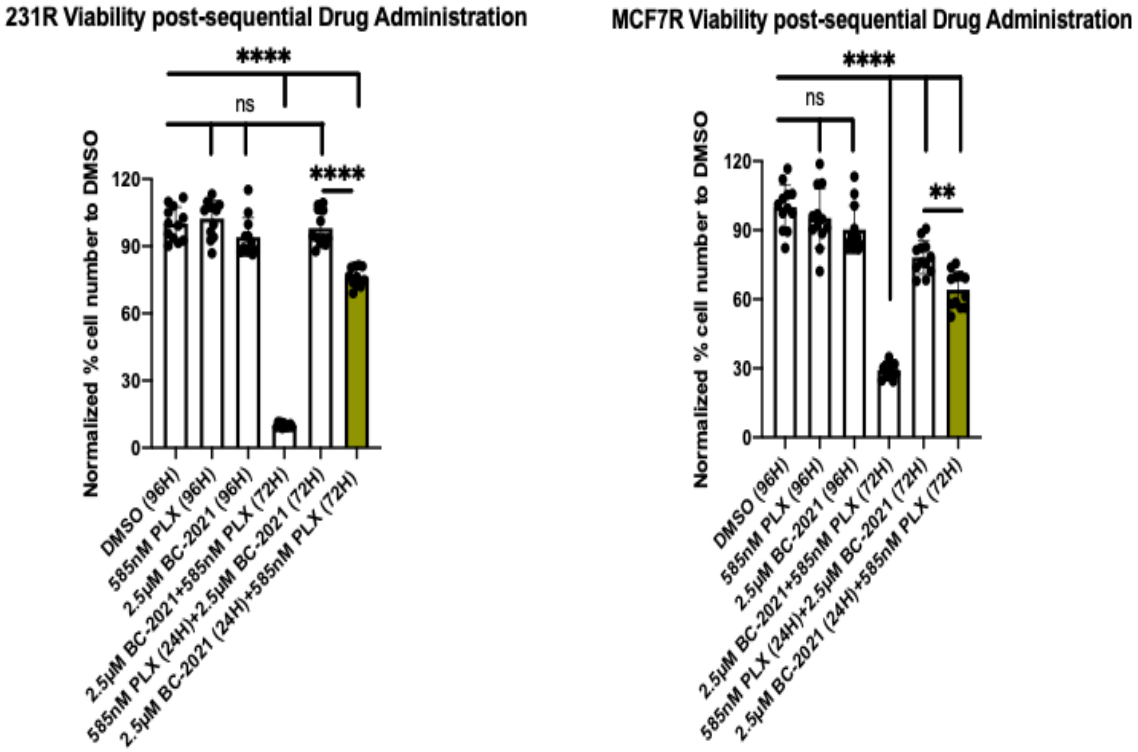


**Figure 3.4. BC-2021 and PLX selectively downregulate 231R and MCF7R cell viability by disposing 231R and MCF7R cells, but not sensitive counterparts, to PLX cytotoxicity.** A) Normalized 231S and MCF7S cell count following treatment with DMSO, 2.5μM of BC-2021, 5nM of PLX, and the combination of 2.5μM BC-2021 and 5nM of PLX for 24, 48, and 72 hours. B) Single and double-agent sequential administration paradigm of BC-2021 and PLX on 231R and MCF7R cells. C) Normalized 231R and MCF7R cell count following the paradigm outlined in (B) in relative to the DMSO-treated control group. Data are expressed as the mean ± s.d. of triplicates (n=3). NS indicates $P>0.05$, ** indicates $P \leq 0.01$, *** indicates $P \leq 0.001$, and **** indicates $P \leq 0.0001$.

### 3.5 Bcl-2 family genes and other survival-regulating genes do not underlie combinatorial drug-mediated cell death

Apoptotic cell death in cancer following chemotherapeutic challenges often involves Bcl-2 family genes and other survival-regulating genes, such as tumor protein 53 (p53), activating transcription factor 2 (ATF2), retinoblastoma protein 1 (RB1), transforming growth factor β (TGF-β), and tumor necrosis factor (TNF-α) (206-212). To investigate whether these genes were involved in combinatorial regimen-mediated cell death, we treated 231R cells with DMSO, 1μM, and 2.5μM of BC-2021 in combination with 585nM of PLX for 16 hours and evaluated the functional expression of these candidate genes using quantitative reverse transcription polymerase chain reaction (RT-qPCR). 231R cells did not exhibit explicit dose-dependent transcriptional regulation of these candidate genes (Figure 3.5). The apparent lack of up-regulation of pro-apoptotic genes, such as *BAX*, *Bim*, *p53*, and *RB1*, and concurrent downregulation of pro-survival genes, such as *Bcl-2* and *Bcl-xL*, indicates that neither Bcl-2 family genes nor the survival-regulating candidate genes were sufficient to account for the acute apoptotic cell death post-combinatorial drug treatment.

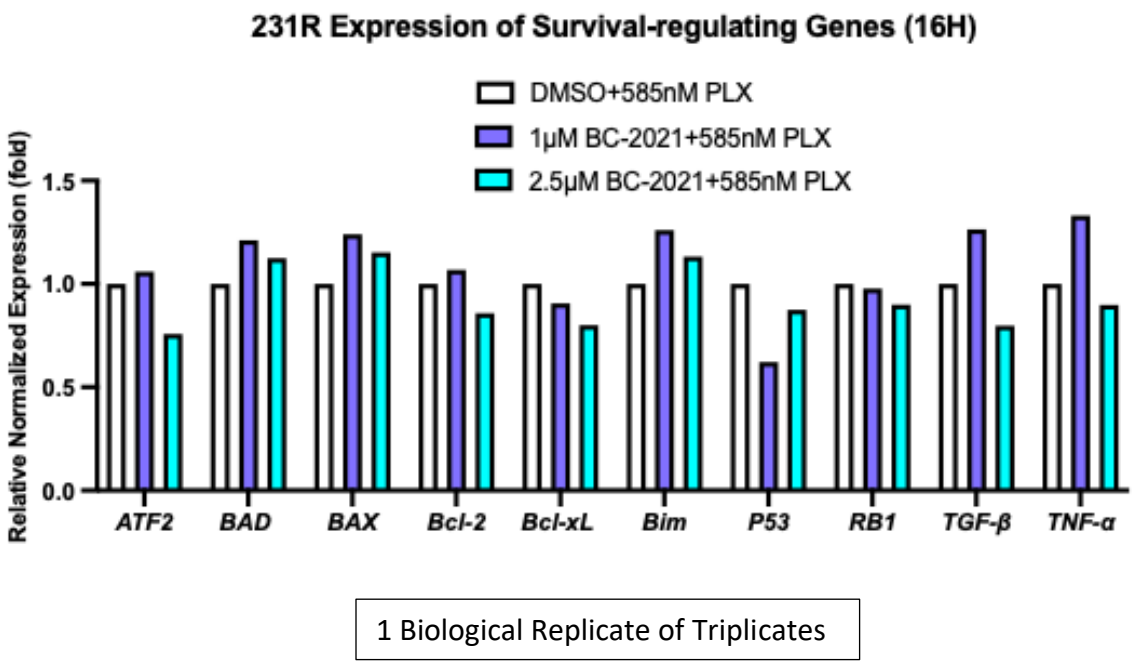


**Figure 3.5. Bcl-2 family genes and candidate survival-regulating genes are not prominent cell death mediators of 231R cells post-combinatorial drug treatment.** Relative level of expression of Bcl-2 family genes and other candidate survival-regulating genes extracted from 231R cells treated with 0, 1, and 2.5μM of BC-2021 in combination with 585nM of PLX. Gene expression level was assessed by RT-qPCR. DMSO and 585nM of PLX-treated cells were used for normalization. Data are expressed as the mean of triplicates in one biological replicate (n=1).

### 3.6 BC-2021 and PLX-mediated cell death does not involve induction of reactive oxygen species

Generated primarily as a by-product of mitochondrial oxidative phosphorylation, reactive oxygen species (ROS), such as superoxide anion ($O_2^-$), hydroxyl radical ($OH^{\cdot}$), and hydrogen peroxide ($H_2O_2$), carry out the critical roles of maintaining cellular redox balance, regulating cell cycle progression, and modulating immune responses at moderate levels (213-215). Excessive ROS reacts with organic substrates, including lipids, proteins, and DNA, leading to cell death (216). Strikingly, many chemotherapeutic agents, including paclitaxel, mediate cancer cell death by increasing ROS levels (217). To investigate whether ROS elevation served as the basis for drug-induced cell death, using ROS indicators, CM-$H_2$DCFDA (total ROS) and MitoSOX (mitochondrial ROS) for flow cytometry (Figure 3.6 A-B), we measured total cellular (tROS) and mitochondrial ROS (mROS) on live 231R and MCF7R cells following 8, 16, and 24 hours of treatment with either BC-2021 alone (Figure 3.6 C-D) or BC-2021 and PLX (Figure 3.6 E-F). Neither tROS nor mROS was up-regulated in live 231R and MCF7R cells following 0, 1, and 2.5µM of BC-2021 treatment alone over the 8, 16, and 24 intervals. Interestingly, even in the combinatorial regimen-treated 231R and MCF7R cells, we did not detect consistent and sustained upregulation of tROS and mROS, suggesting that overall ROS elevation did not serve as the primary mechanism leading to deaths of 231R and MCF7R cells following treatment with BC-2021 and PLX.

## A Positive Controls for tROS

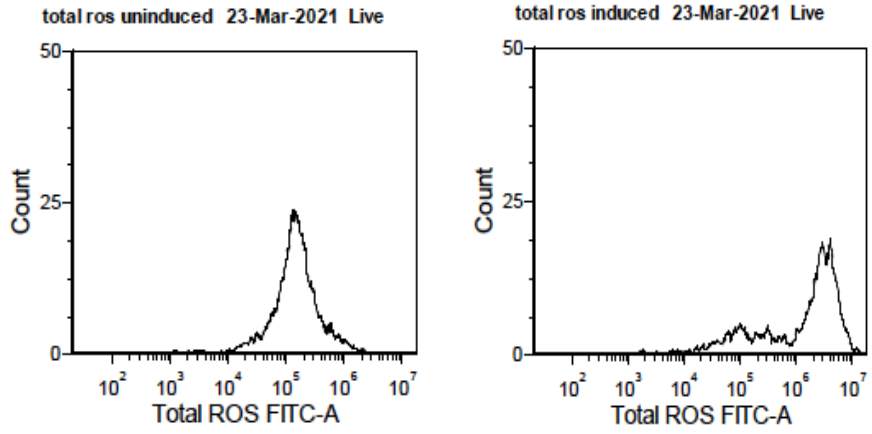


## B. Positive Controls for mROS

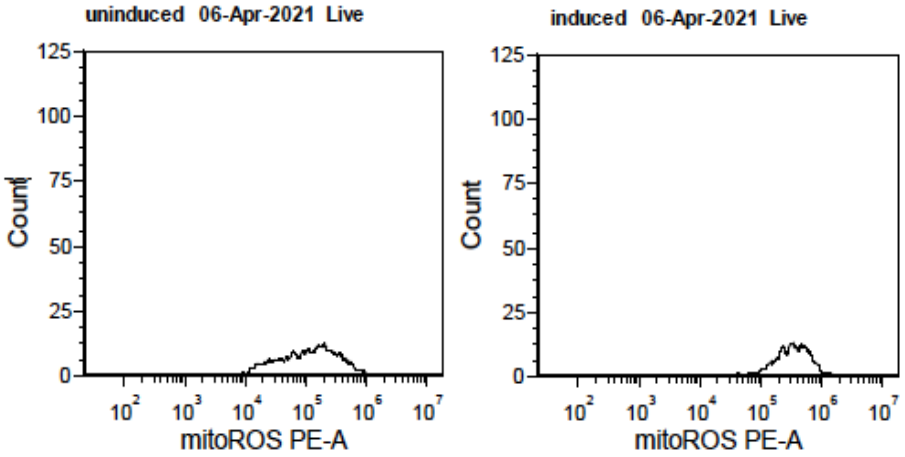

**C**

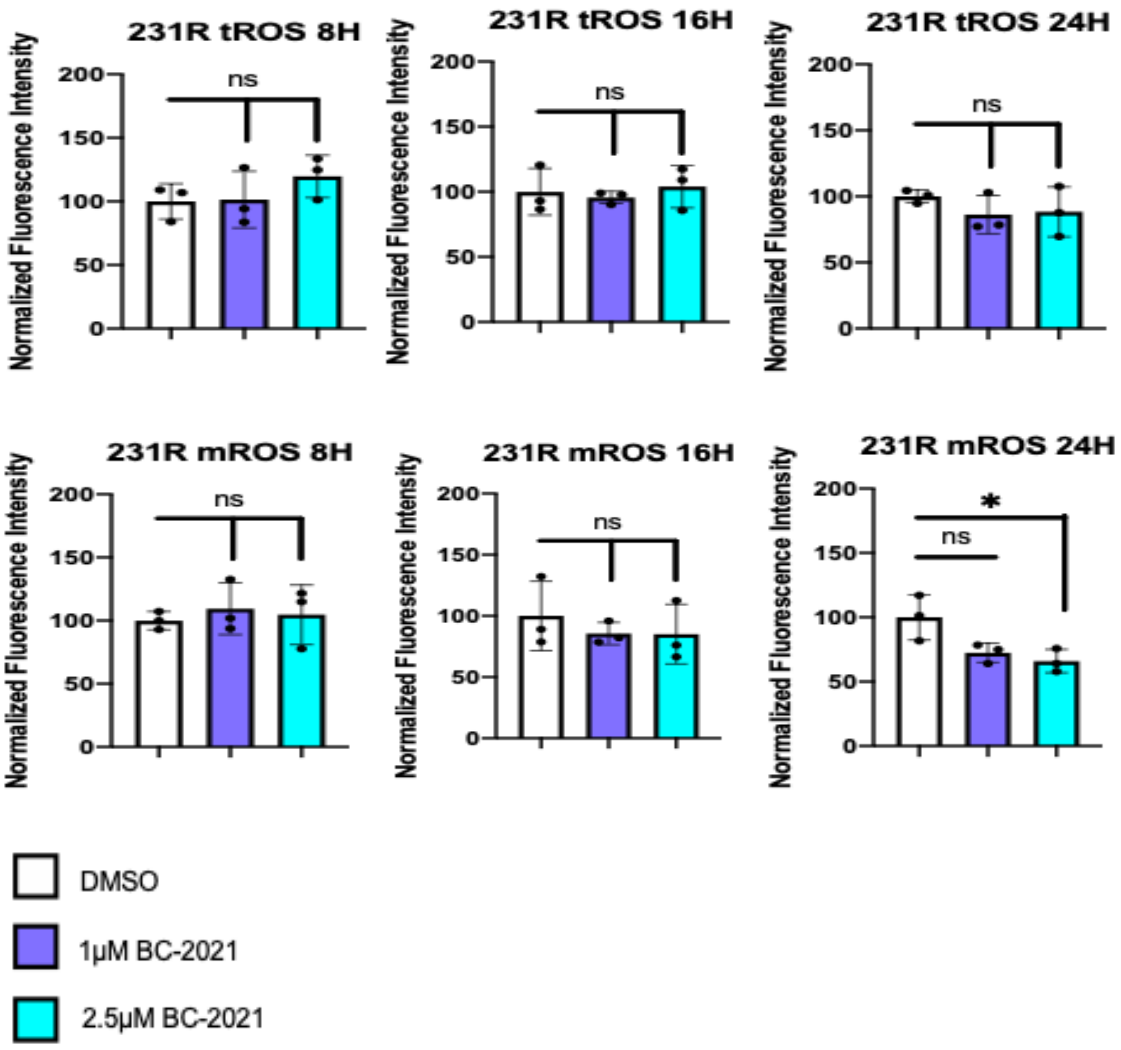
231R tROS 8H
231R tROS 16H
231R tROS 24H
231R mROS 8H
231R mROS 16H
231R mROS 24H
Normalized Fluorescence Intensity
ns
*
0
50
100
150
200
DMSO
1μM BC-2021
2.5μM BC-2021

**D**

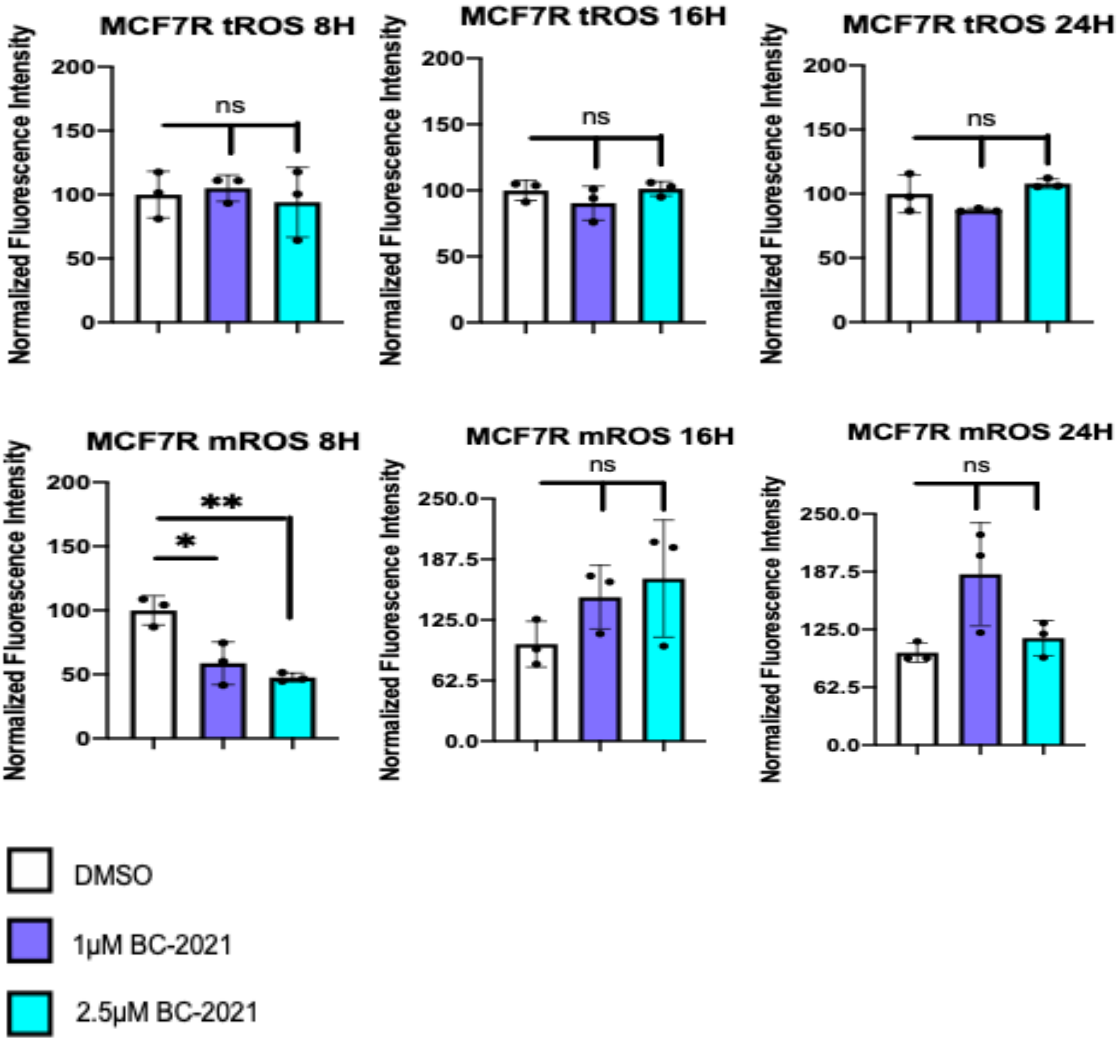
MCF7R tROS 8H
MCF7R tROS 16H
MCF7R tROS 24H
MCF7R mROS 8H
MCF7R mROS 16H
MCF7R mROS 24H
Normalized Fluorescence Intensity
ns
*
**
DMSO
1μM BC-2021
2.5μM BC-2021

E

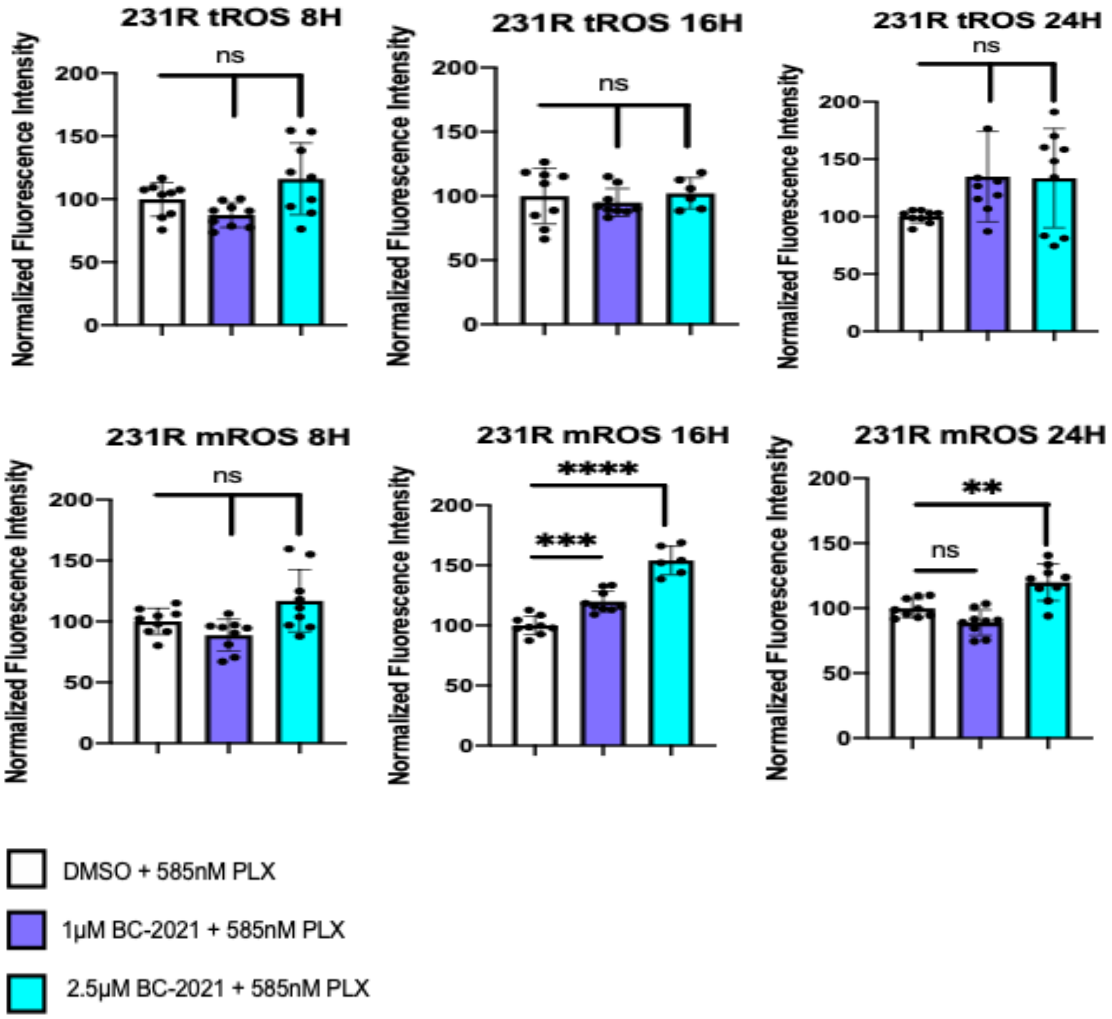
231R tROS 8H
231R tROS 16H
231R tROS 24H
231R mROS 8H
231R mROS 16H
231R mROS 24H
Normalized Fluorescence Intensity
ns
****
***
**
0
50
100
150
200
DMSO + 585nM PLX
1μM BC-2021 + 585nM PLX
2.5μM BC-2021 + 585nM PLX

**F**

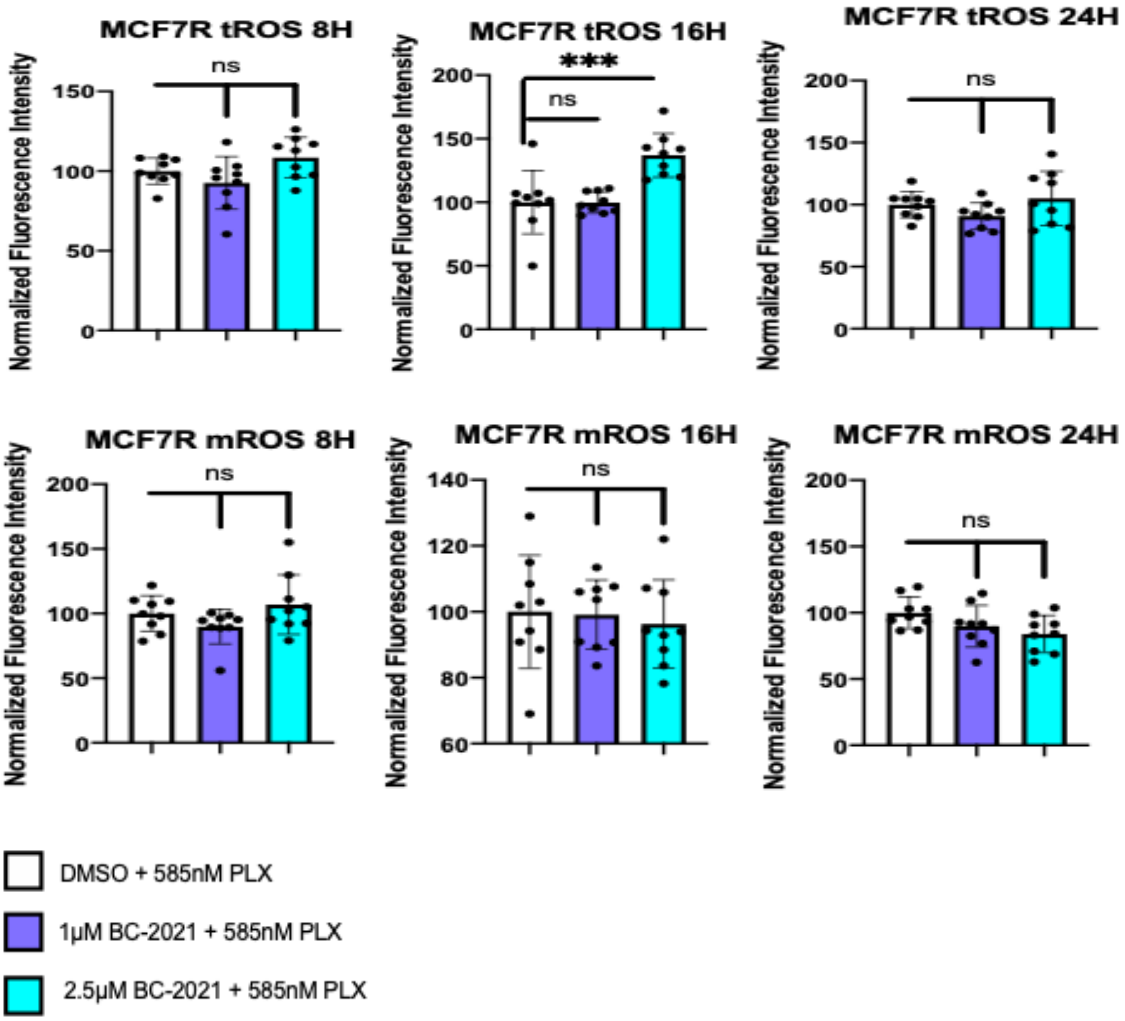
MCF7R tROS 8H
MCF7R tROS 16H
MCF7R tROS 24H
MCF7R mROS 8H
MCF7R mROS 16H
MCF7R mROS 24H
Normalized Fluorescence Intensity
ns
***
DMSO + 585nM PLX
1μM BC-2021 + 585nM PLX
2.5μM BC-2021 + 585nM PLX

**Figure 3.6. BC-2021 and PLX-treated 231R and MCF7R cells do not exhibit elevated ROS.** A) Histogram distribution of fluorescence intensity of total ROS-sensitive dye, CM-$H_2$DCFDA, and B) mitochondrial-ROS dye, MitoSOX Red, of uninduced and induced 231R cells according to 2.5.5 and 2.5.6 of Materials and Methods. Time-course flow cytometric measurements of tROS and mROS of live C) 231R and D) MCF7R cells following 8, 16, and 24 hours of BC-2021 treatment alone or (E-F) BC-2021 in combination with PLX. Despite statistically significant elevation of mROS in 231R cells following 24-hour treatment with 2.5μM BC-2021 and 585nM of PLX, the miniscule extent of ROS induction is not sufficient to account for the ensuing drastic cell death. Data are expressed as the mean ± s.d. of triplicates (n=3). NS indicates P>0.05, * indicates P ≤ 0.05, ** indicates P ≤ 0.01, *** indicates P ≤ 0.001, and **** indicates P ≤ 0.0001.

### 3.7 BC-2021 and PLX-treated 231R and MCF7R cells do not die through elevated nitric oxide

Through crosstalk with reactive oxygen species and induction of nitrosative stress, elevated nitric oxide (NO) and their chemical derivatives lead to DNA damage and cell death (218). To investigate whether NO upregulation underlies combination treatment-mediated cell death, 231R and MCF7R cells subjected to either BC-2021 alone or BC-2021 and PLX for 8, 16, and 24 hours were assessed for NO levels using flow cytometry (Figure 3.7. A-C). Compared to the vehicle control DMSO and 585nM PLX group, NO was not particularly upregulated, especially at the 8 and 16-hour drug treatment periods where pronounced cell death already began to occur, following treatment of 1µM and 2.5µM BC-2021 in combination with 585nM PLX, suggesting that NO elevation did not precede cell death and, therefore, was not likely to account for combinatorial drug-induced cell death.

**A Positive Control**

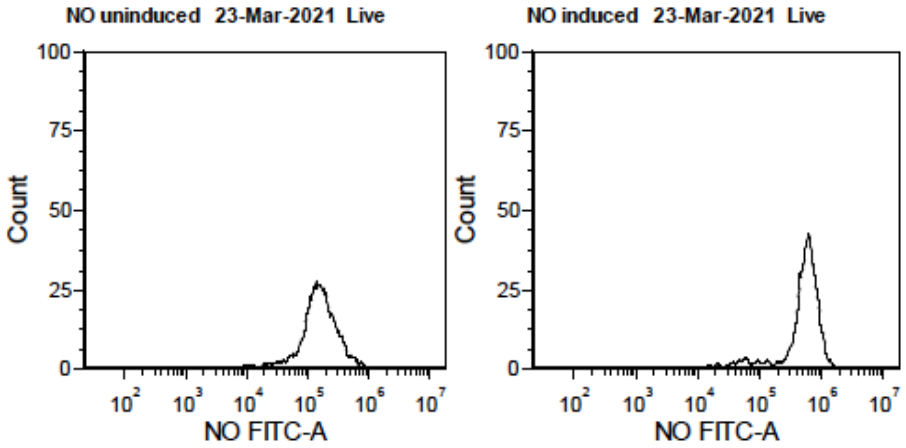


**B**

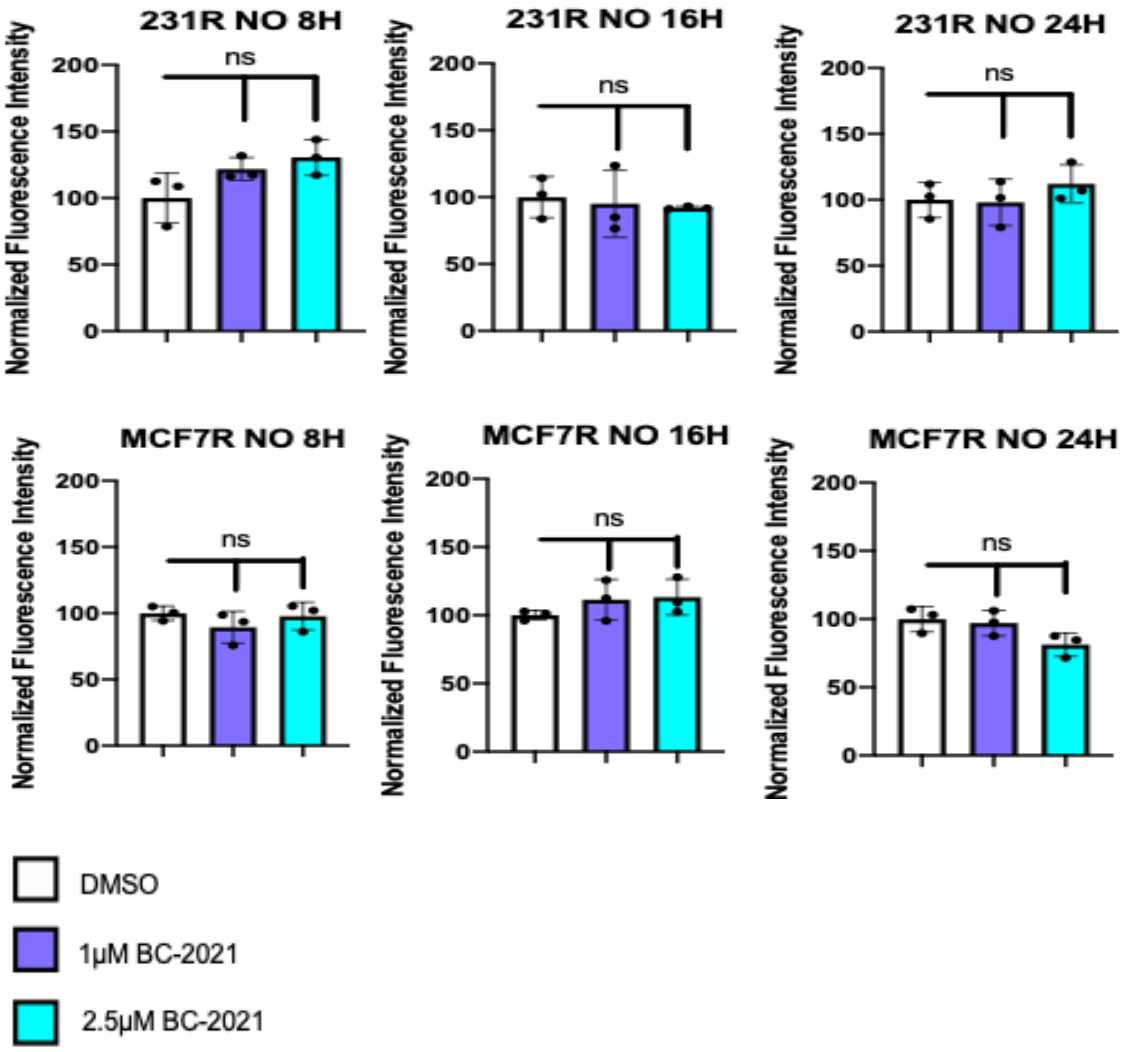

C

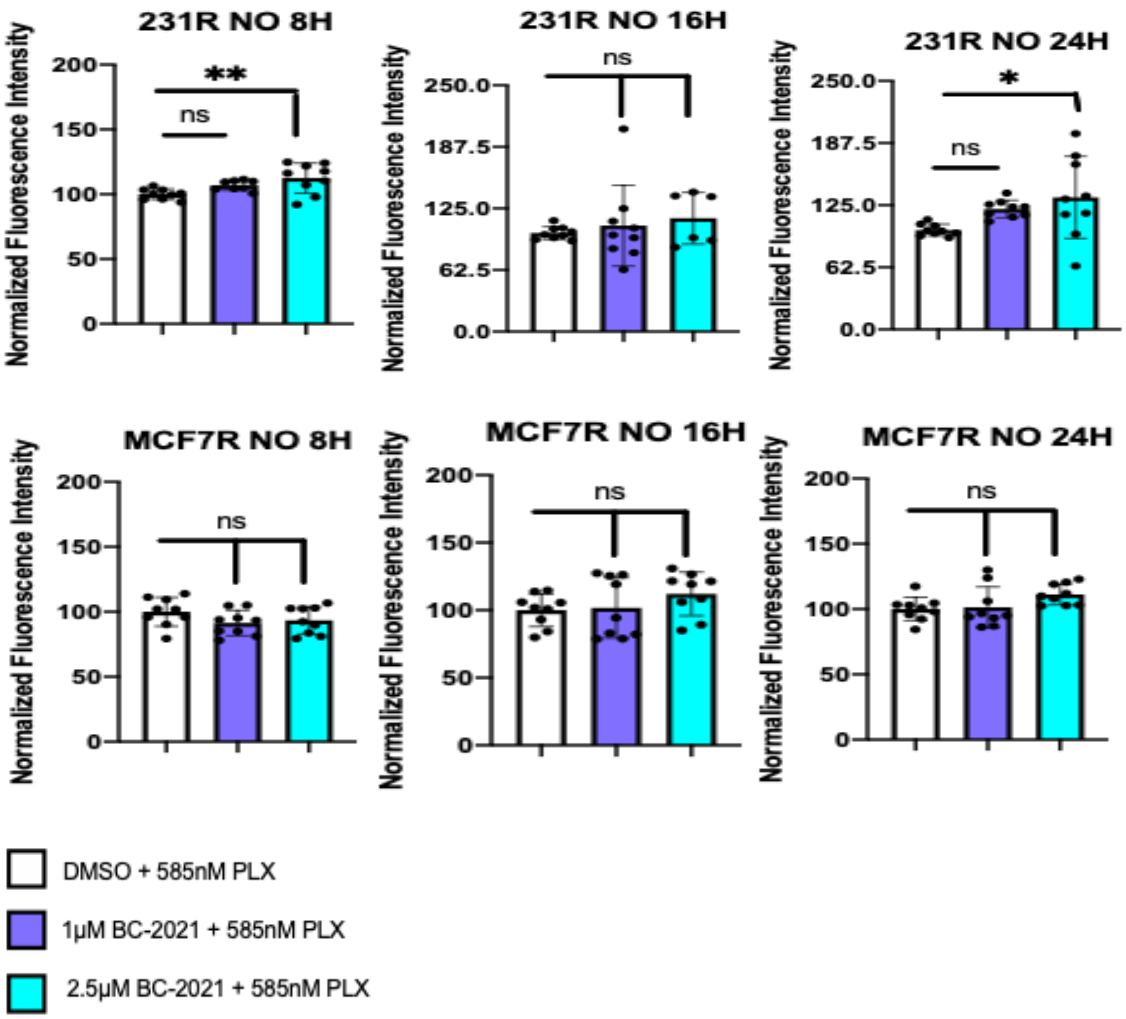
231R NO 8H
231R NO 16H
231R NO 24H
MCF7R NO 8H
MCF7R NO 16H
MCF7R NO 24H
Normalized Fluorescence Intensity
ns
**
*
DMSO + 585nM PLX
1μM BC-2021 + 585nM PLX
2.5μM BC-2021 + 585nM PLX

**Figure 3.7 BC-2021 and PLX-treated 231R and MCF7R cells do not die through elevated nitric oxide.** A) Histogram distribution of fluorescence intensity of the NO-sensitive dye, DAF-FM Diacetate, on untreated 231R cells and 231R cells induced for NO according to 2.5.7 of Materials and Methods. B) 8, 16, and 24-hour BC-2021 treatment alone did not induce NO level on 231R and MCF7R cells, so did C) combinatorial treatment with BC-2021 and 585nM of PLX, suggesting that NO upregulation was not chiefly responsible for combinatorial drug-induced cell death. Data are expressed as the mean ± s.d. of triplicates (n=3). NS indicates $P>0.05$, * indicates $P \leq 0.05$, and ** indicates $P \leq 0.01$.

### 3.8 BC-2021 treatment alone attenuates autophagy in 231R and MCF7R cells

Autophagy has been dubbed as a double-edged sword in regulating cell viability. Sufficient autophagy recycles biomolecules to sustain cellular bioenergetics. Excessive autophagy, however, may result in autophagic cell death, where cytoplasmic content collapses and becomes chemically degraded (219). Reducing autophagy, on the other hand, has been adopted as a functional basis for the design of chemo-sensitizers to combat drug-resistant cancers as attenuated autophagic degradation machineries are linked to increased cytoplasmic bioavailability of chemotherapeutic agents (220, 221). To determine whether autophagic dysregulation mediates drug-induced cell death, we monitored cellular autophagy on 231R and MCF7R cells following 8, 16, and 24 hours of BC-2021 treatment alone (Figure 3.8 A) or BC-2021 in combination with PLX (Figure 3.8 B) using autophagy dye-based flow cytometry. Interestingly, we demonstrated that BC-2021, on its own, impairs autophagy in both 231R and MCF7R cells 24 hours post-treatment. This reduction in autophagy was, however, not evident in 231R cells but was observed in MCF7R cells post-combinatorial treatment with BC-2021 and PLX, suggesting the likely differential regulation of autophagy across hormone-receptor and negative breast cancer subtypes. Nevertheless, BC-2021 treatment alone attenuated cellular autophagy in both 231R and MCF7R in a time-dependent manner, suggesting that autophagy inhibition may be one, among many other means, that contributed to reversal of chemoresistance.

**A**

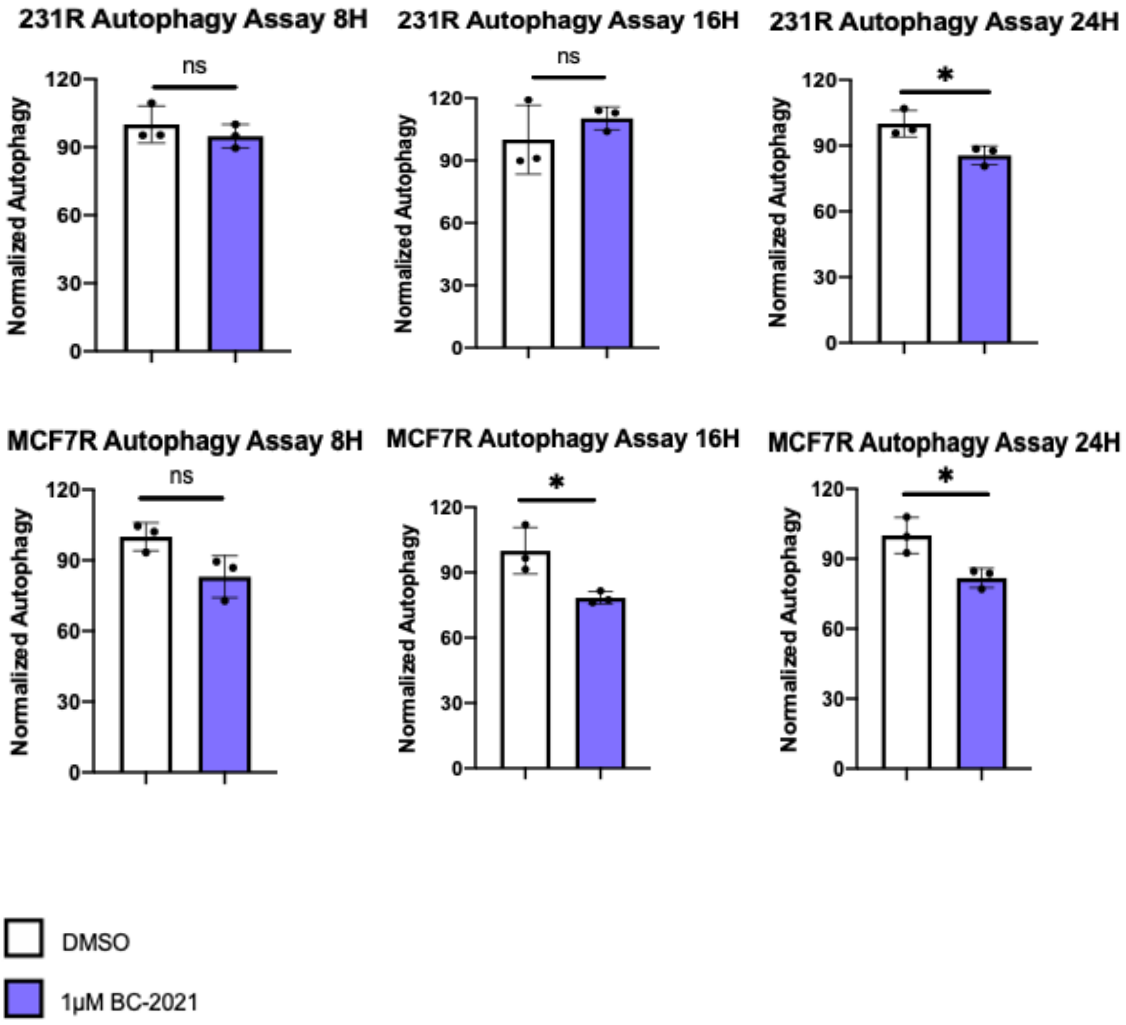
231R Autophagy Assay 8H
231R Autophagy Assay 16H
231R Autophagy Assay 24H
MCF7R Autophagy Assay 8H
MCF7R Autophagy Assay 16H
MCF7R Autophagy Assay 24H
Normalized Autophagy
ns
*
0
30
60
90
120
DMSO
1μM BC-2021

**B**

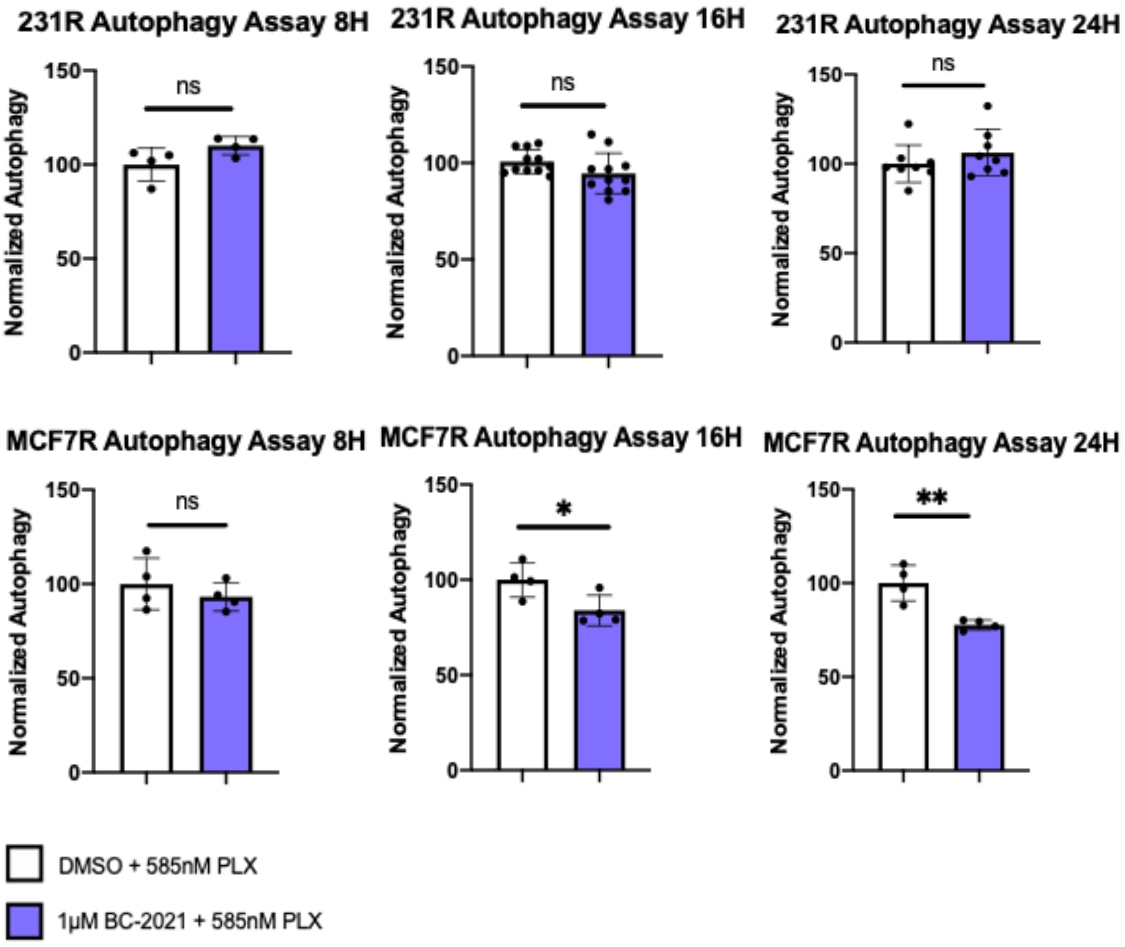
231R Autophagy Assay 8H
231R Autophagy Assay 16H
231R Autophagy Assay 24H
MCF7R Autophagy Assay 8H
MCF7R Autophagy Assay 16H
MCF7R Autophagy Assay 24H
Normalized Autophagy
150
100
50
0
ns
*
**
DMSO + 585nM PLX
1μM BC-2021 + 585nM PLX

**Figure 3.8. BC-2021 alone attenuates autophagy in 231R and MCF7R cells.** Cellular autophagy was monitored using an autophagic vacuole-selective dye through time-course flow cytometry on 231R and MCF7R cells treated with BC-2021 alone or BC-2021 in combination with PLX over 8, 16, and 24 hours. A) 1µM of BC-2021 alone attenuates autophagic activity of both 231R and MCF7R cells. B) Combinatorial administration of 1µM BC-2021 and 585nM PLX left no impact on autophagy in 231R cells over the 24-hour window but decreased autophagic activity in MCF7R cells 16 and 24 hours of drug treatment, suggesting possible differential regulation of autophagy across triple-negative and receptor-positive breast cancer cells. Data are expressed as the mean ± s.d. of triplicates (n=3). NS indicates $P>0.05$, * indicates $P \leq 0.05$, and ** indicates $P \leq 0.01$.

### 3.9 BC-2021 and PLX collectively induces drastic G2/M phase cell cycle arrest on 231R and MCF7R cells

Cellular survival and proliferation requires controlled progression of cell cycle. Perturbations of cell cycle can lead to cell death (222). To assess the functional regulation of cell cycle post-drug treatment, we compared cell cycle progression of live 231R and MCF7R cells treated with either BC-2021 alone to that of cells treated with BC-2021 in combination PLX for 24 hours by monitoring the population-wide distribution of the fluorescence intensity of propidium iodide, a DNA-intercalating agent. BC-2021 alone did not alter cell cycle progression (Figure 3.9 A), however, when in combination with PLX, BC-2021 induced drastic G2/M phase cell cycle arrest on both 231R and MCF7R cells in a dose-dependent manner (Figure 3.9 B). Notably, following 24-hour treatment with 2.5μM of BC-2021 and 585nM of PLX, roughly 80% of live cells underwent G2/M phase cell cycle arrest, the magnitude of which was in concomitance with the extent of cell death observed at later time point. Collectively, cell cycle arrest at the G2/M phase served as a critical mechanism underlying combinatorial drug therapy-mediated cell death.

A

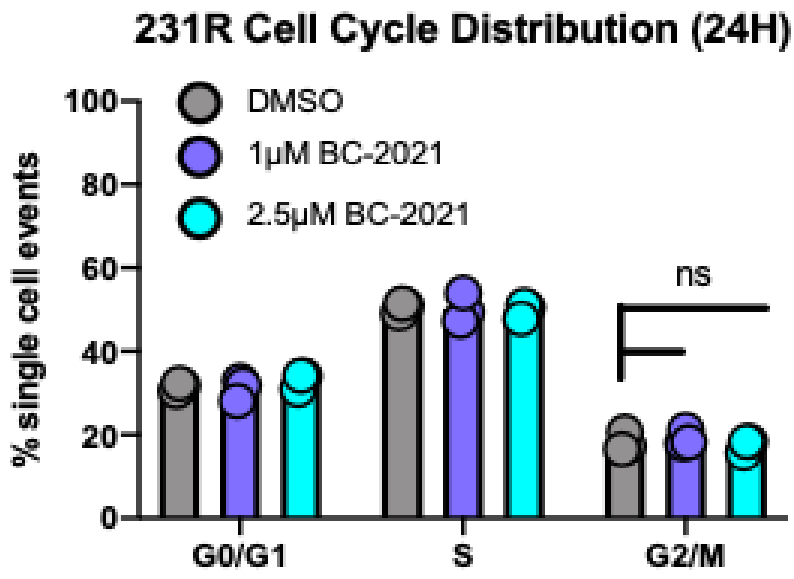
231R Cell Cycle Distribution (24H)
% single cell events
100
80
60
40
20
0
DMSO
1μM BC-2021
2.5μM BC-2021
ns
G0/G1
S
G2/M

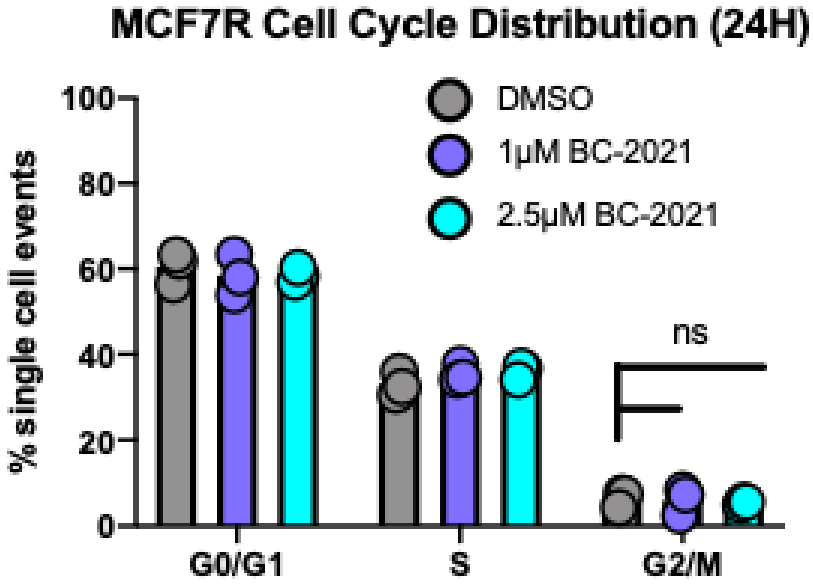
MCF7R Cell Cycle Distribution (24H)
% single cell events
100
80
60
40
20
0
DMSO
1μM BC-2021
2.5μM BC-2021
ns
G0/G1
S
G2/M

**B**

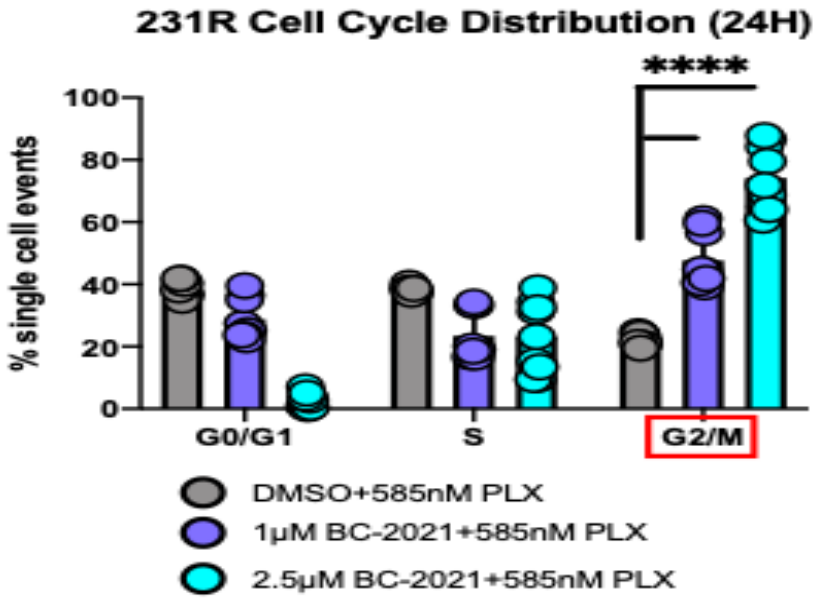
231R Cell Cycle Distribution (24H)
****
% single cell events
100
80
60
40
20
0
G0/G1
S
G2/M
DMSO+585nM PLX
1μM BC-2021+585nM PLX
2.5μM BC-2021+585nM PLX

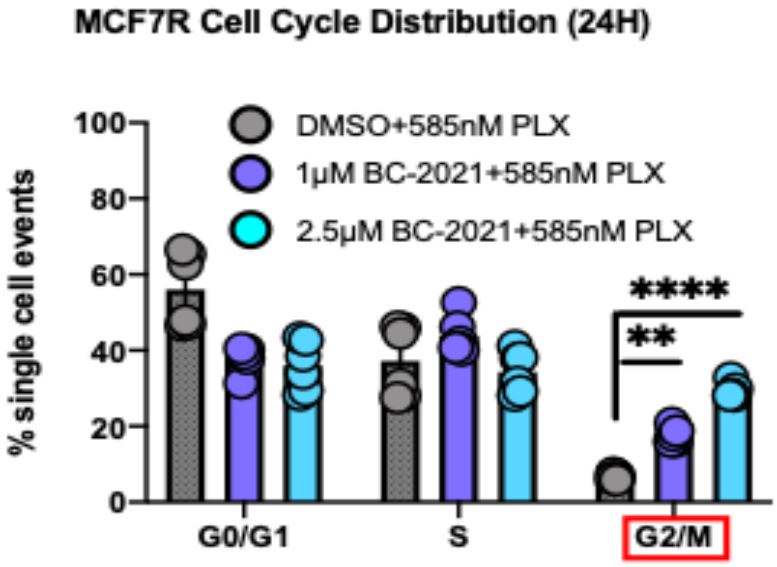
MCF7R Cell Cycle Distribution (24H)
DMSO+585nM PLX
1μM BC-2021+585nM PLX
2.5μM BC-2021+585nM PLX
% single cell events
100
80
60
40
20
0
****
**
G0/G1
S
G2/M

**Figure 3.9 BC-2021 and PLX treatment leads to substantial G2/M phase cell cycle arrest in 231R and MCF7R cells.** Cells were incubated with various drug regimen for 24 hours before being co-stained with eFluor™ 780 Fixable Viability dye as well as propidium iodide and analyzed via flow cytometry. A) BC-2021 treatment alone did not impact 231R and MCF7R cell cycle progression. B) Extensive G2/M phase cell cycle arrest was detected in 231R and MCF7R cells treated with combinatorial regimen consisting of 1μM or 2.5μM of BC-2021 and 585nM PLX. Data are expressed as the mean ± s.d. of triplicates (n=3). NS indicates $P>0.05$, ** indicates $P \leq 0.01$, and **** indicates $P \leq 0.0001$.

# CHAPTER 4 Conclusion

## 4.1 Discussion

Our work provides *in vitro* insights into a novel combination regimen consisting of 1μM of BC-2021, a chemo-sensitizer, and 585nM of PLX, the gold-standard chemotherapeutic agent indicated for advanced breast cancer patients, in the management of multidrug-resistant hormone receptor-positive (MCF7) and triple-negative (MDA-MB-231) breast cancer cells. Through cell counting and flow cytometric analysis, the concurrent administration of 1μM of BC-2021 and 585nM of PLX exerted potentiated acute (≤72 hours) and prolonged (14 days) cytotoxicity on drug-resistant breast cancer cells than either drug alone. Notably, we determined that cell cycle abnormality, particularly G2/M phase cell cycle arrest, served as the principal mediator leading to drug-induced apoptosis and its associated nuclear fragmentation.

Our study revealed that drug-resistant breast cancer cells exposed to 24-hour treatment with BC-2021 and PLX underwent systemic G2/M phase cell cycle arrest, the degree of which was comparable to that of cell death obtained through cell counting experiments. In agreement with our results, Hwang and colleagues observed sustained G2/M phase cell cycle arrest in concomitance with DNA damage in cisplatin-resistant epithelial ovarian cancer cells subjected to cisplatin treatment in combination with the chemosensitizer chloroquine (223). Furthermore, Sanchez-Carranza and colleagues discovered that Achillin could enhance the chemosensitivity of drug-resistant hepatocellular carcinoma cells to PLX and potentiate its effect on G2/M phase cell cycle arrest (224). It is worth mentioning that this G2/M phase cell cycle arrest was observed

with high concentration of chemosensitizer (100µM of Achillin) and low dosage (25nM) of PLX as opposed to a low dosage of chemosensitizer (1µM of BC-2021) and high concentration (585nM) of PLX as was the case in our study. These findings collectively demonstrate the critical need of proper cell cycle regulation in supporting cell survival and the ubiquity of G2/M phase cell cycle arrest in mediating drug-induced cell death. Conversely, our finding, however, differs from Vinod and colleagues' work, where resveratrol, along with docetaxel, another taxane with similar anti-tumor spectra as PLX, induced sub-G0 phase accumulation and chemo-sensitized HER2-overexpressing breast cancer cells to docetaxel challenge (225). Such difference can be explained by the drastically lower dosages of docetaxel utilized by Vinod and colleagues during cell cycle analysis, offering a contextualized landscape for the interpretation of cell cycle abnormality in response to drug treatment. Indeed, in agreement with this interpretation, high dosages (100nM) of docetaxel lead to G2/M phase cell cycle arrest in breast cancer cell lines, whereas lower dosages (2-4 nM) generally target other cell cycle stages (226). As a result, our and similar studies collectively illustrate that though chemo-sensitizers and chemotherapeutics utilized in anti-cancer regimens differ, the extent of cell cycle arrest can eventually converge based on the dosages of chemosensitizers and chemotherapeutics administered, offering flexibility in prescribing therapeutics to combat multidrug resistance.

Further, based on flow cytometric analysis of FITC-Annexin V and PI, we demonstrated drug-resistant cells treated with BC-2021 and PLX underwent enhanced apoptosis, rather than other forms of cell death, compared to treatment with either BC-

2021 or PLX alone. The biochemical basis of intrinsic apoptotic cell death begins with cellular insults that lead to loss of mitochondrial integrity, permeability, and subsequent activation of caspases followed by caspase-mediated disintegration or fragmentation of subcellular organelles (227, 228). To enhance the cytotoxic mechanisms of action of existing chemotherapeutic compounds, most chemosensitizers act by tilting the balance of survival-regulating proteins towards apoptotic promotion, rendering drug-resistant cells more susceptible to the initiation of apoptosis. This concept is shown by the work of Cheng and colleagues', where ferulic acid, a bioactive compound found in cereal grains and Chinese herbs, enhances epirubicin-mediated apoptosis by increasing the ratio of pro-apoptotic protein, Bax, to anti-apoptotic protein, Bcl-2, in triple-negative breast cancer cells (229, 230). Working with nasopharyngeal carcinoma cells, Zhou and colleagues also discovered identical mechanism of reverting apoptotic resistance using astragalus polysaccharides and cisplatin, implicating the dysregulated Bax to Bcl-2 ratio in conferring apoptotic resistance in diverse cancers (231). These studies are in line with the macroscopic trend we observed through our preliminary qPCR experiments, indicating potentially increased expression of pro-apoptotic genes, such as *Bax*, *Bad*, and *Bim*, while showing relatively stable and slightly diminished expression of anti-apoptotic genes, such as *Bcl-2* and *Bcl-xL* post-combinatorial drug treatment. However, it is worth noting that the extent of upregulated expression of pro-apoptotic genes and the downregulation of anti-apoptotic genes in our study was rather miniscule compared to those of *Cheng et al.* and *Zhou et al*.. Such discrepancy could be partially accounted by the relatively intensive dosage of PLX being administered onto even the vehicle-control

cells, leaving little room for transcriptional alterations of survival-regulating genes to take place before sizeable cell death takes over. Treating cells with a lower dosage of PLX as part of the combinatorial regimen over a longer treatment period may offer a more stabilized or controlled environment for the measurement of the ratio of *Bax* to *Bcl-2*. Interestingly, while most chemosensitizers act by increasing the propensity of resistant cancer cells to apoptosis, Lin and colleagues' work revealed that graphene oxide, a nanomaterial, sensitizes CT26 colon cancer cells to cisplatin by provoking primarily necrotic cell death likely through non-canonical autophagy-dependent processes (232). This atypical necrotic mode of cell death, albeit contradictory to our results, exemplifies the versatility, complexity, and abundant points of interventions for chemo-sensitization to take place.

Moreover, the advantage of our chemo-sensitizer, BC-2021, in comparison to many of the chemo-sensitizers mentioned previously, graphene oxide, for instance, is its superior safety profile (233). Indeed, our results indicated that treatment with low micro-molar BC-2021 had minimal cytotoxicity on non-cancerous MCF10A breast epithelial cells and BHK kidney fibroblasts over 72 hours. This finding was particularly encouraging as it served as a solid basis for further *in vivo* toxicity assessment of BC-2021.

Lastly, to contextualize our results, it is critical to recognize that our work was built upon a two-dimensional *in vitro* setting, where drug-resistant breast cancer cells were cultured in the form of platted sheets deprived of stromal interactions and endocrine signaling as in the case of an *in vivo* environment (234). Even though we

reported drastic and sustained combination regimen-mediated cytotoxicity against resistant breast cancer cells, our mechanistic understanding was, after all, limited, and questions remained on the penetration, efficacy, tolerance, and utility of our combinatorial regimen in three-dimensional *in vivo* models.

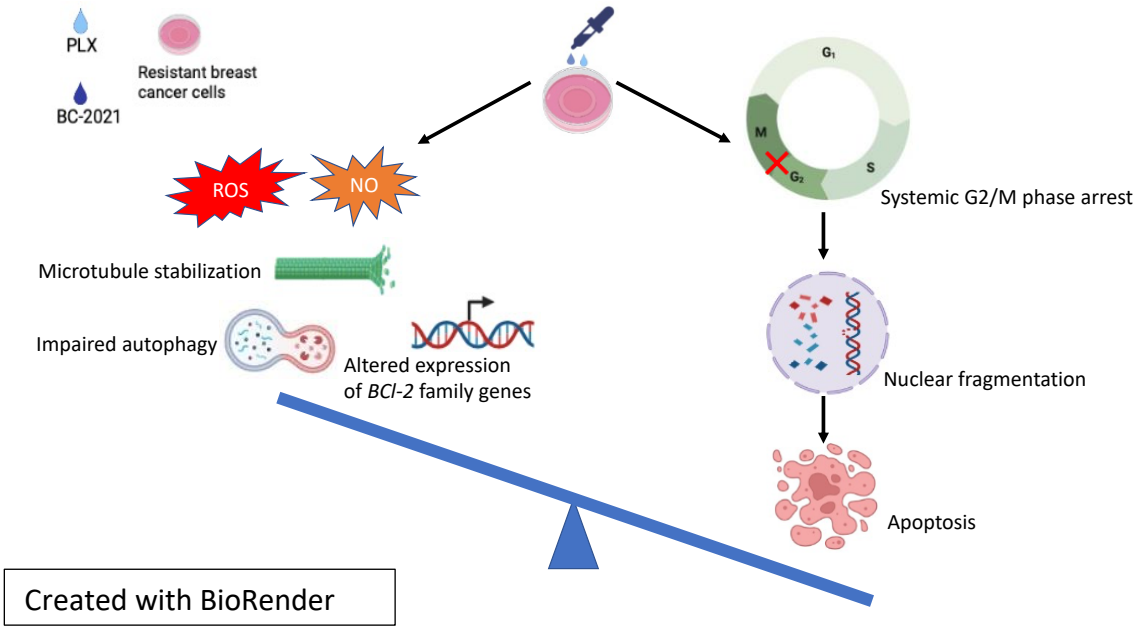


**Figure 4.1. Schematic summary of the combinatorial regimen consisting of BC-2021 and PLX and its principal mode of cytotoxicity**. Concurrent treatment of drug-resistant breast cancer cells with 1µM of BC-2021 and 585nM of PLX resulted in acute apoptosis that is independent of ROS and NO induction, microtubule stabilization (Appendix Figure 2), autophagic impairment, and altered expression of the *Bcl-2* family genes. Cell cycle analysis revealed global G2/M phase cell cycle arrest upon incorporation of BC-2021 into PLX treatment, resulting in nuclear fragmentation and subsequent apoptosis of drug-resistant breast cancer cells. To conclude, our research identified that 1µM of BC-2021 and 585nM of PLX induce apoptosis through cell cycle arrest, the effect of which outweighs other potential mediators of cell death.

## 4.2 Limitations

### 4.2.1 Limited control panels

The control experiments described in this thesis suffer from two sources of limitations – the absence of PLX-alone control group and high dosage of PLX used as part of the combinatorial regimen.

For a thorough layout of control conditions for the cell counting, colony assay, cell cycle analysis, ROS as well as NO measurements, and confocal microscopy, we should have also tested the effects of PLX alone without the addition of the DMSO vehicle control. Even though administering 585nM of PLX to resistant breast cancer cells would not cause drastic cell death over at least 24 hours, there may be background effects on cell cycle regulation, ROS, NO, and microtubule stabilization in comparison to the untreated cells. Being able to take background effects into consideration when analyzing data across experimental groups helps elucidate how these parameters could be affected by the combinatorial regimen.

Furthermore, the 585nM of PLX used in the combinatorial regimen may not represent the most ideal dosage for biochemical studies, providing limited context for understanding the biological processes potentially perturbed by the combinatorial regimen. The levels of NO, total, and mitochondrial ROS often increase in cancer cells upon PLX challenge (235-237). The fact that 1μM of BC-2021 and 585nM of PLX led to roughly 25% cell death following 24 hours of drug treatment but failed to induce significantly higher levels of ROS and NO compared to those of the vehicle control (DMSO+585nM PLX) group suggests that cells were already experiencing the highest

possible ROS and NO when treated with DMSO+585nM PLX and that even the tiniest increase of ROS and/or NO may lead to cell death. Indeed, these drug-resistant cells, were only able to endure up to 585nM of PLX challenge without exhibiting significant decline in viability. In alignment with the MTT assay measuring cell viability in response to PLX challenge, 585nM of PLX demarcated the cell viability threshold. Had the flow cytometry staining of NO and ROS been conducted on resistant cells treated with lower concentrations of PLX, there would have been a significant increase in ROS and NO levels upon introducing BC-2021.

### 4.2.2 Primitive RT-qPCR results

Though performed in three technical replicates, the RT-qPCR experiment was conducted only on one biological sample. As a result, the validity of the data is weak. In addition, since paclitaxel can enter the cell either through passive diffusion across the plasma membrane or through OATP transporters as described in the Introduction section 1.3.2.1, gene expression profiles of various members of the OATP family transporters along with efflux transporters should also be conducted and repeated on three biological specimens of resistant breast cancer cells to speculate on the disposition and transport of PLX.

### 4.2.3 Incomprehensive assessment of autophagy

Autophagy plays a cytoprotective role during PLX challenge (238, 239). Our flow cytometry staining of an autophagy-specific dye indicated that 24-hour treatment of

1µM of BC-2021 impaired overall autophagy of resistant breast cancer cells, which was likely to set the stage for enhancing PLX-mediated cell death due to the abrogation of cytoprotective autophagy. To make a stronger case of this, it is necessary to conduct Western blotting and RT-qPCR on markers of autophagy, such as microtubule-associated protein light chain 3 I (LC3 I) and II (LC3 II) and autophagy-related proteins (ATGs) (240). Furthermore, modulation of autophagy through siRNA-mediated genetic knockdown or overexpression of these autophagy markers may be used as a validatory step to either enhance or attenuate BC-2021-mediated synergy of PLX response of resistant breast cancer cells, respectively. Alternatively, to determine whether attenuated autophagy, presumably due to BC-2021 administration, may lead to increased cytoplasmic PLX content, studying the intracellular trafficking and deposition of PLX using fluorescent paclitaxel derivative Flutax-1 (Green) may be of interest for future studies (241).

### 4.2.4 Insufficient validation of microtubule dynamicity

The primary investigative endpoint used to quantify the extent of microtubule stabilization in this thesis is mean fluorescence intensity of exogenously stained tubulin proteins as tubulin stabilization is often manifested in stronger tubulin staining in other studies (242, 243). Other recognized markers of stabilized microtubules include acetylated tubulin and de-tyrosinated tubulin (244, 245). These post-translational modifications of the microtubules can be detected via Western blot. Had these Western blots been conducted along with confocal microscopy imaging of microtubules, there

would have been more clues as to whether microtubule stabilization contributed to the death of multi-drug resistant breast cancer cells treated with BC-2021 and PLX.

### 4.3 Future Directions

Throughout this project, various attempts were made to explore potential subcellular pathways through which BC-2021 in combination with PLX act to kill multi-drug resistant breast cancer cells. This effort started with a preliminary qPCR screen for candidate genes regulating cell survival. When none of the candidate genes seemed to be significantly biologically upregulated or downregulated in an explicit dose-dependent manner, generic mediators of cell death, such as NO, total, and mitochondrial ROS, were assessed. These attempts neither defined a specific subcellular pathway nor elucidated a subcellular target of the combinatorial drug regimen, rendering the lack of mechanistic insights a jarring weakness of this work. Herein, we propose several directions on which future work can focus.

#### 4.3.1 Assessment of membrane transporters in therapeutic resistance

As mentioned in 1.3.2.1, aberrant membrane transporters are fundamental to drug resistance in breast cancer. These membrane transporters mainly fall into the solute carrier (SLC) and ABC superfamilies, mediating the influx and efflux for a broad spectrum of substrates, respectively (246). Future studies should focus on investigating the functional correlation between the expression as well as activity of these

transporters and sensitivity to therapy. To execute this goal, future experiments could implement micro-array analyses of SLC and ABC family transporters in conjunction to published large-scale datasets on drug resistance, such as the Cancer Cell Line Encyclopedia and the Catalogue of Somatic Mutations in Cancer (247-250). Furthermore, future studies can also incorporate biophysical approaches by utilizing fluorescent tracer dyes, such as rhodamine and acetoxymethyl calcein, to measure the kinetics of SLC and ABC transporters across drug-sensitive and resistant cells (251, 252).

### 4.3.2 Transcriptomic profiling of multidrug-resistant breast cancer cells

Functional genomics may offer robust mechanistic insights into transcriptional alterations associated with acquired chemoresistance. Differentially expressed transcripts in drug resistant breast cancer cells can be identified and subsequently clustered by *DESeq2* Bioconductor (253). Clustered datasets can then be fed into gene set enrichment analysis (GSEA) to further identify the most impacted cellular pathways across different biological states. A significant advantage of using GSEA is that it does not set a “threshold value” in defining whether genes are significantly altered or not, allowing a holistic evaluation of gene enrichment in a specific biological context (254). This genomic pipeline is critical as it can not only reveal transcriptional alterations associated with multi-drug resistance but also reveal cellular targets of BC-2021 in restoring the chemosensitivity of previously resistant cancer cells.

### 4.3.3 3D spheroids for drug efficacy and toxicity characterization

Even though *in vitro* experiments confirmed that 1μM of BC-2021 and 585nM of PLX induced potent cytotoxicity against resistant breast cancer cells, this did not guarantee that the combinatorial drug regimen would work in a three-dimensional solid tumor mass or in the actual bodily tumor microenvironment. It may be of interest to establish and cultivate 3D spheroid models to assess the penetration, bioavailability, toxicity, and efficacy of BC-2021 alone before transitioning to *in vivo* studies.

### 4.3.4 Patient-derived xenograft as *in vivo* model

As directly implanting established human cancer cell lines, which have adapted to *in vitro* growth, into immunodeficient mice does not embody clinical characteristics of cancer due to the lack of proper tumor microenvironment and texture, obtaining and culturing original biopsy or surgical resections of human tumor specimens as patient-derived xenografts (PDX) serves as a more representative method for preclinical drug validation (255). PDX models are excellent sources for predicting and characterizing drug efficacy and response, offering a route toward personalized treatment (256). As PDX models have been previously adopted in research on breast cancer therapeutic resistance, future research may employ such *in vivo* model (257).

### 4.3.5 Drug-drug interactions and pharmacokinetics

This research proposes that the combination of BC-2021 and PLX effectively targets drug-resistant breast cancer cells; however, it is possible that other conventional chemotherapeutic agents can also have synergistic effects in killing resistant cancer cells when being combined with BC-2021. An *in vitro* screen coupled with Combination Index analysis may provide preliminary insights on this question (258). In addition to uncovering the mechanism of action, or the pharmacodynamic properties, of BC-2021 and PLX in overcoming drug resistance, future research should also strive to understand the metabolism and excretion of the drug combination through different routes/sites of administration. To determine the therapeutic potential of our combination regimen, an understanding of the half-life, bioavailability, and potential interaction with drug-metabolizing enzymes, such as the cytochrome P450 superfamily enzymes, *in vivo* is required. These insights will serve as strong foundation for future predictive work evaluating patient response and the design of individualized anti-cancer therapy for not just breast cancer but also potentially other cancers.

## Appendix

### The cytotoxic profile BC-2021 on non-cancerous mammalian cell lines

To establish a preliminary toxicity profile of BC-2021 *in vitro*, various micromolar dosages of BC-2021 alone were administered to non-cancerous mammalian cell lines, MCF10A (Non-tumorigenic Human Breast Epithelium) and BHK (Baby Hamster Kidney fibroblasts). Cell counting following 24, 48, and 72-hr incubation indicates that BC-2021 is not acutely cytotoxic on MCF10A and BHK cells at the 1µM concentration (Appendix Figure 1).

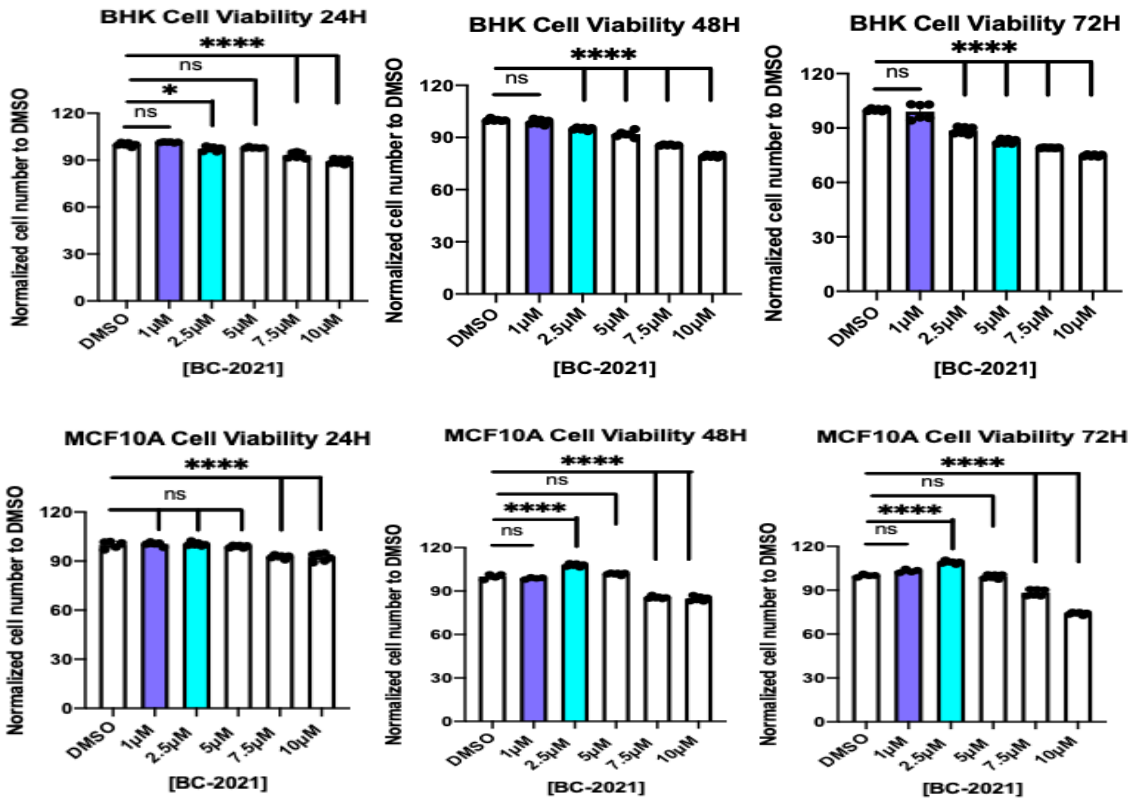


**Appendix Figure 1. 1μM of BC-2021 was not toxic to non-cancerous MCF10A and BHK cells.** Micromolar ranges of BC-2021 were tested on two non-cancerous mammalian cell lines. Interestingly, incubation with 1 μM of BC-2021 did not lead to cell MCF10A and BHK cell death within the 72-hour treatment period. Data are expressed as the mean ± s.d. of triplicates (n=3). NS indicates P>0.05 and **** indicates P ≤ 0.0001.

**BC-2021 and PLX combinatorial regimen does not enhance microtubule stabilization**

Microtubules dynamically regulate cell division and shape. As mentioned previously, PLX inhibits microtubule dynamicity and promotes microtubule stabilization, resulting in apoptotic cell death. While culturing 231R and MCF7R cells, we discovered that cells shrunk in response to PLX treatment alone and the combination of BC-2021 and PLX. To evaluate whether BC-2021 increased the extent of PLX-mediated microtubule stabilization within the combinatorial regimen, 231R cells were treated with the DMSO vehicle and 1 μM of BC-2021 along with 585nM of PLX and observed for microtubule stabilization phenotype using a fluorescent tubulin-binding agent at the 1, 3, and 6-hour treatment intervals (Appendix Figure 2 A-D), before noticeable cell death occurred. Interestingly, at these time frames, microtubule stabilization, as reflected in the average tubulin fluorescence intensity, was not enhanced in combinatorial drug-treated 231R cells compared to the DMSO+585nM PLX-treated control. Strikingly, tubulin fluorescence intensity was decreased, rather than increased, at the 1-hour treatment period, suggesting that BC-2021 and PLX combinatorial regimen does not lead to resistant breast cancer cell death through intensifying microtubule stabilization.

**A**

Untreated R231

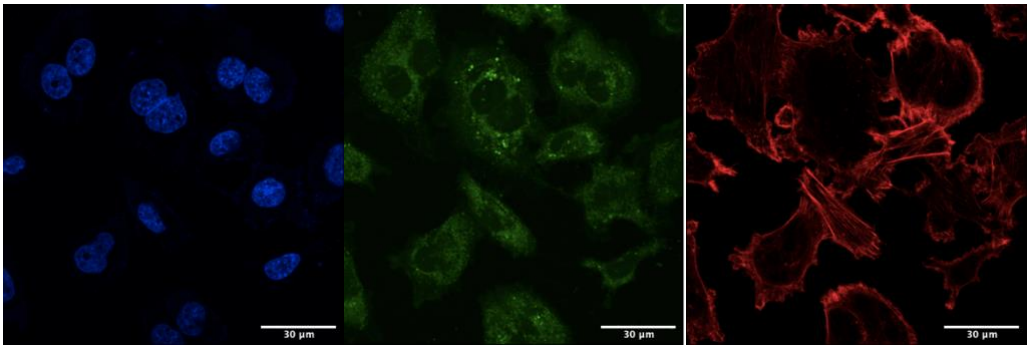


Nuclei Tubulin F-actin

**B**

1H DMSO+585nM PLX R231

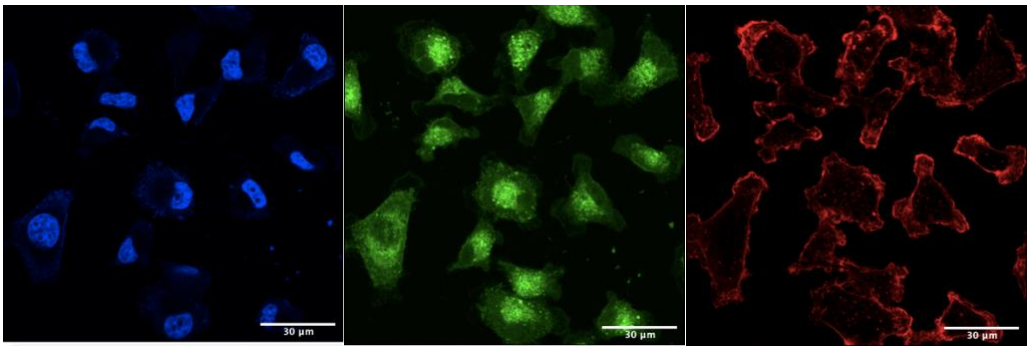


Nuclei Tubulin F-actin

1H 1µM BC-2021+585nM PLX R231

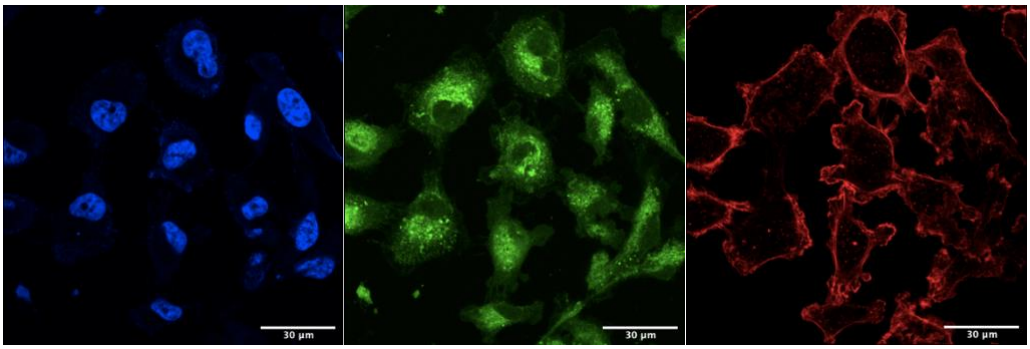


Nuclei Tubulin F-actin

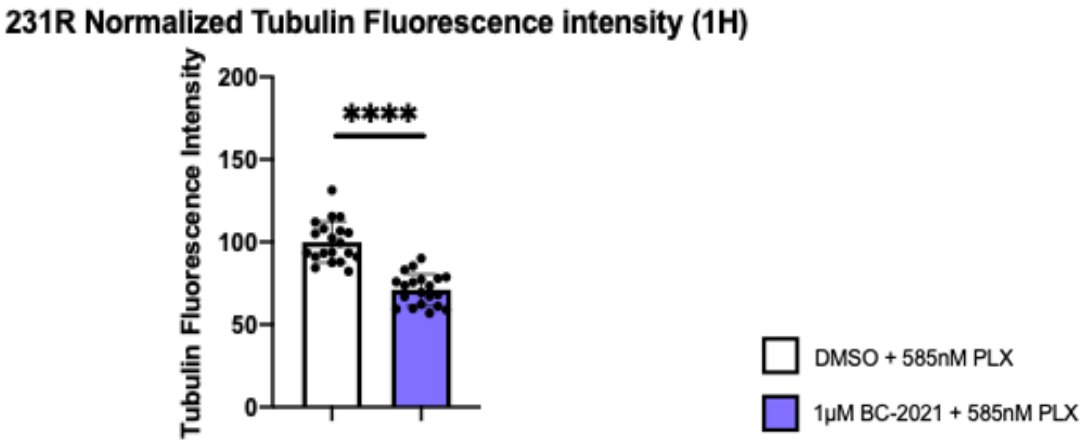


**C**

3H DMSO+585nM PLX R231

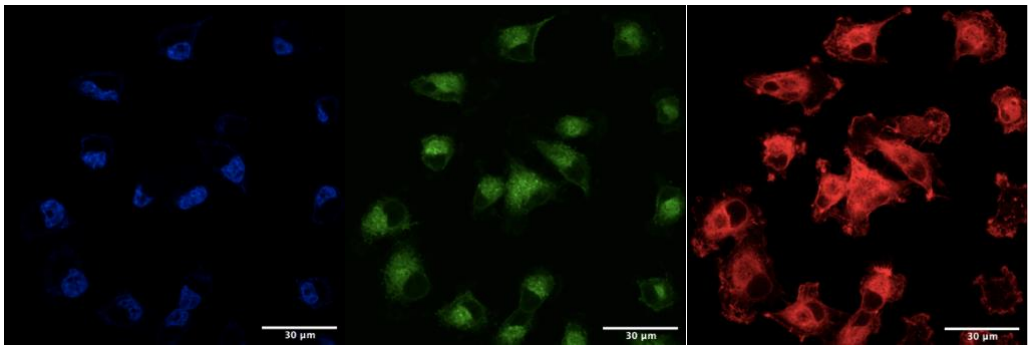


Nuclei

Tubulin

F-actin

3H 1µM BC-2021+585nM PLX R231

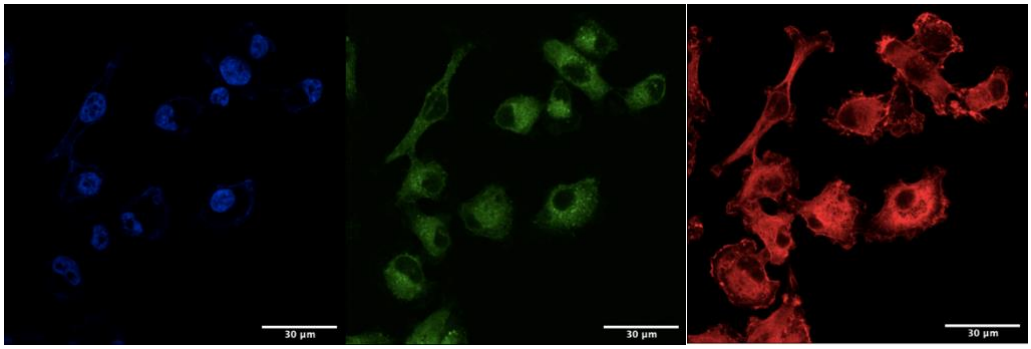


Nuclei

Tubulin

F-actin

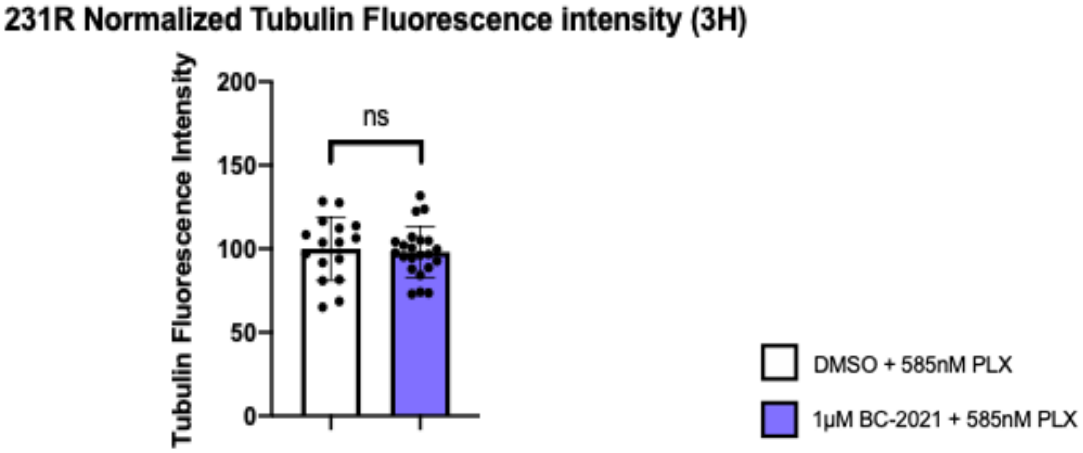

**D**

6H DMSO+585nM PLX R231

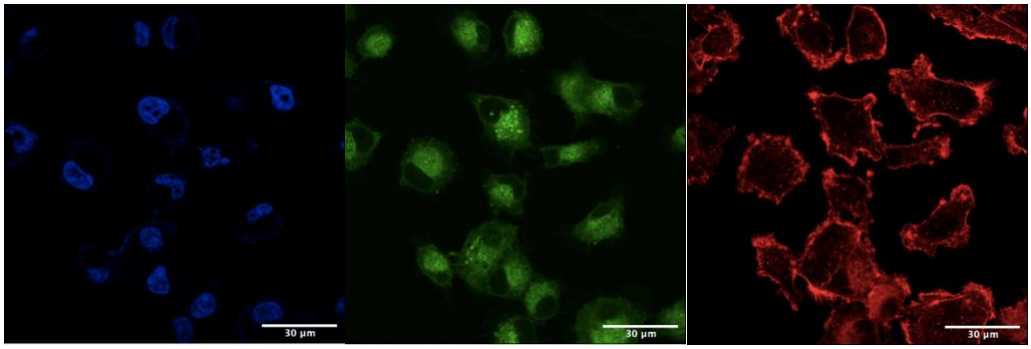


Nuclei Tubulin F-actin

6H 1µM BC-2021+585nM PLX R231

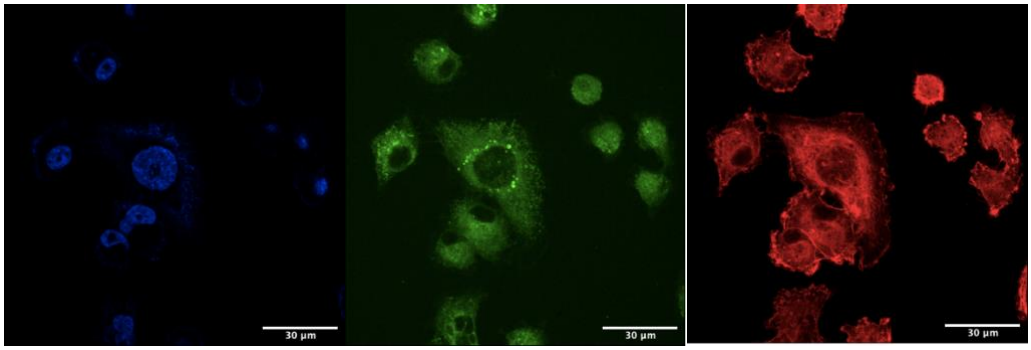


Nuclei Tubulin F-actin

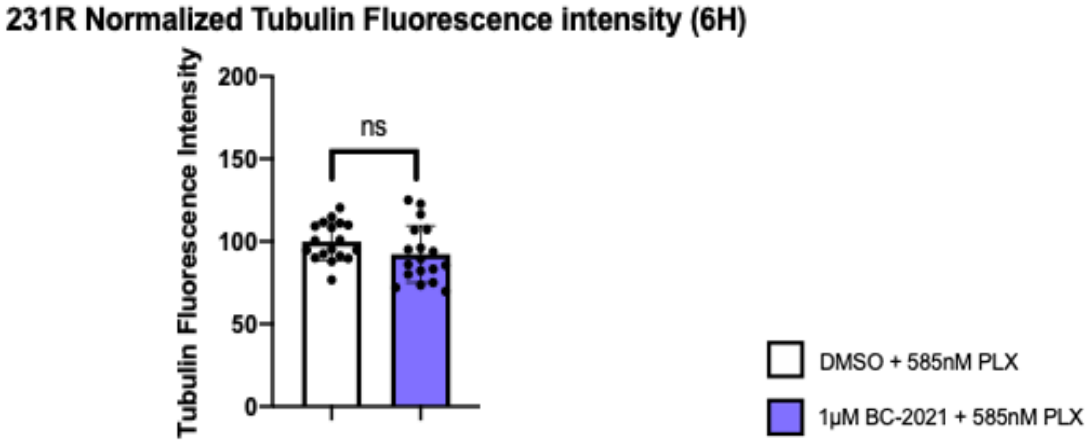

**Appendix Figure 2. BC-2021 in combination with PLX does not potentiate microtubule stabilization.** 231R cells treated with drug regimen for desired periods of time were fixed and stained with Hoechst 33342, Oregon Green™ 488 Conjugate paclitaxel derivative, and phalloidin to label nuclei, tubulins, and F-actin, respectively. These subcellular structures were visualized using Zeiss LSM 710 Confocal Microscope at 63X magnification. A) Spatial distribution of nucleus, tubulin, and F-actin in untreated 231R cells. Tubulin is, for the most part, spread out throughout the cytoplasm enclosed within the actin cytoskeleton boundary. B-D) Time-course measurements of mean fluorescence intensity of Oregon Green™ 488 Conjugate paclitaxel derivative in 231R cells 1, 3, and 6 hours following vehicle control and combinatorial drug-treatment. Data are expressed as the mean ± s.d. of triplicates (n=3). NS indicates $P>0.05$ and **** indicates $P \leq 0.0001$.

**BC-2021 and PLX combination does not impair cellular migration**

Cellular migration was measured by gap closure assay. For this assay, a gap was induced among fully adherent 231R and MCF7R cells, and cells were allowed to migrate to fill the gap. To suppress cell division while maintaining cell viability, 0.5% FBS-supplemented culture media was supplied along with various drug combinations for the entire duration of the migration period. BC-2021 and PLX combination did not impair cell migration (Appendix Figure 3 A-B).

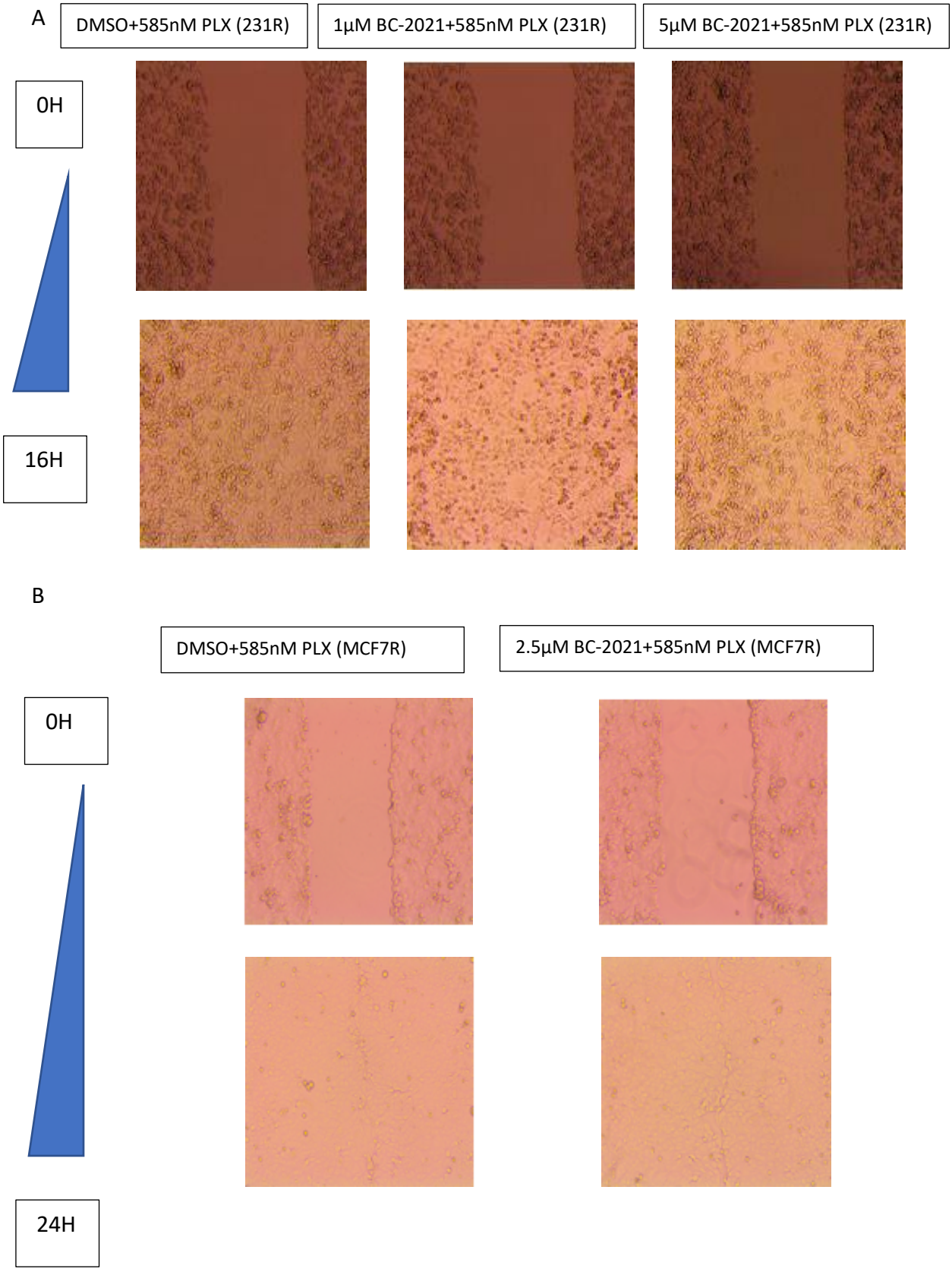
A
DMSO+585nM PLX (231R)
1μM BC-2021+585nM PLX (231R)
5μM BC-2021+585nM PLX (231R)
0H
16H
B
DMSO+585nM PLX (MCF7R)
2.5μM BC-2021+585nM PLX (MCF7R)
0H
24H

**Appendix Figure 3. BC-2021 along with PLX did not impair cell migration.**

A)231R and B) MCF7R cells immersed in culture medium containing various drug regimen were allowed to migrate to fill equally-sized gaps over 16 and 24 hours, respectively. BC-2021 and PLX incubation did not impair cell migration. All images were acquired using inverted light microscope at the 10X magnification. Experiment was repeated three times to confirm reproducibility. Data shows one representative image from three separate experiments.

## References


1. Lteif A, Javed A. Development of the Human Breast. *Seminars in Plastic Surgery*. 2013;27(1):5-12. doi:10.1055/s-0033-1343989
2. Macias H, Hinck L. Mammary gland development. *Wiley Interdisciplinary Reviews: Developmental Biology*. 2012;1(4):533-557. doi:10.1002/wdev.35
3. Hassiotou F, Geddes D. Anatomy of the human mammary gland: Current status of knowledge. *Clinical Anatomy*. 2012;26(1):29-48. doi:10.1002/ca.22165
4. Jackson-Fisher AJ, Bellinger G, Ramabhadran R, Morris JK, Lee K-F ., Stern DF. ErbB2 is required for ductal morphogenesis of the mammary gland. *Proceedings of the National Academy of Sciences*. 2004;101(49):17138-17143. doi:10.1073/pnas.0407057101
5. Andrechek ER, White D, Muller WJ. Targeted disruption of ErbB2/Neu in the mammary epithelium results in impaired ductal outgrowth. *Oncogene*. 2004;24(5):932-937. doi:10.1038/sj.onc.1208230
6. Jatoi I, Benson J, Sbitany H. Anatomy. *Atlas of Breast Surgery*. Published online 2020:9-25. doi:10.1007/978-3-030-45951-2_2
7. Lopez ME, Olutoye OO. Breast Embryology, Anatomy, and Physiology. *Endocrine Surgery in Children*. Published online August 2, 2017:365-376. doi:10.1007/978-3-662-54256-9_27

8. Brisken C, Scabia V. 90 years of progesterone: Progesterone receptor signaling in the normal breast and its implications for cancer. *Journal of Molecular Endocrinology*. 2020;65(1):T81-T94. doi:10.1530/jme-20-0091
9. Hilton HN, Clarke CL, Graham JD. Estrogen and progesterone signalling in the normal breast and its implications for cancer development. *Molecular and Cellular Endocrinology*. 2018;466:2-14. doi:10.1016/j.mce.2017.08.011
10. Goff SL, Danforth DN. The Role of Immune Cells in Breast Tissue and Immunotherapy for the Treatment of Breast Cancer. *Clinical Breast Cancer*. Published online July 2020. doi:10.1016/j.clbc.2020.06.011
11. Arendt LM, Rudnick JA, Keller PJ, Kuperwasser C. Stroma in Breast Development and Disease. *Seminars in cell & developmental biology*. 2010;21(1):11-18. doi:10.1016/j.semcdb.2009.10.003
12. Morsing M, Kim J, Villadsen R, et al. Fibroblasts direct differentiation of human breast epithelial progenitors. *Breast Cancer Research*. 2020;22(1). doi:10.1186/s13058-020-01344-0
13. Vass RA, Kemeny A, Dergez T, et al. Distribution of bioactive factors in human milk samples. *International Breastfeeding Journal*. 2019;14(1). doi:10.1186/s13006-019-0203-3
14. Gila-Diaz A, Arribas SM, Algara A, et al. A Review of Bioactive Factors in Human Breastmilk: A Focus on Prematurity. *Nutrients*. 2019;11(6):1307. doi:10.3390/nu11061307

15. Sriraman NK. The Nuts and Bolts of Breastfeeding: Anatomy and Physiology of Lactation. *Current Problems in Pediatric and Adolescent Health Care*. 2017;47(12):305-310. doi:10.1016/j.cppeds.2017.10.001
16. Wise NJ, Frangos E, Komisaruk BR. Activation of sensory cortex by imagined genital stimulation: an fMRI analysis. *Socioaffective Neuroscience & Psychology*. 2016;6(1):31481. doi:10.3402/snp.v6.31481
17. Mugea TT. Breast Development and Aging. *Aesthetic Surgery of the Breast*. Published online September 11, 2014:45-55. doi:10.1007/978-3-662-43407-9_6
18. Lee S. Breast cancer statistics. Canadian Cancer Society. Published 2020. https://cancer.ca/en/cancer-information/cancer-types/breast/statistics
19. Brenner DR, Weir HK, Demers AA, et al. Projected estimates of cancer in Canada in 2020. *CMAJ*. 2020;192(9):E199-E205. doi:10.1503/cmaj.191292
20. World Health Organization. Breast cancer. www.who.int. Published March 26, 2021. https://www.who.int/news-room/fact-sheets/detail/breast-cancer
21. BreastCancer.org. U.S. Breast Cancer Statistics | Breastcancer.org. Breastcancer.org. Published June 25, 2020. https://www.breastcancer.org/symptoms/understand_bc/statistics
22. Breast cancer statistics | World Cancer Research Fund International. WCRF International. https://www.wcrf.org/dietandcancer/breast-cancer-statistics/

23. Ontario Cancer Statistics. *5-Year Relative Survival for All Cancers Combined 63%*. Accessed November 8, 2021. https://www.cancercareontario.ca/sites/ccocancercare/files/assets/OCSChapterFour.pdf

24. Survival Rates for Breast Cancer. Cancer.org. Published 2014. https://www.cancer.org/cancer/breast-cancer/understanding-a-breast-cancer-diagnosis/breast-cancer-survival-rates.html

25. Cancer.org. Published 2019. https://www.cancer.org/cancer/breast-cancer/screening-tests-and-early-detection/breast-biopsy.html

26. National Cancer Institute. Cancer Staging. National Cancer Institute. Published 2015. https://www.cancer.gov/about-cancer/diagnosis-staging/staging

27. Akram M, Iqbal M, Daniyal M, Khan AU. Awareness and current knowledge of breast cancer. *Biological Research*. 2017;50(1). doi:10.1186/s40659-017-0140-9

28. Kalli S, Semine A, Cohen S, Naber SP, Makim SS, Bahl M. American Joint Committee on Cancer's Staging System for Breast Cancer, Eighth Edition: What the Radiologist Needs to Know. *RadioGraphics*. 2018;38(7):1921-1933. doi:10.1148/rg.2018180056

29. Bansal C, Singh US, Misra S, Sharma KL, Tiwari V, Srivastava AN. Comparative evaluation of the modified Scarff-Bloom-Richardson grading system on breast carcinoma aspirates and histopathology. *CytoJournal*. 2012;9:4. doi:10.4103/1742-6413.92550

30. Chand P, Garg A, Singla V, Rani N. Evaluation of Immunohistochemical Profile of Breast Cancer for Prognostics and Therapeutic Use. *Nigerian Journal of Surgery : Official Publication of the Nigerian Surgical Research Society*. 2018;24(2):100-106. doi:10.4103/njs.NJS_2_18

31. Johnson KS, Conant EF, Soo MS. Molecular Subtypes of Breast Cancer: A Review for Breast Radiologists. *Journal of Breast Imaging*. Published online December 30, 2020. doi:10.1093/jbi/wbaa110

32. Wesolowski R, Ramaswamy B. Gene Expression Profiling: Changing Face of Breast Cancer Classification and Management. *Gene Expression*. 2018;15(3):105-115. Accessed November 9, 2021. https://www.ncbi.nlm.nih.gov/pmc/articles/PMC3772713/

33. Tsang JYS, Tse GM. Molecular Classification of Breast Cancer. *Advances In Anatomic Pathology*. Published online April 2019:1. doi:10.1097/pap.0000000000000232

34. Raj-Kumar P-K, Liu J, Hooke JA, et al. PCA-PAM50 improves consistency between breast cancer intrinsic and clinical subtyping reclassifying a subset of luminal A tumors as luminal B. *Scientific Reports*. 2019;9(1):7956. doi:10.1038/s41598-019-44339-4

35. Yersal O. Biological subtypes of breast cancer: Prognostic and therapeutic implications. *World Journal of Clinical Oncology*. 2014;5(3):412. doi:10.5306/wjco.v5.i3.412

36. Yin L, Duan J-J, Bian X-W, Yu S. Triple-negative breast cancer molecular subtyping and treatment progress. *Breast Cancer Research*. 2020;22(1). doi:10.1186/s13058-020-01296-5

37. Testa U, Castelli G, Pelosi E. Breast Cancer: A Molecularly Heterogenous Disease Needing Subtype-Specific Treatments. *Medical Sciences*. 2020;8(1). doi:10.3390/medsci8010018

38. Bradley R, Braybrooke J, Gray R, et al. Trastuzumab for early-stage, HER2-positive breast cancer: a meta-analysis of 13 864 women in seven randomised trials. *The Lancet Oncology*. 2021;22(8):1139-1150. doi:10.1016/S1470-2045(21)00288-6

39. Damaskos C, Garmpi A, Nikolettos K, et al. Triple-Negative Breast Cancer: The Progress of Targeted Therapies and Future Tendencies. *Anticancer Research*. 2019;39(10):5285-5296. doi:10.21873/anticanres.13722

40. Hwang S-Y, Park S, Kwon Y. Recent therapeutic trends and promising targets in triple negative breast cancer. *Pharmacology & Therapeutics*. 2019;199:30-57. doi:10.1016/j.pharmthera.2019.02.006

41. Deciding when to use adjuvant chemotherapy for hormone receptor-positive, HER2-negative breast cancer. www.uptodate.com. Accessed November 9, 2021. https://www.uptodate.com/contents/deciding-when-to-use-adjuvant-chemotherapy-for-hormone-receptor-positive-her2-negative-breast-cancer/print

42. Tremont A, Lu J, Cole JT. Endocrine Therapy for Early Breast Cancer: Updated Review. *The Ochsner Journal*. 2017;17(4):405-411. https://www.ncbi.nlm.nih.gov/pmc/articles/PMC5718454/

43. Comparisons between different polychemotherapy regimens for early breast cancer: meta-analyses of long-term outcome among 100 000 women in 123 randomised trials. *The Lancet*. 2012;379(9814):432-444. doi:10.1016/s0140-6736(11)61625-5

44. Mazouni C, Kau S-W ., Frye D, et al. Inclusion of taxanes, particularly weekly paclitaxel, in preoperative chemotherapy improves pathologic complete response rate in estrogen receptor-positive breast cancers. *Annals of Oncology: Official Journal of the European Society for Medical Oncology*. 2007;18(5):874-880. doi:10.1093/annonc/mdm008

45. Venkatesh P, Kasi A. Anthracyclines. PubMed. Published 2020. https://www.ncbi.nlm.nih.gov/books/NBK538187/

46. McGowan JV, Chung R, Maulik A, Piotrowska I, Walker JM, Yellon DM. Anthracycline Chemotherapy and Cardiotoxicity. *Cardiovascular Drugs and Therapy*. 2017;31(1):63-75. doi:10.1007/s10557-016-6711-0

47. Weaver BA. How Taxol/paclitaxel kills cancer cells. Bement W, ed. *Molecular Biology of the Cell*. 2014;25(18):2677-2681. doi:10.1091/mbc.e14-04-0916

48. St. George M, Ayoub AT, Banerjee A, et al. Designing and Testing of Novel Taxanes to Probe the Highly Complex Mechanisms by Which Taxanes Bind to Microtubules and Cause Cytotoxicity to Cancer Cells. Sung S-Y, ed. *PLOS ONE*. 2015;10(6):e0129168. doi:10.1371/journal.pone.0129168

49. Choi YH, Yoo YH. Taxol-induced growth arrest and apoptosis is associated with the upregulation of the Cdk inhibitor, p21WAF1/CIP1, in human breast cancer cells. *Oncology Reports*. 2012;28(6):2163-2169. doi:10.3892/or.2012.2060

50. Cai F, Luis M, Lin X, et al. Anthracycline-induced cardiotoxicity in the chemotherapy treatment of breast cancer: Preventive strategies and treatment (Review). *Molecular and Clinical Oncology*. Published online May 8, 2019. doi:10.3892/mco.2019.1854

51. Jones SE, Savin MA, Holmes FA, et al. Phase III trial comparing doxorubicin plus cyclophosphamide with docetaxel plus cyclophosphamide as adjuvant therapy for operable breast cancer. *Journal of Clinical Oncology: Official Journal of the American Society of Clinical Oncology*. 2006;24(34):5381-5387. doi:10.1200/JCO.2006.06.5391

52. Bertucci F, Borie N, Ginestier C, et al. Identification and validation of an ERBB2 gene expression signature in breast cancers. *Oncogene*. 2004;23(14):2564-2575. doi:10.1038/sj.onc.1207361

53. Harari D, Yarden Y. Molecular mechanisms underlying ErbB2/HER2 action in breast cancer. *Oncogene*. 2000;19(53):6102-6114. doi:10.1038/sj.onc.1203973

54. Mitri Z, Constantine T, O'Regan R. The HER2 Receptor in Breast Cancer: Pathophysiology, Clinical Use, and New Advances in Therapy. *Chemotherapy Research and Practice*. 2012;2012:1-7. doi:10.1155/2012/743193

55. Tarantino P, Hamilton E, Tolaney SM, et al. HER2-Low Breast Cancer: Pathological and Clinical Landscape. *Journal of Clinical Oncology*. 2020;38(17):1951-1962. doi:10.1200/jco.19.02488

56. Marchiò C, Annaratone L, Marques A, Casorzo L, Berrino E, Sapino A. Evolving concepts in HER2 evaluation in breast cancer: Heterogeneity, HER2-low carcinomas and beyond. *Seminars in Cancer Biology*. Published online February 2020. doi:10.1016/j.semcancer.2020.02.016

57. Debiasi M, Polanczyk CA, Ziegelmann P, et al. Efficacy of Anti-HER2 Agents in Combination With Adjuvant or Neoadjuvant Chemotherapy for Early and Locally Advanced HER2-Positive Breast Cancer Patients: A Network Meta-Analysis. *Frontiers in Oncology*. 2018;8:156. doi:10.3389/fonc.2018.00156

58. Nicolazzi MA, Carnicelli A, Fuorlo M, et al. Anthracycline and trastuzumab-induced cardiotoxicity in breast cancer. *European Review for Medical and Pharmacological Sciences*. 2018;22(7):2175-2185. doi:10.26355/eurrev_201804_14752

59. Tolaney SM, Guo H, Pernas S, et al. Seven-Year Follow-Up Analysis of Adjuvant Paclitaxel and Trastuzumab Trial for Node-Negative, Human Epidermal Growth Factor Receptor 2–Positive Breast Cancer. *Journal of Clinical Oncology*. 2019;37(22):1868-1875. doi:10.1200/jco.19.00066

60. Slamon D, Eiermann W, Robert N, et al. Adjuvant Trastuzumab in HER2-Positive Breast Cancer. *New England Journal of Medicine*. 2011;365(14):1273-1283. doi:10.1056/nejmoa0910383

61. Palmirotta R, Carella C, Silvestris E, et al. SNPs in predicting clinical efficacy and toxicity of chemotherapy: walking through the quicksand. *Oncotarget*. 2018;9(38). doi:10.18632/oncotarget.25256

62. Le Morvan V, Litière S, Laroche-Clary A, et al. Identification of SNPs associated with response of breast cancer patients to neoadjuvant chemotherapy in the EORTC-10994 randomized phase III trial. *The Pharmacogenomics Journal*. 2015;15(1):63-68. doi:10.1038/tpj.2014.24

63. Lopresti ML, Bian JJ, Sakr BJ, et al. Neoadjuvant weekly paclitaxel and carboplatin with trastuzumab and pertuzumab in HER2-positive breast cancer: a Brown University Oncology Research Group (BrUOG) study. *Breast Cancer Research and Treatment*. 2021;189(1):93-101. doi:10.1007/s10549-021-06266-9

64. Singh RK, Kumar S, Prasad DN, Bhardwaj TR. Therapeutic journery of nitrogen mustard as alkylating anticancer agents: Historic to future perspectives. *European Journal of Medicinal Chemistry*. 2018;151:401-433. doi:10.1016/j.ejmech.2018.04.001

65. Kellogg EH, Hejab NMA, Howes S, et al. Insights into the Distinct Mechanisms of Action of Taxane and Non-Taxane Microtubule Stabilizers from Cryo-EM Structures. *Journal of Molecular Biology*. 2017;429(5):633-646. doi:10.1016/j.jmb.2017.01.001

66. Thadani-Mulero M, Nanus DM, Giannakakou P. AR on the move; boarding the microtubule expressway to the nucleus. *Cancer research*. 2012;72(18):4611-4615. doi:10.1158/0008-5472.CAN-12-0783

67. Kampan NC, Madondo MT, McNally OM, Quinn M, Plebanski M. Paclitaxel and Its Evolving Role in the Management of Ovarian Cancer. *BioMed Research International*. 2015;2015:413076. doi:10.1155/2015/413076

68. Longley DB, Harkin DP, Johnston PG. 5-fluorouracil: mechanisms of action and clinical strategies. *Nature reviews Cancer*. 2003;3(5):330-338. doi:10.1038/nrc1074

69. Liang X, Wu Q, Luan S, et al. A comprehensive review of topoisomerase inhibitors as anticancer agents in the past decade. *European Journal of Medicinal Chemistry*. 2019;171:129-168. doi:10.1016/j.ejmech.2019.03.034

70. Skok Ž, Zidar N, Kikelj D, Ilaš J. Dual Inhibitors of Human DNA Topoisomerase II and Other Cancer-Related Targets. *Journal of Medicinal Chemistry*. 2019;63(3):884-904. doi:10.1021/acs.jmedchem.9b00726

71. Pogoda K, Niwińska A, Sarnowska E, et al. Effects of BRCA Germline Mutations on Triple-Negative Breast Cancer Prognosis. *Journal of Oncology*. 2020;2020:1-10. doi:10.1155/2020/8545643

72. Zeng Z, Du H, Xiong L, et al. BRCA1 protects cardiac microvascular endothelial cells against irradiation by regulating p21-mediated cell cycle arrest. *Life Sciences*. 2020;244:117342. doi:10.1016/j.lfs.2020.117342

73. Deng C-X. BRCA1: cell cycle checkpoint, genetic instability, DNA damage response and cancer evolution. *Nucleic Acids Research*. 2006;34(5):1416-1426. doi:10.1093/nar/gkl010

74. Andreopoulou E, Kelly CM, McDaid HM. Therapeutic Advances and New Directions for Triple-Negative Breast Cancer. *Breast Care*. 2017;12(1):20-27. doi:10.1159/000455821

75. Poggio F, Bruzzone M, Ceppi M, et al. Platinum-based neoadjuvant chemotherapy in triple-negative breast cancer: a systematic review and meta-analysis. *Annals of Oncology*. Published online June 4, 2018. doi:10.1093/annonc/mdy127

76. Garutti M, Pelizzari G, Bartoletti M, et al. Platinum Salts in Patients with Breast Cancer: A Focus on Predictive Factors. *International Journal of Molecular Sciences*. 2019;20(14):3390. doi:10.3390/ijms20143390

77. Gerratana L, Fanotto V, Pelizzari G, Agostinetto E, Puglisi F. Do platinum salts fit all triple negative breast cancers? *Cancer Treatment Reviews*. 2016;48:34-41. doi:10.1016/j.ctrv.2016.06.004

78. Tutt A, Tovey H, Cheang MCU, et al. Carboplatin in BRCA1/2-mutated and triple-negative breast cancer BRCAness subgroups: the TNT Trial. *Nature Medicine*. 2018;24(5):628-637. doi:10.1038/s41591-018-0009-7

79. Li Y, Zhao Y, Gong C, et al. Cisplatin shows greater efficacy than gemcitabine when combined with nab-paclitaxel in metastatic triple-negative breast cancer. *Scientific Reports*. 2019;9(1):3563. doi:10.1038/s41598-019-39314-y

80. Jin J, Tao Z, Cao J, Li T, Hu X. DNA damage response inhibitors: An avenue for TNBC treatment. *Biochimica et Biophysica Acta (BBA) - Reviews on Cancer*. 2021;1875(2):188521. doi:10.1016/j.bbcan.2021.188521

81. Coussy F, El-Botty R, Château-Joubert S, et al. BRCAness, SLFN11, and RB1 loss predict response to topoisomerase I inhibitors in triple-negative breast cancers. *Science Translational Medicine*. 2020;12(531). doi:10.1126/scitranslmed.aax2625

82. Rodriguez AA, Makris A, Harrison MK, et al. BRCA1 gene expression signature predicts for anthracycline-chemosensitivity in triple-negative breast cancer. *Cancer Research*. 2009;69(2 Supplement):6039. doi:10.1158/0008-5472.SABCS-6039

83. Thomssen C, Lüftner D, Untch M, et al. International Consensus Conference for Advanced Breast Cancer, Lisbon 2019: ABC5 Consensus – Assessment by a German Group of Experts. *Breast Care*. 2020;15(1):82-95. doi:10.1159/000505957

84. Medina MA, Oza G, Sharma A, et al. Triple-Negative Breast Cancer: A Review of Conventional and Advanced Therapeutic Strategies. *International Journal of Environmental Research and Public Health*. 2020;17(6):2078. doi:10.3390/ijerph17062078

85. Mansoori B, Mohammadi A, Davudian S, Shirjang S, Baradaran B. The Different Mechanisms of Cancer Drug Resistance: A Brief Review. *Advanced Pharmaceutical Bulletin*. 2017;7(3):339-348. doi:10.15171/apb.2017.041

86. Sharma P, Hu-Lieskovan S, Wargo JA, Ribas A. Primary, Adaptive, and Acquired Resistance to Cancer Immunotherapy. *Cell*. 2017;168(4):707-723. doi:10.1016/j.cell.2017.01.017

87. Wang Q, Wu X. Primary and acquired resistance to PD-1/PD-L1 blockade in cancer treatment. *International Immunopharmacology*. 2017;46:210-219. doi:10.1016/j.intimp.2017.03.015

88. Prieto-Vila M, Takahashi R, Usuba W, Kohama I, Ochiya T. Drug Resistance Driven by Cancer Stem Cells and Their Niche. *International Journal of Molecular Sciences*. 2017;18(12):2574. doi:10.3390/ijms18122574

89. Vaish M. Mismatch repair deficiencies transforming stem cells into cancer stem cells and therapeutic implications. *Molecular Cancer*. 2007;6(1):26. doi:10.1186/1476-4598-6-26

90. Najafi M, Farhood B, Mortezaee K. Cancer stem cells (CSCs) in cancer progression and therapy. *Journal of Cellular Physiology*. 2018;234(6):8381-8395. doi:10.1002/jcp.27740

91. Song K, Farzaneh M. Signaling pathways governing breast cancer stem cells behavior. *Stem Cell Research & Therapy*. 2021;12(1). doi:10.1186/s13287-021-02321-w

92. Yang F, Xu J, Tang L, Guan X. Breast cancer stem cell: the roles and therapeutic implications. *Cellular and Molecular Life Sciences*. 2016;74(6):951-966. doi:10.1007/s00018-016-2334-7

93. Mazzoldi EL, Pastò A, Pilotto G, et al. Comparison of the Genomic Profile of Cancer Stem Cells and Their Non-Stem Counterpart: The Case of Ovarian Cancer. *Journal of Clinical Medicine*. 2020;9(2):368. doi:10.3390/jcm9020368

94. Machida K. Existence of cancer stem cells in hepatocellular carcinoma: myth or reality? *Hepatology International*. 2016;11(2):143-147. doi:10.1007/s12072-016-9777-7

95. Lopez-Bertoni H, Laterra J. The cancer stem cell phenotype: You can't win until you learn how to lose it. *Molecular & Cellular Oncology*. 2015;2(3):e989760. doi:10.4161/23723556.2014.989760

96. Kim C, Gao R, Sei E, et al. Chemoresistance Evolution in Triple-Negative Breast Cancer Delineated by Single-Cell Sequencing. *Cell*. 2018;173(4):879-893.e13. doi:10.1016/j.cell.2018.03.041

97. Cao L, Zhou Y, Li X, Lin S, Tan Z, Guan F. Integrating transcriptomics, proteomics, glycomics and glycoproteomics to characterize paclitaxel resistance in breast cancer cells. *Journal of Proteomics*. 2021;243:104266. doi:10.1016/j.jprot.2021.104266

98. Worm J, Kirkin AF, Dzhandzhugazyan KN, Guldberg P. Methylation-dependent Silencing of the Reduced Folate Carrier Gene in Inherently Methotrexate-resistant Human Breast Cancer Cells. *Journal of Biological Chemistry*. 2001;276(43):39990-40000. doi:10.1074/jbc.m103181200

99. Jo Y, Choi N, Kim K, Koo H-J, Choi J, Kim HN. Chemoresistance of Cancer Cells: Requirements of Tumor Microenvironment-mimicking In Vitro Models in Anti-Cancer Drug Development. *Theranostics*. 2018;8(19):5259-5275. doi:10.7150/thno.29098

100. Liberti MV, Locasale JW. The Warburg Effect: How Does it Benefit Cancer Cells? *Trends in Biochemical Sciences*. 2016;41(3):211-218. doi:10.1016/j.tibs.2015.12.001

101. Schulte RR, Ho RH. Organic Anion Transporting Polypeptides: Emerging Roles in Cancer Pharmacology. *Molecular Pharmacology*. 2019;95(5):490-506. doi:10.1124/mol.118.114314

102. Dorman SN, Baranova K, Knoll JHM, et al. Genomic signatures for paclitaxel and gemcitabine resistance in breast cancer derived by machine learning. *Molecular Oncology*. 2015;10(1):85-100. doi:10.1016/j.molonc.2015.07.006

103. de Morrée ES, Böttcher R, van Soest RJ, et al. Loss of SLCO1B3 drives taxane resistance in prostate cancer. *British Journal of Cancer*. 2016;115(6):674-681. doi:10.1038/bjc.2016.251

104. Takano M, Otani Y, Tanda M, Kawami M, Nagai J, Yumoto R. Paclitaxel-resistance conferred by altered expression of efflux and influx transporters for paclitaxel in the human hepatoma cell line, HepG2. *Drug Metabolism and Pharmacokinetics*. 2009;24(5):418-427. doi:10.2133/dmpk.24.418

105. Muley H, Fadó R, Rodríguez-Rodríguez R, Casals N. Drug uptake-based chemoresistance in breast cancer treatment. *Biochemical Pharmacology*. 2020;177:113959. doi:10.1016/j.bcp.2020.113959

106. Dorman SN, Baranova K, Knoll JHM, et al. Genomic signatures for paclitaxel and gemcitabine resistance in breast cancer derived by machine learning. *Molecular Oncology*. 2015;10(1):85-100. doi:10.1016/j.molonc.2015.07.006

107. Sun Y-L, Patel A, Kumar P, Chen Z-S. Role of ABC transporters in cancer chemotherapy. *Chinese Journal of Cancer*. 2012;31(2):51-57. doi:10.5732/cjc.011.10466

108. Levi M, Muscatello LV, Brunetti B, et al. High Intrinsic Expression of P-glycoprotein and Breast Cancer Resistance Protein in Canine Mammary Carcinomas Regardless of Immunophenotype and Outcome. *Animals*. 2021;11(3):658. doi:10.3390/ani11030658

109. Thomas C, Tampé R. Structural and Mechanistic Principles of ABC Transporters. *Annual Review of Biochemistry*. 2020;89(1):605-636. doi:10.1146/annurev-biochem-011520-105201

110. Giddings EL, Champagne DP, Wu M-H, et al. Mitochondrial ATP fuels ABC transporter-mediated drug efflux in cancer chemoresistance. *Nature Communications*. 2021;12(1). doi:10.1038/s41467-021-23071-6

111. Xiao H, Zheng Y, Ma L, Tian L, Sun Q. Clinically-Relevant ABC Transporter for Anti-Cancer Drug Resistance. *Frontiers in Pharmacology*. 2021;12. doi:10.3389/fphar.2021.648407

112. Reed K, Hembruff SL, Sprowl JA, Parissenti AM. The temporal relationship between ABCB1 promoter hypomethylation, ABCB1 expression and acquisition of drug resistance. *The Pharmacogenomics Journal*. 2010;10(6):489-504. doi:10.1038/tpj.2010.1

113. Mosca L, Ilari A, Fazi F, Assaraf YG, Colotti G. Taxanes in cancer treatment: Activity, chemoresistance and its overcoming. *Drug Resistance Updates*. 2021;54:100742. doi:10.1016/j.drup.2020.100742

114. Phang-Lyn S, Llerena VA. Biochemistry, Biotransformation. PubMed. Published 2020. https://www.ncbi.nlm.nih.gov/books/NBK544353/

115. Jancova P, Anzenbacher P, Anzenbacherova E. Phase II drug metabolizing enzymes. *Biomedical papers of the Medical Faculty of the University Palacky, Olomouc, Czechoslovakia*. 2010;154(2):103-116. doi:10.5507/bp.2010.017

116. de Almagro MC, Selga E, Thibaut R, Porte C, Noé V, Ciudad CJ. UDP-glucuronosyltransferase 1A6 overexpression in breast cancer cells resistant to methotrexate. *Biochemical Pharmacology*. 2011;81(1):60-70. doi:10.1016/j.bcp.2010.09.008

117. Allain EP, Rouleau M, Lévesque E, Guillemette C. Emerging roles for UDP-glucuronosyltransferases in drug resistance and cancer progression. *British Journal of Cancer*. 2020;122(9):1277-1287. doi:10.1038/s41416-019-0722-0

118. Yang S-J, Wang D-D, Li J, et al. Predictive role of GSTP1-containing exosomes in chemotherapy-resistant breast cancer. *Gene*. 2017;623:5-14. doi:10.1016/j.gene.2017.04.031

119. Arai T, Miyoshi Y, Kim SJ, et al. Association of GSTP1 expression with resistance to docetaxel and paclitaxel in human breast cancers. *European Journal of Surgical Oncology: The Journal of the European Society of Surgical Oncology and the British Association of Surgical Oncology*. 2008;34(7):734-738. doi:10.1016/j.ejso.2007.07.008

120. Dong X, Yang Y, Zhou Y, et al. Glutathione S-transferases P1 protects breast cancer cell from adriamycin-induced cell death through promoting autophagy. *Cell Death & Differentiation*. 2019;26(10):2086-2099. doi:10.1038/s41418-019-0276-y

121. Chen X, Chen S, Yu D. Metabolic Reprogramming of Chemoresistant Cancer Cells and the Potential Significance of Metabolic Regulation in the Reversal of Cancer Chemoresistance. *Metabolites*. 2020;10(7):289. doi:10.3390/metabo10070289

122. Zhai X, El Hiani Y. Getting Lost in the Cell–Lysosomal Entrapment of Chemotherapeutics. *Cancers*. 2020;12(12):3669. doi:10.3390/cancers12123669

123. Poisson LM, Munkarah A, Madi H, et al. A metabolomic approach to identifying platinum resistance in ovarian cancer. *Journal of Ovarian Research*. 2015;8(1). doi:10.1186/s13048-015-0140-8

124. Geisslinger F, Müller M, Vollmar AM, Bartel K. Targeting Lysosomes in Cancer as Promising Strategy to Overcome Chemoresistance—A Mini Review. *Frontiers in Oncology*. 2020;10. doi:10.3389/fonc.2020.01156

125. Lucien F, Lavoie RR, Dubois CM. Targeting endosomal pH for cancer chemotherapy. *Molecular & Cellular Oncology*. Published online March 13, 2018:e1435184. doi:10.1080/23723556.2018.1435184

126. Yamagishi T, Sahni S, Sharp DM, Arvind A, Jansson PJ, Richardson DR. P-glycoprotein Mediates Drug Resistance via a Novel Mechanism Involving Lysosomal Sequestration. *Journal of Biological Chemistry*. 2013;288(44):31761-31771. doi:10.1074/jbc.m113.514091

127. Abd El-Aziz Yomna S, Spillane Andrew J, Jansson Patric J, Sahni S. Role of ABCB1 in mediating chemoresistance of triple-negative breast cancers. *Bioscience Reports*. 2021;41(2). doi:10.1042/bsr20204092

128. Cook KL, Wärri A, Soto-Pantoja DR, et al. Hydroxychloroquine inhibits autophagy to potentiate antiestrogen responsiveness in ER+ breast cancer. *Clinical cancer research : an official journal of the American Association for Cancer Research*. 2014;20(12):3222-3232. doi:10.1158/1078-0432.CCR-13-3227

129. Ajabnoor GMA, Crook T, Coley HM. Paclitaxel resistance is associated with switch from apoptotic to autophagic cell death in MCF-7 breast cancer cells. *Cell Death & Disease*. 2012;3(1):e260-e260. doi:10.1038/cddis.2011.139

130. Zhitomirsky B, Yunaev A, Kreiserman R, Kaplan A, Stark M, Assaraf YG. Lysosomotropic drugs activate TFEB via lysosomal membrane fluidization and consequent inhibition of mTORC1 activity. *Cell Death & Disease*. 2018;9(12). doi:10.1038/s41419-018-1227-0

131. Palmieri M, Impey S, Kang H, et al. Characterization of the CLEAR network reveals an integrated control of cellular clearance pathways. *Human Molecular Genetics*. 2011;20(19):3852-3866. doi:10.1093/hmg/ddr306

132. Zhao B, Dierichs L, Gu J-N, et al. TFEB-mediated lysosomal biogenesis and lysosomal drug sequestration confer resistance to MEK inhibition in pancreatic cancer. *Cell Death Discovery*. 2020;6(1). doi:10.1038/s41420-020-0246-7

133. Otte J, Dyberg C, Pepich A, Johnsen JI. MYCN Function in Neuroblastoma Development. *Frontiers in Oncology*. 2021;10. doi:10.3389/fonc.2020.624079

134. Schafer JM, Lehmann BD, Gonzalez-Ericsson PI, et al. Targeting MYCN-expressing triple-negative breast cancer with BET and MEK inhibitors. *Science translational medicine*. 2020;12(534):eaaw8275. doi:10.1126/scitranslmed.aaw8275

135. Yi X, Lou L, Wang J, Xiong J, Zhou S. Honokiol antagonizes doxorubicin resistance in human breast cancer via miR-188-5p/FBXW7/c-Myc pathway. *Cancer Chemotherapy and Pharmacology*. 2021;87(5):647-656. doi:10.1007/s00280-021-04238-w

136. Wang W, Zhang L, Wang Y, et al. Involvement of miR-451 in resistance to paclitaxel by regulating YWHAZ in breast cancer. *Cell Death & Disease*. 2017;8(10):e3071-e3071. doi:10.1038/cddis.2017.460

137. Iqbal N, Iqbal N. Human Epidermal Growth Factor Receptor 2 (HER2) in Cancers: Overexpression and Therapeutic Implications. *Molecular Biology International*. 2014;2014(1):1-9. doi:10.1155/2014/852748

138. Moasser MM. The oncogene HER2: its signaling and transforming functions and its role in human cancer pathogenesis. *Oncogene*. 2007;26(45):6469-6487. doi:10.1038/sj.onc.1210477

139. Cao X, Hou J, An Q, Assaraf YG, Wang X. Towards the overcoming of anticancer drug resistance mediated by p53 mutations. *Drug Resistance Updates*. 2020;49:100671. doi:10.1016/j.drup.2019.100671

140. Lisek K, Campaner E, Ciani Y, Walerych D, Del Sal G. Mutant p53 tunes the NRF2-dependent antioxidant response to support survival of cancer cells. *Oncotarget*. 2018;9(29):20508-20523. doi:10.18632/oncotarget.24974

141. Galmarini CM, Clarke ML, Falette N, Puisieux A, Mackey JR, Dumontet C. Expression of a non-functional p53 affects the sensitivity of cancer cells to gemcitabine. *International Journal of Cancer*. 2002;97(4):439-445. doi:10.1002/ijc.1628

142. Selle F, Gligorov J, Soares DG, Lotz J-P. [High-dose chemotherapy as a strategy to overcome drug resistance in solid tumors]. *Bulletin Du Cancer*. 2016;103(10):861-868. doi:10.1016/j.bulcan.2016.08.002

143. Maurya SK, Shadab GGHA, Siddique HR. Chemosensitization of Therapy Resistant Tumors: Targeting Multiple Cell Signaling Pathways by Lupeol, A Pentacyclic Triterpene. *Current Pharmaceutical Design*. 2020;26(4):455-465. doi:10.2174/1381612826666200122122804

144. Dong J, Qin Z, Zhang W-D, et al. Medicinal chemistry strategies to discover P-glycoprotein inhibitors: An update. *Drug Resistance Updates*. 2020;49:100681. doi:10.1016/j.drup.2020.100681

145. Bordoloi D, K. Roy N, Monisha J, Padmavathi G, B. Kunnumakkara A. Multi-Targeted Agents in Cancer Cell Chemosensitization: What We Learnt from Curcumin Thus Far. *Recent Patents on Anti-Cancer Drug Discovery*. 2016;11(1):67-97. doi:10.2174/1574892810666151020101706

146. Abotaleb M, Kubatka P, Caprnda M, et al. Chemotherapeutic agents for the treatment of metastatic breast cancer: An update. *Biomedicine & Pharmacotherapy*. 2018;101:458-477. doi:10.1016/j.biopha.2018.02.108

147. Škubník J, Pavlíčková V, Ruml T, Rimpelová S. Current Perspectives on Taxanes: Focus on Their Bioactivity, Delivery and Combination Therapy. *Plants*. 2021;10(3):569. doi:10.3390/plants10030569

148. Hortobagyi GN. Paclitaxel-based combination chemotherapy for breast cancer. *Oncology (Williston Park, NY)*. 1997;11(3 Suppl 2):29-37. Accessed November 9, 2021. https://pubmed.ncbi.nlm.nih.gov/9110340/

149. Fisusi FA, Akala EO. Drug Combinations in Breast Cancer Therapy. *Pharmaceutical Nanotechnology*. 2019;07. doi:10.2174/2211738507666190122111224

150. Liu C, Shengjing Hospital. Albumin-bound Paclitaxel Combined With Carboplatin Versus Epirubicin Combined With Docetaxel as Neoadjuvant Therapy for Triple-negative Breast Cancer: a Multicenter Randomized Controlled Phase IV Clinical Trial. clinicaltrials.gov. Published July 18, 2021. Accessed November 9, 2021. https://clinicaltrials.gov/ct2/show/NCT04136782

151. Bines J, Earl H, Buzaid AC, Saad ED. Anthracyclines and taxanes in the neo/adjuvant treatment of breast cancer: does the sequence matter? *Annals of Oncology*. 2014;25(6):1079-1085. doi:10.1093/annonc/mdu007

152. Hilaj E, Ymeri A, Shpati KP. The Impact of Adding Taxanes to Anthracyclines on Women with Breast Cancer Receiving Adjuvant Chemotherapy. *Cureus*. Published online February 27, 2020. doi:10.7759/cureus.7117

153. Liu M, Liu S, Yang L, Wang S. Comparison between nab-paclitaxel and solvent-based taxanes as neoadjuvant therapy in breast cancer: a systematic review and meta-analysis. *BMC Cancer*. 2021;21(1). doi:10.1186/s12885-021-07831-7

154. Kundranda M, Niu J. Albumin-bound paclitaxel in solid tumors: clinical development and future directions. *Drug Design, Development and Therapy*. Published online July 2015:3767. doi:10.2147/dddt.s88023

155. Škubník J, Pavlíčková V, Ruml T, Rimpelová S. Current Perspectives on Taxanes: Focus on Their Bioactivity, Delivery and Combination Therapy. *Plants*. 2021;10(3):569. doi:10.3390/plants10030569

156. Szikriszt B, Póti Á, Németh E, Kanu N, Swanton C, Szüts D. A comparative analysis of the mutagenicity of platinum-containing chemotherapeutic agents reveals direct and indirect mutagenic mechanisms. *Mutagenesis*. 2021;36(1):75-86. doi:10.1093/mutage/geab005

157. Muggia FM. Overview of carboplatin: replacing, complementing, and extending the therapeutic horizons of cisplatin. *Seminars in Oncology*. 1989;16(2 Suppl 5):7-13. Accessed November 9, 2021. https://pubmed.ncbi.nlm.nih.gov/2655099/

158. Zhou L, Xu S, Yin W, et al. Weekly paclitaxel and cisplatin as neoadjuvant chemotherapy with locally advanced breast cancer: a prospective, single arm, phase II study. *Oncotarget*. 2017;8(45):79305-79314. doi:10.18632/oncotarget.17954

159. Wang J, Zheng R, Wang Z, Yang Y, Wang M, Zou W. Efficacy and Safety of Vinorelbine Plus Cisplatin vs. Gemcitabine Plus Cisplatin for Treatment of Metastatic Triple-Negative Breast Cancer After Failure with Anthracyclines and Taxanes. *Medical Science Monitor: International Medical Journal of Experimental and Clinical Research*. 2017;23:4657-4664. doi:10.12659/msm.905300

160. Apostolou P, Toloudi M, Chatziioannou M, et al. Anvirzel™ in combination with cisplatin in breast, colon, lung, prostate, melanoma and pancreatic cancer cell lines. *BMC Pharmacology & Toxicology*. 2013;14:18. doi:10.1186/2050-6511-14-18

161. Tanabe M. Combination Chemotherapy of Mitomycin C and Methotrexate Was Effective on Metastatic Breast Cancer Resistant to Eribulin, Vinorelbine, and Bevacizumab after Anthracycline, Taxane, and Capecitabine. *Case Reports in Oncology*. 2016;9(2):422-426. doi:10.1159/000447770

162. Walko CM, Lindley C. Capecitabine: a review. *Clinical Therapeutics*. 2005;27(1):23-44. doi:10.1016/j.clinthera.2005.01.005

163. Terjung A, Kummer S, Friedrich M. Simultaneous 24 h-infusion of high-dose 5-fluorouracil and sodium-folinate as alternative to capecitabine in advanced breast cancer. *Anticancer Research*. 2014;34(12):7233-7238. Accessed November 9, 2021. https://pubmed.ncbi.nlm.nih.gov/25503154/

164. Martín M, Ruiz A, Muñoz M, et al. Gemcitabine plus vinorelbine versus vinorelbine monotherapy in patients with metastatic breast cancer previously treated with anthracyclines and taxanes: final results of the phase III Spanish Breast Cancer Research Group (GEICAM) trial. *The Lancet Oncology*. 2007;8(3):219-225. doi:10.1016/S1470-2045(07)70041-4

165. Lao J, Madani J, Puértolas T, et al. Liposomal Doxorubicin in the Treatment of Breast Cancer Patients: A Review. *Journal of Drug Delivery*. 2013;2013:1-12. doi:10.1155/2013/456409

166. Mirzaei SA, Gholamian Dehkordi N, Ghamghami M, Amiri AH, Dalir Abdolahinia E, Elahian F. ABC-transporter blockage mediated by xanthotoxin and bergapten is the major pathway for chemosensitization of multidrug-resistant cancer cells. *Toxicology and Applied Pharmacology*. 2017;337:22-29. doi:10.1016/j.taap.2017.10.018

167. Lee H-J, Choi C-H. Characterization of SN38-Resistant T47D Breast Cancer Cell Sublines Overexpressing BCRP, MRP1, MRP2, MRP3, and MRP4. Published online January 12, 2021. doi:10.21203/rs.3.rs-141966/v1

168. Yu S, Kim T, Yoo KH, Kang K. The T47D cell line is an ideal experimental model to elucidate the progesterone-specific effects of a luminal A subtype of breast cancer. *Biochemical and Biophysical Research Communications*. 2017;486(3):752-758. doi:10.1016/j.bbrc.2017.03.114

169. Li P, Zhong D, Gong P. Synergistic effect of paclitaxel and verapamil to overcome multi-drug resistance in breast cancer cells. *Biochemical and Biophysical Research Communications*. 2019;516(1):183-188. doi:10.1016/j.bbrc.2019.05.189

170. Al-malky HS, Damanhouri ZA, Al Aama JY, et al. Diltiazem potentiation of doxorubicin cytotoxicity and cellular uptake in human breast cancer cells. *Breast Cancer Management*. 2019;8(4):BMT31. doi:10.2217/bmt-2019-0018

171. Nanayakkara AK, Follit CA, Chen G, Williams NS, Vogel PD, Wise JG. Targeted inhibitors of P-glycoprotein increase chemotherapeutic-induced mortality of multidrug resistant tumor cells. *Scientific Reports*. 2018;8(1):967. doi:10.1038/s41598-018-19325-x

172. Famta P, Shah S, Chatterjee E, et al. Exploring new Horizons in overcoming P-glycoprotein-mediated multidrug-resistant breast cancer via nanoscale drug delivery platforms. *Current Research in Pharmacology and Drug Discovery*. 2021;2:100054. doi:10.1016/j.crphar.2021.100054

173. Palmeira A, Sousa E, H. Vasconcelos M, M. Pinto M. Three Decades of P-gp Inhibitors: Skimming Through Several Generations and Scaffolds. *Current Medicinal Chemistry*. 2012;19(13):1946-2025. doi:10.2174/092986712800167392

174. Costales C, Lin J, Kimoto E, et al. Quantitative prediction of breast cancer resistant protein mediated drug-drug interactions using physiologically-based pharmacokinetic modeling. *CPT: Pharmacometrics & Systems Pharmacology*. 2021;10(9):1018-1031. doi:10.1002/psp4.12672

175. Egido E, Müller R, Li-Blatter X, Merino G, Seelig A. Predicting Activators and Inhibitors of the Breast Cancer Resistance Protein (ABCG2) and P-Glycoprotein (ABCB1) Based on Mechanistic Considerations. *Molecular Pharmaceutics*. 2015;12(11):4026-4037. doi:10.1021/acs.molpharmaceut.5b00463

176. Seelig A. P-Glycoprotein: One Mechanism, Many Tasks and the Consequences for Pharmacotherapy of Cancers. *Frontiers in Oncology*. 2020;10. doi:10.3389/fonc.2020.576559

177. Follit CA, Brewer FK, Wise JG, Vogel PD. In silico identified targeted inhibitors of P-glycoprotein overcome multidrug resistance in human cancer cells in culture. *Pharmacology Research & Perspectives*. 2015;3(5):e00170. doi:10.1002/prp2.170

178. Brewer FK, Follit CA, Vogel PD, Wise JG. In silico screening for inhibitors of p-glycoprotein that target the nucleotide binding domains. *Molecular Pharmacology*. 2014;86(6):716-726. doi:10.1124/mol.114.095414

179. Lee S, Ju M, Jeon H, et al. Reactive oxygen species induce epithelial-mesenchymal transition, glycolytic switch, and mitochondrial repression through the Dlx-2/Snail signaling pathways in MCF-7 cells. *Molecular Medicine Reports*. Published online July 3, 2019. doi:10.3892/mmr.2019.10466

180. Zhu D, Shen Z, Liu J, et al. The ROS-mediated activation of STAT-3/VEGF signaling is involved in the 27-hydroxycholesterol-induced angiogenesis in human breast cancer cells. *Toxicology Letters*. 2016;264:79-86. doi:10.1016/j.toxlet.2016.11.006

181. Sarmiento-Salinas FL, Delgado-Magallón A, Montes-Alvarado JB, et al. Breast Cancer Subtypes Present a Differential Production of Reactive Oxygen Species (ROS) and Susceptibility to Antioxidant Treatment. *Frontiers in Oncology*. 2019;9. doi:10.3389/fonc.2019.00480

182. Reczek CR, Chandel NS. The Two Faces of Reactive Oxygen Species in Cancer. *Annual Review of Cancer Biology*. 2017;1(1):79-98. doi:10.1146/annurev-cancerbio-041916-065808

183. Cockfield JA, Schafer ZT. Antioxidant Defenses: A Context-Specific Vulnerability of Cancer Cells. *Cancers*. 2019;11(8):1208. doi:10.3390/cancers11081208

184. Yang M, Li Y, Shen X, et al. CLDN6 promotes chemoresistance through GSTP1 in human breast cancer. *Journal of Experimental & Clinical Cancer Research*. 2017;36(1). doi:10.1186/s13046-017-0627-9

185. Lewis-Wambi JS, Kim HR, Wambi C, et al. Buthionine sulfoximine sensitizes antihormone-resistant human breast cancer cells to estrogen-induced apoptosis. *Breast Cancer Research : BCR*. 2008;10(6):R104. doi:10.1186/bcr2208

186. Yang Q, Xiao H, Cai J, Xie Z, Wang Z, Jing X. Nanoparticle mediated delivery of a GST inhibitor ethacrynic acid for sensitizing platinum based chemotherapy. *RSC Advances*. 2014;4(105):61124-61132. doi:10.1039/C4RA12040J

187. Joo M-K, Shin S, Ye D-J, et al. Combined treatment with auranofin and trametinib induces synergistic apoptosis in breast cancer cells. *Journal of Toxicology and Environmental Health, Part A*. 2020;84(2):84-94. doi:10.1080/15287394.2020.1835762

188. Ye D-J, Kwon Y-J, Baek H-S, Cho E, Kwon T-U, Chun Y-J. Combination treatment with auranofin and nutlin-3a induces synergistic cytotoxicity in breast cancer cells. *Journal of Toxicology and Environmental Health Part A*. 2019;82(10):626-637. doi:10.1080/15287394.2019.1635934

189. Beatty A, Fink LS, Singh T, et al. Metabolite Profiling Reveals the Glutathione Biosynthetic Pathway as a Therapeutic Target in Triple-Negative Breast Cancer. *Molecular Cancer Therapeutics*. 2018;17(1):264-275. doi:10.1158/1535-7163.MCT-17-0407

190. Triple-negative breast cancer therapeutic resistance: Where is the Achilles' heel? *Cancer Letters*. 2021;497:100-111. doi:10.1016/j.canlet.2020.10.016

191. Bansal P, Christopher A, Kaur R, Kaur G, Kaur A, Gupta V. MicroRNA therapeutics: Discovering novel targets and developing specific therapy. *Perspectives in Clinical Research*. 2016;7(2):68. doi:10.4103/2229-3485.179431

192. Chakraborty C, Sharma AR, Sharma G, Lee S-S. Therapeutic advances of miRNAs: A preclinical and clinical update. *Journal of Advanced Research*. 2021;28:127-138. doi:10.1016/j.jare.2020.08.012

193. Zhang S, Cheng Z, Wang Y, Han T. The Risks of miRNA Therapeutics: In a Drug Target Perspective. *Drug Design, Development and Therapy*. 2021;15:721-733. doi:10.2147/DDDT.S288859

194. Dastmalchi N, Safaralizadeh R, Hosseinpourfeizi MA, Baradaran B, Khojasteh SMB. MicroRNA-424-5p enhances chemosensitivity of breast cancer cells to Taxol and regulates cell cycle, apoptosis, and proliferation. *Molecular Biology Reports*. 2021;48(2):1345-1357. doi:10.1007/s11033-021-06193-4

195. Chen D, Bao C, Zhao F, et al. Exploring Specific miRNA-mRNA Axes With Relationship to Taxanes-Resistance in Breast Cancer. *Frontiers in Oncology*. 2020;10. doi:10.3389/fonc.2020.01397

196. Deng X, Cao M, Zhang J, et al. Hyaluronic acid-chitosan nanoparticles for co-delivery of MiR-34a and doxorubicin in therapy against triple negative breast cancer. *Biomaterials*. 2014;35(14):4333-4344. doi:10.1016/j.biomaterials.2014.02.006

197. Zhang Y-K, Wang Y-J, Gupta P, Chen Z-S. Multidrug Resistance Proteins (MRPs) and Cancer Therapy. *The AAPS Journal*. 2015;17(4):802-812. doi:10.1208/s12248-015-9757-1

198. Liang Z, Wu H, Xia J, et al. Involvement of miR-326 in chemotherapy resistance of breast cancer through modulating expression of multidrug resistance-associated protein 1. *Biochemical pharmacology*. 2010;79(6):817-824. doi:10.1016/j.bcp.2009.10.017

199. Xie M, Fu Z, Cao J, et al. MicroRNA-132 and microRNA-212 mediate doxorubicin resistance by down-regulating the PTEN-AKT/NF-κB signaling pathway in breast cancer. *Biomedicine & Pharmacotherapy*. 2018;102:286-294. doi:10.1016/j.biopha.2018.03.088

200. Deshmukh RR, Kim S, Elghoul Y, Dou QP. P-Glycoprotein Inhibition Sensitizes Human Breast Cancer Cells to Proteasome Inhibitors. *Journal of Cellular Biochemistry*. 2017;118(5):1239-1248. doi:10.1002/jcb.25783

201. Zhong P, Chen X, Guo R, et al. Folic Acid-Modified Nanoerythrocyte for Codelivery of Paclitaxel and Tariquidar to Overcome Breast Cancer Multidrug Resistance. *Molecular Pharmaceutics*. 2020;17(4):1114-1126. doi:10.1021/acs.molpharmaceut.9b01148

202. Wen S, Su S, Liou B, Lin C, Lee K. Sulbactam-enhanced cytotoxicity of doxorubicin in breast cancer cells. *Cancer Cell International*. 2018;18. doi:10.1186/s12935-018-0625-9

203. Li S, Yuan S, Zhao Q, Wang B, Wang X, Li K. Quercetin enhances chemotherapeutic effect of doxorubicin against human breast cancer cells while reducing toxic side effects of it. *Biomedicine & Pharmacotherapy = Biomedecine & Pharmacotherapie*. 2018;100:441-447. doi:10.1016/j.biopha.2018.02.055

204. Li K, Liu W, Zhao Q, et al. Combination of tanshinone IIA and doxorubicin possesses synergism and attenuation effects on doxorubicin in the treatment of breast cancer. *Phytotherapy Research*. 2019;33(6):1658-1669. doi:10.1002/ptr.6353

205. Bao L, Hazari S, Mehra S, Kaushal D, Moroz K, Dash S. Increased expression of P-glycoprotein and doxorubicin chemoresistance of metastatic breast cancer is regulated by miR-298. *The American Journal of Pathology*. 2012;180(6):2490-2503. doi:10.1016/j.ajpath.2012.02.024

206. Naumova N, Šachl R. Regulation of Cell Death by Mitochondrial Transport Systems of Calcium and Bcl-2 Proteins. *Membranes*. 2020;10(10):299. doi:10.3390/membranes10100299

207. Soond SM, Savvateeva LV, Makarov VA, Gorokhovets NV, Townsend PA, Zamyatnin AA. Making Connections: p53 and the Cathepsin Proteases as Co-Regulators of Cancer and Apoptosis. *Cancers*. 2020;12(11):3476. doi:10.3390/cancers12113476

208. Fearnley GW, Latham AM, Hollstein M, Odell AF, Ponnambalam S. ATF-2 and Tpl2 regulation of endothelial cell cycle progression and apoptosis. *Cellular Signalling*. 2020;66:109481. doi:10.1016/j.cellsig.2019.109481

209. Zacksenhaus E, Shrestha M, Liu JC, et al. Mitochondrial OXPHOS Induced by RB1 Deficiency in Breast Cancer: Implications for Anabolic Metabolism, Stemness, and Metastasis. *Trends in Cancer*. 2017;3(11):768-779. doi:10.1016/j.trecan.2017.09.002

210. Indovina P, Pentimalli F, Conti D, Giordano A. Translating RB1 predictive value in clinical cancer therapy: Are we there yet? *Biochemical Pharmacology*. 2019;166:323-334. doi:10.1016/j.bcp.2019.06.003

211. Xu X, Zhang L, He X, et al. TGF-β plays a vital role in triple-negative breast cancer (TNBC) drug-resistance through regulating stemness, EMT and apoptosis. *Biochemical and Biophysical Research Communications*. 2018;502(1):160-165. doi:10.1016/j.bbrc.2018.05.139

212. Zhang Z, Lin G, Yan Y, et al. Transmembrane TNF-alpha promotes chemoresistance in breast cancer cells. *Oncogene*. 2018;37(25):3456-3470. doi:10.1038/s41388-018-0221-4

213. Helfinger V, Schröder K. Redox control in cancer development and progression. *Molecular Aspects of Medicine*. 2018;63:88-98. doi:10.1016/j.mam.2018.02.003

214. Roy J, Galano J, Durand T, Le Guennec J, Chung-Yung Lee J. Physiological role of reactive oxygen species as promoters of natural defenses. *The FASEB Journal*. 2017;31(9):3729-3745. doi:10.1096/fj.201700170r

215. Di Meo S, Reed TT, Venditti P, Victor VM. Role of ROS and RNS Sources in Physiological and Pathological Conditions. *Oxidative Medicine and Cellular Longevity*. 2016:1-44. doi:10.1155/2016/1245049

216. Perillo B, Di Donato M, Pezone A, et al. ROS in cancer therapy: the bright side of the moon. *Experimental & Molecular Medicine*. 2020;52(2):192-203. doi:10.1038/s12276-020-0384-2

217. Zhang J, Lei W, Chen X, Wang S, Qian W. Oxidative stress response induced by chemotherapy in leukemia treatment (Review). *Molecular and Clinical Oncology*. Published online January 10, 2018. doi:10.3892/mco.2018.1549

218. Kamm A, Przychodzen P, Kuban-Jankowska A, et al. Nitric oxide and its derivatives in the cancer battlefield. *Nitric Oxide*. 2019;93:102-114. doi:10.1016/j.niox.2019.09.005

219. Denton D, Kumar S. Autophagy-dependent cell death. *Cell Death & Differentiation*. 2018;26(4):605-616. doi:10.1038/s41418-018-0252-y

220. Gąsiorkiewicz BM, Koczurkiewicz-Adamczyk P, Piska K, Pękala E. Autophagy modulating agents as chemosensitizers for cisplatin therapy in cancer. *Investigational New Drugs*. 2020;39(2):538-563. doi:10.1007/s10637-020-01032-y

221. Liao M, Wang C, Yang B, et al. Autophagy Blockade by Ai Du Qing Formula Promotes Chemosensitivity of Breast Cancer Stem Cells Via GRP78/β-Catenin/ABCG2 Axis. *Frontiers in Pharmacology*. 2021;12. doi:10.3389/fphar.2021.659297

222. Wiman KG, Zhivotovsky B. Understanding cell cycle and cell death regulation provides novel weapons against human diseases. *Journal of Internal Medicine*. 2017;281(5):483-495. doi:10.1111/joim.12609

223. Hwang JR, Kim WY, Cho Y-J, et al. Chloroquine reverses chemoresistance via upregulation of p21WAF1/CIP1 and autophagy inhibition in ovarian cancer. *Cell Death & Disease*. 2020;11(12). doi:10.1038/s41419-020-03242-x

224. Sanchez-Carranza JN, González-Maya L, Razo-Hernández RS, et al. Achillin Increases Chemosensitivity to Paclitaxel, Overcoming Resistance and Enhancing Apoptosis in Human Hepatocellular Carcinoma Cell Line Resistant to Paclitaxel (Hep3B/PTX). *Pharmaceutics*. 2019;11(10):512. doi:10.3390/pharmaceutics11100512

225. Vinod BS, Nair HH, Vijayakurup V, et al. Resveratrol chemosensitizes HER-2-overexpressing breast cancer cells to docetaxel chemoresistance by inhibiting docetaxel-mediated activation of HER-2–Akt axis. *Cell Death Discovery*. 2015;1(1). doi:10.1038/cddiscovery.2015.61

226. Hernández-Vargas H, Palacios J, Moreno-Bueno G. Molecular profiling of docetaxel cytotoxicity in breast cancer cells: uncoupling of aberrant mitosis and apoptosis. *Oncogene*. 2006;26(20):2902-2913. doi:10.1038/sj.onc.1210102

227. Elmore S. Apoptosis: A Review of Programmed Cell Death. *Toxicologic Pathology*. 2007;35(4):495-516. doi:10.1080/01926230701320337

228. Galluzzi L, Vitale I, Aaronson SA, et al. Molecular mechanisms of cell death: recommendations of the Nomenclature Committee on Cell Death 2018. *Cell Death & Differentiation*. 2018;25(3):486-541. doi:10.1038/s41418-017-0012-4

229. Cheng W-J, Zhang P-P, Luo Q-Q, Deng S-M, Jia A-Q. The chemosensitizer ferulic acid enhances epirubicin-induced apoptosis in MDA-MB-231 cells. *Journal of Functional Foods*. 2020;73:104130. doi:10.1016/j.jff.2020.104130

230. Kumar N, Pruthi V. Potential applications of ferulic acid from natural sources. *Biotechnology Reports*. 2014;4:86-93. doi:10.1016/j.btre.2014.09.002

231. Zhou Z, Meng M, Ni H. Chemosensitizing Effect of Astragalus Polysaccharides on Nasopharyngeal Carcinoma Cells by Inducing Apoptosis and Modulating Expression of Bax/Bcl-2 Ratio and Caspases. *Medical Science Monitor*. 2017;23:462-469. doi:10.12659/msm.903170

232. Lin K-C, Lin M-W, Hsu M-N, et al. Graphene oxide sensitizes cancer cells to chemotherapeutics by inducing early autophagy events, promoting nuclear trafficking and necrosis. *Theranostics*. 2018;8(9):2477-2487. doi:10.7150/thno.24173

233. Qu G, Liu S, Zhang S, et al. Graphene Oxide Induces Toll-like Receptor 4 (TLR4)-Dependent Necrosis in Macrophages. *ACS Nano*. 2013;7(7):5732-5745. doi:10.1021/nn402330b

234. Kapałczyńska M, Kolenda T, Przybyła W, et al. 2D and 3D cell cultures – a comparison of different types of cancer cell cultures. *Archives of Medical Science*. 2016;14(4). doi:10.5114/aoms.2016.63743

235. Jiang H, Zhang X, Liao Q, Wu W, Liu Y, Huang W. Electrochemical Monitoring of Paclitaxel-Induced ROS Release from Mitochondria inside Single Cells. *Small*. 2019;15(48):1901787. doi:10.1002/smll.201901787

236. Gorini S, De Angelis A, Berrino L, Malara N, Rosano G, Ferraro E. Chemotherapeutic Drugs and Mitochondrial Dysfunction: Focus on Doxorubicin, Trastuzumab, and Sunitinib. *Oxidative Medicine and Cellular Longevity*. 2018;2018:1-15. doi:10.1155/2018/7582730

237. Hu Y, Xiang J, Su L, Tang X. The regulation of nitric oxide in tumor progression and therapy. *Journal of International Medical Research*. 2020;48(2):030006052090598. doi:10.1177/0300060520905985

238. Chatterjee A, Chattopadhyay D, Chakrabarti G. miR-17-5p Downregulation Contributes to Paclitaxel Resistance of Lung Cancer Cells through Altering Beclin1 Expression. Mari B, ed. *PLoS ONE*. 2014;9(4):e95716. doi:10.1371/journal.pone.0095716

239. Guo Y, Huang C, Li G, Chen T, Li J, Huang Z. Paxilitaxel induces apoptosis accompanied by protective autophagy in osteosarcoma cells through hypoxia-inducible factor-1α pathway. *Molecular Medicine Reports*. 2015;12(3):3681-3687. doi:10.3892/mmr.2015.3860

240. Yoshii SR, Mizushima N. Monitoring and Measuring Autophagy. *International Journal of Molecular Sciences*. 2017;18(9). doi:10.3390/ijms18091865

241. Rodrigues-Ferreira S, Nehlig A, Kacem M, Nahmias C. ATIP3 deficiency facilitates intracellular accumulation of paclitaxel to reduce cancer cell migration and lymph node metastasis in breast cancer patients. *Scientific Reports*. 2020;10(1). doi:10.1038/s41598-020-70142-7

242. Park H-S, Han J-H, Jung S-H, Lee D-H, Heo K-S, Myung C-S. Anti-apoptotic effects of autophagy via ROS regulation in microtubule-targeted and PDGF-stimulated vascular smooth muscle cells. *The Korean Journal of Physiology & Pharmacology*. 2018;22(3):349. doi:10.4196/kjpp.2018.22.3.349

243. Lukina MM, Dudenkova VV, Ignatova NI, et al. Metabolic cofactors NAD(P)H and FAD as potential indicators of cancer cell response to chemotherapy with paclitaxel. *Biochimica et Biophysica Acta (BBA) - General Subjects*. 2018;1862(8):1693-1700. doi:10.1016/j.bbagen.2018.04.021

244. Janke C, Montagnac G. Causes and Consequences of Microtubule Acetylation. *Current Biology*. 2017;27(23):R1287-R1292. doi:10.1016/j.cub.2017.10.044

245. Magiera MM, Janke C. Post-translational modifications of tubulin. *Current Biology*. 2014;24(9):R351-R354. doi:10.1016/j.cub.2014.03.032

246. Lin L, Yee SW, Kim RB, Giacomini KM. SLC Transporters as Therapeutic Targets: Emerging Opportunities. *Nature reviews Drug discovery*. 2015;14(8):543-560. doi:10.1038/nrd4626

247. Shen Y, Yan Z. Systematic prediction of drug resistance caused by transporter genes in cancer cells. *Scientific Reports*. 2021;11(1). doi:10.1038/s41598-021-86921-9

248. Ghandi M, Huang FW, Jané-Valbuena J, et al. Next-generation characterization of the Cancer Cell Line Encyclopedia. *Nature*. 2019;569(7757):503-508. doi:10.1038/s41586-019-1186-3

249. Tate JG, Bamford S, Jubb HC, et al. COSMIC: the Catalogue Of Somatic Mutations In Cancer. *Nucleic Acids Research*. 2018;47(D1):D941-D947. doi:10.1093/nar/gky1015

250. Januchowski R, Sterzyńska K, Zawierucha P, et al. Microarray-based detection and expression analysis of new genes associated with drug resistance in ovarian cancer cell lines. *Oncotarget*. 2017;8(30). doi:10.18632/oncotarget.18278

251. Fardel O, Le Vee M, Jouan E, Denizot C, Parmentier Y. Nature and uses of fluorescent dyes for drug transporter studies. *Expert Opinion on Drug Metabolism & Toxicology*. 2015;11(8):1233-1251. doi:10.1517/17425255.2015.1053462

252. Di Giacomo S, Briz O, Monte MJ, et al. Chemosensitization of hepatocellular carcinoma cells to sorafenib by β-caryophyllene oxide-induced inhibition of ABC export pumps. *Archives of Toxicology*. 2019;93(3):623-634. doi:10.1007/s00204-019-02395-9

253. Love MI, Huber W, Anders S. Moderated estimation of fold change and dispersion for RNA-seq data with DESeq2. *Genome Biology*. 2014;15(12). doi:10.1186/s13059-014-0550-8

254. Dunlap JC, Moore JH. *Computational Methods for Genetics of Complex Traits*. Academic Press; 2010.

255. Porru M, Pompili L, Caruso C, Leonetti C. Xenograft as In Vivo Experimental Model. *Methods in Molecular Biology (Clifton, NJ)*. 2018;1692:97-105. doi:10.1007/978-1-4939-7401-6_9

256. Pompili L, Porru M, Caruso C, Biroccio A, Leonetti C. Patient-derived xenografts: a relevant preclinical model for drug development. *Journal of Experimental & Clinical Cancer Research*. 2016;35(1). doi:10.1186/s13046-016-0462-4

257. Malaney P, Nicosia SV, Davé V. One mouse, one patient paradigm: New avatars of personalized cancer therapy. *Cancer Letters*. 2014;344(1):1-12. doi:10.1016/j.canlet.2013.10.010

258. Chou T-C. The combination index (CI < 1) as the definition of synergism and of synergy claims. *Synergy*. 2018;7:49-50. doi:10.1016/j.synres.2018.04.001